Study of a kinesin adaptor in axonal transport and synapse formation

Dissertation
for the award of the degree
"Doctor rerum naturalium"
Division of Mathematics and Natural Sciences
of the Georg-August-Universität Göttingen

within the doctoral program Molecular Biology
of the Georg-August University School of Science (GAUSS)

Submitted by

Tahere Kalantary Dehaghi

from Tehran, Iran

Göttingen, 2018

Thesis advisory committee:

Dr. John Chua (Advisor, Reviewer)
Department of Physiology
Yong Loo Lin School of Medicine
National University of Singapore

Dr. Dieter Klopfenstein (Reviewer)
Department of Biophysics
Third Institute of Physics
University of Göttingen

Prof. Dr. Stefan Jakobs
Department of NanoBiophotonics
Max Planck Institute for Biophysical Chemistry

Date of the oral examination:

27 June 2018

I hereby declare that I prepared my doctoral thesis entitled "Study of a kinesin adaptor in axonal transport and synapse formation" on my own and with no other sources and aids than those cited.

Tahere Kalantary Dehaghi

May 2018, Göttingen

به پدر و مادرم

برای مهر و پشتیبانی همیشگی شان

Contents

List of Figures

List of Tables

Abbreviations

AD	Alzheimer's disease
ALS	Amyotrophic lateral sclerosis
AMPA	α-amino-3-hydroxy-5-methyl-4-isoxazolepropionic acid
AMPAR	AMPA receptor
APP	Amyloid-ß precursor protein
AZ	Active zone
BDNF	Brain-derived neurotrophic factor
CAZ	Cytomatrix assembled at the active zone
CNS	Central nervous system
DENN/MADD	Differentially expressed in normal and neoplastic cells/MAP kinase activating death domain
DISC1	Disrupted-in-Schizophrenia-1
DNC	Dorsal nerve cord
EB	End binding protein
FEZ1	Fasciculation and elongation protein zeta-1
GABA	γ-aminobutyric acid
HRP	Horseradish peroxidase
HSP	Hereditary spastic paraplegia
imac	immaculate connections (Kinesin-3 homolog)
JIP1	c-Jun NH2-terminal kinase-interacting protein 1

JNK	c-Jun NH2-terminal kinase
KLC	Kinesin light chain
MT	Microtubules
NMJ	Neuromuscular junction
PSD	Post synaptic density
PTVs	Piccolo Bassoon transport vesicles
RIM	Rab3 interacting molecule
RIM-BP	RIM binding protein
ROI	Region of interest
RRP	Readily releasable pool
RT	Room temperature
SGZ	Subgranular zone
SNARE	n-ethylmaleimide-sensitive factor attachment protein receptor
STV	Synaptic vesicle protein transport vesicle
SV	Synaptic Vesicle
SVP	Synaptic vesicle precursor
SVP	Synaptic vesicle precursors
VGAT	gamma-aminobutyric acid
VGLUT-1	Vesicular glutamate transporter-1
VNC	Ventral nerve cord

Abstract

To form a synaptic terminal, various components have to be targeted to specific sites in the axon. Presynaptic proteins are synthesized in the cell soma, packaged in vesicular cargos and transported by the motor complexes traveling along microtubules. During synapse development and maturation, the intracellular transport of proteins is highly regulated by mechanisms governing the interactions and movement of motor proteins. Additional specificity and regulation is provided by interaction of motor proteins with their cargos through adaptor and scaffolding proteins.

Previous studies have shown that FEZ1 acts as an adaptor for kinesin-1 and its binding to the motor is regulated by serine-58 phosphorylation. FEZ1/kinesin-1 complex partakes in presynapse formation by transporting syntaxin and Munc18 in the axon. Identification of numerous synaptic vesicle and active zone proteins in the FEZ1/kinesin-1 immunoisolated vesicles suggested the association and transport of these components with this complex. Although functional studies in *Caenorhabditis elegans* showed synaptic disorganization, the relevance of mammalian FEZ1 in neurons have not yet been investigated.

In this study, the mobility of FEZ1 and its phosphomutants were characterized in mammalian neurons. Furthermore, the role of FEZ1-mediated transport in formation of presynaptic and postsynaptic specializations was investigated by ablating the expression of FEZ1 using CRISPR/cas9 knockdown system. The data in this study show that mobility of neuronal FEZ1 is a result of precise modulation of its binding to kinesin-1 by serine-58 phosphorylation. This study also provides evidence for FEZ1 role in transport of active zone components and synaptic vesicle precursors, albeit in distinct mechanisms. Additionally, FEZ1 impacts neuronal development by regulating dendritic branching in young neurons, and dendritic spine formation during later stages.

1. Introduction

The brain is the central part of the mammalian nervous system. Proper brain function hinges on accurate development of its regions and their functional modules, known as neural circuits. Neural circuits are anatomical and functional entities, and can refer to a cluster of interconnected brain regions which translate large amounts of information into appropriate behavioral or cognitive responses. On a lower scale, neural circuits may also refer to an ensemble of interconnected neurons that receives, modifies and eventually transmits electrical and chemical information to other circuits [1].

Neural circuits are able to accomplish complicated functions due to their distinguished cellular building blocks, known as neurons. Neurons, as evident from their distinct morphology, are specialized for long-distance signaling. The extensive branching observed in neurons is the main morphological feature of neurons, specializing them in communication. A typical neuron has elaborate arborization stemming from the cell body known as dendrites, and a long projection called the axon, which can reach tens of centimeters in length [2].

During neonatal and early postnatal periods of development, neural circuits are initially formed through progressive events such as cell migration, neurite growth, target recognition and synaptogenesis. The communication in the brain is facilitated by neuronal connections known as synapses. Navigating axons reach distant target regions and form synapses either at the terminal region (terminal bouton) or along the axoplasm (en passant synapse) [3]. Neural circuits are later refined through regressive events, during which exuberant or unused synapses are removed. Regressive events encompass processes such as synapse elimination and axon and dendrite pruning [4].

1.1. The synapse

Synapses are intercellular conjunctions between a presynaptic neuron and another cell, often also a neuron. Synapses are able to integrate and transmit electrical

stimulation in the form of action potentials to chemical neurotransmission [5, 6]. Synaptic transmission is made possible by the precise juxtaposition of the presynaptic and the postsynaptic specializations. At the presynapse, a highly specialized region within the axon, synaptic vesicles filled with neurotransmitters are ready to be exocytosed and release their content in the synaptic cleft, while the postsynaptic plasma membrane is decorated with numerous neurotransmitter receptors [7].

Although synapses demonstrate a wide diversity with regards to their morphology, neurotransmitter type, release probability and postsynaptic receptors, they essentially share a basic architecture. All synapses are composed of three main cellular compartments: the presynaspe, the synaptic cleft, and the postsynaptic specialization. The presynapse is characterized by clusters of synaptic vesicles (SVs) filled with neurotransmitters, which undergo Ca^{2+}-triggered fusion with the plasma membrane upon arrival of action potential and release their content into the synaptic cleft [8]. Synaptic fusion occurs in a specialized membrane region in the presynapse, known as the active zone (AZ) [9, 6]. The postsynaptic side receives the neurotransmitter signal through various receptors and converts it into electrical and chemical changes in the cell. In the CNS, the excitatory and inhibitory postsynaptic specializations are distinguished by the characteristic ligand gated channels; glutamate and gamma-aminobutyric acid (GABA) receptors, respectively. In addition to their receptors, excitatory and inhibitory synapses differ morphologically and in their molecular organization [10].

1.1.1. The active zone

The active zone is a specialized region of the presynapse, with a set of evolutionary conserved core components, where synaptic vesicle exocytosis occurs. This region can be observed as an electron-dense region in the presynapse [11]. In the CNS neurons of vertebrates, active zones are disc-like structures with a diameter of about 0.2 to 0.5 µm.

The active zone spatially and functionally organizes neurotransmission by integrating three key roles [6, 12]:

1. The active zone organizes the synaptic vesicle pools and facilitates tethering, docking and priming the SVs.

2. It recruits the voltage-gated Ca^{2+} channels necessary for synchronous coupling of electrical stimulation and neurotransmitter release. This process, known as 'positional priming', spatially regulates neurotransmission by bringing the fusion machinery and the calcium source in close proximity.

3. The active zone facilitates the precise alignment of the pre- and postsynapse by proper localization of trans-synaptic cell adhesion molecules and tethering synaptic vesicles and Ca^{2+} channels to synaptic adhesion proteins.

Given the crucial organizational roles of the AZ in steps preceding and during fusion, it is not surprising this specialization is also involved in short and long term plasticity [13]. This process is regulated by the AZ either by directly responding to Ca^{2+} signals through release, or indirectly by recruiting other proteins responsible for plasticity.

1.1.1.1. Active zone components

The collection of proteins enriched in the active zone are known as the cytomatrix at the active zone (CAZ). The majority of the CAZ proteins are scaffolding proteins, each harboring multiple protein-protein interaction domains and few catalytic domains. The core components of the active zone consist of five evolutionary conserved proteins: RIM (for Rab3-interacting molecules), Munc13, RIM-binding proteins (RIM-BP), α-Liprin and ELKS/ERCs/CAST proteins [6]. These five components form a single large protein complex, which docks and primes the SVs, recruits the calcium channels, and tethers the SVs and the calcium channels to the trans-synaptic adhesion molecules. In addition to these core proteins, Bassoon and Piccolo, two large homologous proteins, are also associated with the active zone in vertebrates [14].

RIMs RIMs have five main interacting domains: an N-terminal zinc finger domain, a PDZ domain, and a proline rich domain flanked by two non-Ca^{2+} binding C2 domains. They bind to numerous proteins present at the AZ as well as associate with synaptic vesicles. Therefore, RIMs are considered to be the central organizers of the active zone [15, 16]. There are 4 RIM genes expressed in vertebrates, among which only RIM1 and RIM2 genes produce proteins including all domains, known as RIM1α and RIM2α, respectively. RIM3 and RIM4 genes produce short isoforms, known as RIM3γ and RIM4γ proteins, expressing only the last C-terminal C2 domain [16].

Several studies in *C. elegans* and mice have shown that RIMs are involved in both vesicle docking and priming [17, 18, 19, 20, 21, 22], recruiting the Ca^{2+} channels to active zones [20], and synaptic plasticity [18, 23]. In addition to its functions in regulation of release, RIM also tethers ELKS and N- and P/Q-type calcium channels in the active zone through its central PDZ domain, thereby acting as an organizing hub at the presynapse [24, 25].

RIM-BP   RIM binding proteins are multi-domain proteins, expressed by three genes in vertebrates and only one in *Drosophila* [26, 27, 28]. They form a complex with RIMs, and assist them in recruiting Ca^{2+} channels to the presynapse [26, 29]. Studies in *Drosophila* have shown that the presence of RIM-BPs is not only essential for accurate organization of the active zone, but also crucial for proper Ca^{2+} channels clustering and Ca^{2+} influx, and its deletion reduces the release probability drastically [28].

Munc13   The main function of mammalian orthologs of UNC-13 in C. elegans, Munc13s, is to prime synaptic vesicles for exocytosis, which they accomplish by priming the SNARE/SM protein fusion machinery. They also influence the short term plasticity by regulating this priming activity [30, 31]. The priming function of Munc13 is activated by binding to RIMs and disruption of Munc13 autoinhibitory homodimers [21].

α-Liprins   α- and β-liprins are related proteins with protein-protein interaction domains in both N- and C-termini, capable of forming homo- and heterodimers in addition to complexes with RIMs [18], ELKS [32, 33], CASK[34], and LAR-type receptor phosphotyrosine phosphatases [35]. The sum of *C. elegans* studies carried out on α-liprin and related proteins suggests that it recruits synaptic vesicles and Ca^{2+} channels to the active zone via linking synaptic cell adhesion molecules to the RIM/Munc13/RIM-BP core complex [36, 33, 37].

ELKS   ELKS are the most enigmatic core components of the active zone. They were initially discovered as an interacting partner for Rab6 [38], then found to be localized in the active zone and renamed CAST [24] or ERC [25]. There is one ELKS-like gene expressed in *C. elegans*, and two highly homologous ELKS proteins expressed in mammals, named ELKS1 and ELKS2 [25]. Interestingly, *Drosophila* expresses an ELKS fusion protein, known as '*bruchpilot*', comprised of N-terminal ELKS-related domain and C-terminal plectin-related domain [39]. ELKS participates in the active zone structure by binding to the PDZ domain of RIMs along with α-liprin [25, 32].

Piccolo and Bassoon   Originally discovered in a screen designed to characterize the rat brain synaptic junctions, these two highly homologous large proteins seem to have redundant as well as distinct roles in CAZ organization [40, 41, 42, 43, 44]. Bassoon and Piccolo are specific to vertebrates, although there are structurally more distant versions expressed in invertebrates which might play a similar organizational

role in the active zone [39, 45, 46]. Deleting the central region of Bassoon in mice did not exhibit an effect on the ultrastructure organization of the active zone, but it led to reduced neurotransmission. Although the number of clustered and docked synaptic vesicles appeared normal, they were unable to fuse [47].

Consistent with the observed diminished neurotransmission in mutant Bassoon mice, a few studies have collectively proposed that Bassoon is important for the accurate positioning of the Ca^{2+} channels in the active zone, in addition to rapid vesicle replenishment in the vacant release sites [48, 49, 50, 51]. With regards to recruitment of Ca^{2+} channels, Bassoon seems to selectively position P/Q-type (and not the N-type) Ca^{2+} channels near the release sites in the hippocampal synapses [52].

RNAi-mediated knockdown of Piccolo in cultured neurons did not affect the formation or morphology of glutamatergic synapses. It is however suggested to negatively regulate SV exocytosis through a calmodulin kinase II-dependent mechanism, influencing the dynamics of synapsin Ia [53]. Cultured neurons and acute slices from Piccolo knockout mice have shown that the absence of Piccolo has no significant effect on neither survival nor synaptic transmission. The same phenotype was observed when Bassoon was also acutely knocked down from these neurons. However, synaptic vesicle clustering was severely reduced in the absence of both Bassoon and Piccolo, leading the authors to propose a redundant function of Bassoon and Piccolo in SV clustering at the nerve terminal [54].

1.1.2. Synaptic vesicles

Synaptic vesicles are the main means of interneuronal communication in the nervous system. These 40-nm trafficking organelles are accumulated at the presynaptic nerve terminals, and are filled with neurotransmitters. Upon the arrival of an action potential and influx of Ca^{2+} into the presynaptic terminal, SVs go through exocytosis and neurotransmitter release in less than a millisecond [55]. SVs can be biochemically purified and their molecular composition has been extensively characterized [56, 57, 58].

Synaptic vesicles are uniform in size and shape, and while the exact stoichiometric ratio of proteins varies among individual SVs, they require at least five distinct members to be able to take up neurotransmitters, respond appropriately to the calcium signal and fuse with the plasma membrane [59]:

1. The soluble n-ethylmaleimide-sensitive factor attachment protein receptor (SNARE) synaptobrevin for fusion with the plasma membrane

2. Synaptotagmin for detection of Ca^{2+} influx before exocytosis

3. The neurotransmitter transporter to fill up the SVs with neurotransmitters

4. SV protein 2, probably involved in release [60]

5. The abundant but poorly understood Synaptophysin [58]

At the nerve terminal, synaptic vesicles have been classically grouped in three distinct subpopulations based on their release capability [61]. The readily releasable pool (RRP) refers to the SVs that are thought to be docked at the AZ and are rapidly depleted upon electrical stimulation or depolarization [62, 63, 64, 65, 66, 67]. The recycling pool is released more slowly that the RRP, and comprise 5-20% of all vesicles [61]. These vesicles are continuously recycling upon stimulation by physiological frequencies [67, 68, 69, 70]. The majority of the vesicles however comprise the reserve pool, from which release only occurs upon prolonged or intense stimulations [71, 72, 66, 67, 68, 70].

1.1.3. Trans-synaptic adhesion molecules

Many synaptic adhesion molecules reside at the synaptic sites in dendrites and axons. These molecules, known as synaptically localized cell adhesion molecules (SAMs), bridge the pre- and postsynaptic specializations and can interact in either homo- or heterophilic fashion across the synaptic cleft. Trans-synaptic adhesion molecules not only facilitate the juxtapositioning of pre- and postsynapses and provide mechanical support, but they also induce formation of new synapses and regulate the function of existing synapses through triggering signaling cascades or secondary protein-protein interactions [73]. Among several well-studied trans-synaptic adhesion molecules, the importance of two is briefly discussed in the following sections.

1.1.3.1. N-cadherins

Cadherins are a large protein family with more than 80 members in a single mammalian species [74]. Initially studied in epithelial cells, N-cadherins have also been shown to play key roles in synaptic formation, maintenance, transmission and plasticity. Classical cadherins, type I and II, have five extracellular repeats which bind to Ca^{2+}, a transmembrane domain, and a cytosolic tail capable of binding to β-catenin, δ-catenin, and α-catenin (via β-catenin). The most widely expressed cadherins in neurons are N-cadherins [74]. They localize evenly along the nascent synapses in young cultured neurons, while clustering more in the active zone in more mature

neurons [75]. N-cadherins are transported with the trafficking packets of active zone components to the sites of synaptic formation [76, 77, 75]. N-cadherins are found in both pre- and postsynaptic compartments, and they exert their functional roles by binding to cytosolic catenins, which in turn interact with their respective signaling molecules. In addition to the structural role of N-cadherin through providing synaptic contact, it has also been shown to play a key role in clustering of synaptic vesicles through indirect interaction with the postsynaptic adhesion molecule neuroligin-1. Microscopy studies have shown that N-cadherin recruits neuroligin-1 in the postsynaptic compartment via the scaffolding molecule S-SCAM, which activates neuroligin and leads to presynaptic vesicle clustering. The functional role of N-cadherin is further highlighted by its role in increasing release probability in mature synapses [78].

1.1.3.2. Neuroligins and neurexins

Another major trans-synaptic adhesion complex inducing synaptogenesis is the neuroligin-neurexin complex. Neuroligins are a class of postsynaptic adhesion molecules with four members [79]. Different subtypes of neuroligins exhibit distinct subcellular localization; while neuroligin-1 and 2 selectively localize to excitatory and inhibitory synapses respectively, neuroligin-3 is found in both types of synapses [79, 80, 81, 82, 83]. On the postsynaptic side, neuroligins interact with PSD95 among other proteins [84], while they extracellularly associate with β-neurexins as their presynaptic binding partners [84, 85]. There has been a line of studies focusing on the mechanisms through which neuroligin-neurexin complex contribute to synaptogenesis. Neuroligin-1 and 2, when expressed on the surface of non-neuronal cells and contacting navigating axons, can recruit presynaptic proteins to these contact sites [86]. Later work also showed that binding of neuroligin to neurexin was sufficient for its clustering, which was in turn sufficient to initiate presynapse formation by recruiting vesicles through interactions mediated by cytosolic domains of neurexin [87, 88].

1.1.4. Synapse formation

Formation of the presynaptic terminals requires the transport of active zone components and synaptic vesicle proteins to the axo-dendritic contacts at the right time. The newly synthesized presynaptic proteins are generally sorted in at least two distinct groups of precursory organelles, PTVs (Piccolo Bassoon transport vesicles) and STVs (synaptic vesicle protein transport vesicles). Numerous studies over the last

two decades have investigated the content and transport dynamics of these trafficking organelles.

1.1.4.1. Assembly of the active zone

PTVs are 80-nm dense-core granulated vesicles carrying the active zone proteins Piccolo and Bassoon, in addition to other proteins involved in exocytosis, such as SNAP25, Munc13, Munc18 and syntaxin [89, 76]. Several studies in the last decade have demonstrated that there are at least three distinct transport vesicles which are carrying Munc13, or complexes between Piccolo-Bassoon-ELKS/CAST, and RIM-Neurexin-CASK-Voltage gated Ca^{+2} channels (VGCCs) [90, 91, 92]. In neurons, PTVs move bidirectionally and in a saltatory manner. They occasionally split into smaller puncta or coalesce into larger clusters [76]. PTVs begin their journey along the axon from the trans-Golgi network [93], and their initial assembly requires Piccolo and Bassoon [92]. They eventually fuse to the plasma membrane and establish the active zone [94, 92].

1.1.4.2. Assembly and delivery of synaptic vesicles

A large body of research in the last decades has investigated how and when the components of SVs assemble on a trafficking organelle and begin their journey towards the nerve terminal. Transporting the SV components in prepackaged structures rather than individually is faster and energetically less demanding on the cell. Indeed, there are several studies suggesting that synaptic proteins travel into the axon by forming vesicular intermediates, and their contents have been studied by biochemical methods, electron microscopy and confocal imaging.

The trafficking organelles containing the synaptic vesicle proteins are a morphologically heterogeneous population, called STVs (synaptic vesicle protein transport vesicles) [95]. It has been shown that synaptic proteins travel along the axon in discrete packets, which in addition to clear SVs, contain dense core vesicles, tubulovesicular structures and pleiomorphic vesicles in different combinations [96]. These structures were also observed by electron microscopy in embedded neurons labeled for SV proteins [97, 98, 90]. Immunolabeling of numerous SV proteins in neurons, such as synaptophysin, synapsin I and SV2 showed a high colocalization in the axons, implying that synaptic vesicle proteins are indeed transported together [96, 99].

Live imaging of young cultured neurons have shown that simimilar to PTVs, STVs also move in a saltatory fashion punctuated with frequent directional changes. They

have been observed to sometimes split off from a stable cluster of STVs into smaller units, or coalesce into larger ones [98, 96, 99]. These trafficking organelles are electrophysiologically active within less than one hour of recruitment to targeted axonal regions [96].

1.1.5. Initiation of synapse formation

In order for a functional synapse to form, navigating axons have to make contact with the dendritic branches. The physical contact has to be further stabilized in the presence of essential synaptic and active zone proteins. While the requirement of an extensive set of proteins is undebatable, there are three different models proposed for the initiation of synaptogenesis.

1.1.5.1. Axo-dendritic contact precedes synaptogenesis

Randomly growing axons can establish cell-cell adhesion contacts with dendritic filopodia, which upon stabilization can eventually differentiate into a fully functional synapse. In this model, the initial contact of axons and dendrites precedes the recruitment of synaptic proteins on either side [100]. Such a mechanism has been observed in a few studies [96, 101, 76]. For instance, in order to resolve a timeline for synaptic bouton formation, it was observed that the new boutons capable of vesicle recycling appear within 30 min of initial axo-dendritic contact. Accumulation of postsynaptic proteins, specifically SAP90/PSD95 and glutamate receptors, was observed 45 min after the appearance of such boutons, leading to a fully assembled synapse within 1-2 h of initial axo-dendritic contact [102].

1.1.5.2. Pre-defined synaptogenic sites within the axon

Contrary to the conventional notion that synapse formation is preceded by axo-dendritic contact, there are a number of studies postulating a model where there are pre-defined sites for synapse formation in the axonal membrane. There is a considerable body of evidence in favor of this hypothesis. PTVs and STVs move bidirectionally in the axons displaying frequent pauses and change of direction [96, 76]. Interestingly, they appear to co-migrate extensively and have the tendency to pause at the same sites as one another [103, 104]. The coordinated transport and pause sites of STVs and PTVs suggest the existence of intrinsic pre-defined areas within the axonal membrane where presynapses eventually form. Additionally, it has been observed that there are many active presynapses in the axons capable of evoked

release, despite the lack of any postsynaptic partners. These orphan presynapses are mobile presynaptic material that have been transiently immobilized at specific regions due to evoked action potentials, and demonstrate the same SV dynamics as mature synapses [105]. Orphan boutons eventually either fuse to existing presynaptic sites or establish new release sites [105, 106]. Lastly, STVs are more prone to pause at the pre-defined sites where a future axo-dendritic contact will occur [95].

Two determinants of pre-defined pause sites within the axon have been proposed. First, the Sec6/8 subunit of the exocyst, a multisubunit protein, has been shown to display a punctate distribution pattern in developing axons of young cultured neurons and to be downregulated as neurons mature [107]. Sec6 also localizes to preferred STV pause sites [95]. In another line of research, lipid rafts have been suggested to play a role in specifying the presynapse location. Lipid rafts are small microdomains in plasma membrane containing high cholesterol and sphingolipid concentration [108]. In one study, BDNF was shown to promote neuronal lipid raft formation, followed by upregulation of presynaptic protein expression, specifically in lipid rafts but not in non-rafts [108, 109].

1.1.5.3. Postsynaptic initiation of synaptogenesis

Similar to axons, there are also pre-defined sites along the dendrites that can promote the establishment of a functional synapse. There are several studies that have reported the non-synaptic clustering of postsynaptic proteins in the dendrites of young neurons [110, 111, 101, 112, 113, 114]. Further analysis of the postsynaptic protein complexes in young cultured neurons has shown that they all contain PSD95, guanylate-kinase-associated protein (GKAP) and Shank. Most of these complexes appeared to be stationary and located at both synaptic and non-synaptic sites. Interestingly, the fraction of the stationary complexes containing neuroligin-1 was able to recruit synaptophysin-containing transport vesicles in the axons, and a presynaptic bouton was able to form within 2 hours on the other side [115]. Consistent with the evidence on PSD proteins, non-synaptic membrane specializations have also been observed in vivo with the help of EM analysis [116, 117, 110, 118].

1.2. Cytoskeleton in neurons

Neurons are highly polarized cells, with their axons reaching targets tens of centimeters away. Efficient transport of various organelles and proteins to distant regions of the cell depends on the neuronal cytoskeleton. Furthermore, the cytoskeleton is also

involved in establishment and maintenance of neuron morphology and polarity. The neuronal cytoskeleton is composed of microtubules (MT), actin filaments and neurofilaments. MT and actin filaments are mainly involved in neurite formation, axonal differentiation and short and long distance transport [119, 120]. Neurofilaments are highly abundant in the axon and are mainly involved in axonal radial growth and conductance [121, 122, 123].

Due to high dynamicity of the cytoskeletal filaments, they have gained much attention in regards to axonal regeneration and neurological disorders. The regenerative ability of the axon is dependent on either the remodeling of the cytoskeleton itself, or on the transport of growth factor receptors to the site of injury [124, 125]. Moreover, disruption in the axonal transport has been implicated in neurological disorders such as amyotrophic lateral sclerosis (ALS) and Alzheimer's disease (AD) [126, 127].

1.2.1. Microtubules

Microtubule protofilaments are composed of stable heterodimers of α and β tubulins, aligned in a head-to-tail polar fashion. Both tubulin monomers have a binding site for GTP. While the GTP bound to α-tubulin is trapped within the dimer structure and cannot be hydrolyzed, the β-tubulin can be found in a GTP or GDP-bound form. Thirteen protofilaments are laterally joined together to form a hollow cylindrical tube with an outer diameter of 25 µm [128]. The protofilaments are always aligned in a parallel fashion with the α-tubulin positioned at one end and the β-tubulin at the other, maintaining an inherent structural polarity in MT. Generally, one end of the microtubule filament is more dynamic, where both growth and disassembly of the filament is occurring at a faster rate. The fast end of the microtubule is called the plus end, while the other is the minus end. MT alternate between phases of slow growth and rapid disassembly, a phenomenon known as dynamic instability [129]. This feature enables the microtubules to grow and explore different regions of the cell, and retract in the absence of appropriate signals [129, 130]. The microtubule plusend is also a major regulatory site [128], where microtubule plus end tracking proteins (+TIPs) are bound. For instance, end binding proteins (EB) regulate MT growth dynamics, in addition to binding to several other MT-related proteins, such as MT motors, actin-associated proteins and signaling proteins [131, 132].

1.2.1.1. Microtubules in neurons

Microtubules have to be in the correct orientation to carry out their function. In the axon and the distal dendrites, microtubules are generally found with the plus-

ends pointing away from the cell body, while exhibiting a mixed polarity in the proximal regions of the dendrites [133, 134, 135, 136, 137]. As one of the three major constituents of the cytoskeleton, microtubules have various functions within two main themes in neurons:

(i) Microtubules are involved in inducing morphological changes during different stages of neuron development:

- Neuron migration: Migration of the neurons is the result of cooperation between both actin filaments and microtubules. Actin filaments facilitate the formation of the leading process by polymerization at its tip, and generating propelling contractions at the rear end of the cell. Meanwhile, microtubules protruding out of the centrosome create a cytoskeletal cage around the nucleus, which is being pulled at the proximal end of the leading process, thereby carrying the nucleus in the same direction as the entire cell [138, 139, 140].

- Neurite initiation: The initial symmetry of the newborn neuron is disrupted by small neurite protrusions [141]. Formation of neurites is facilitated by a combination of microtubule stabilization and forces generated by increased actin dynamics [142, 143].

- Axonal differentiation and elongation: After the initial neurite formation in young neurons, one of the neurites grows longer and eventually differentiates into the axon [144]. Several studies have implicated that axonal differentiation is facilitated by local stabilization of MT [145]. Microtubule stabilization could also explain the targeting of kinesin motors which actually precedes axonal differentiation. Kinesins show a higher affinity for stabilized microtubules, which implies higher membrane trafficking to the future axons [146, 147]. It has been shown that microtubules facilitate axonal elongation by sliding apart, which is powered by the forces generated by motor proteins [148, 149, 150].

(ii) Microtubules provide railways for intracellular transport of vesicles, organelles and soluble proteins by motor proteins. While microtubules, actin filaments and neurofilaments all contribute to neuronal function and morphology, intracellular transport is almost entirely dependent on microtubules. Transport occurs bidirectionally, with cargos moving towards the cell periphery (anterograde transport) mainly done by kinesins, and from the periphery to the cell soma (retrograde transport) by dyneins [151, 152].

1.2.1.2. Microtubules at the synapse

Over the last few decades, many studies have investigated the presence of microtubules within the nerve terminals. Microtubules have been detected in presynaptic membrane fractions associated with both SVs and dense core vesicles [153, 154]. More recent studies have also found tubulin by performing mass spectrometry on presynaptic preparations [155, 156, 157], suggesting that microtubules may interact with the CAZ proteins and direct SVs to the presynaptic membrane or contribute to the organization of AZ [158]. Ultrastructural analysis by EM has shown that presynaptic microtubules are spaced closer together than the axonal microtubules, and they appear to expand to form vesicle-filled varicosities in the presynaptic region [159].

A number of studies in *Drosophila* have attributed a structural and physiological role to microtubules at the presynaptic terminals. Firstly, at the *Drosophila* NMJ, there is an equilibrium between the tubulin monomers and polymers of tubulin [160], and microtubules have been shown to dynamically protrude into the presynaptic terminals forming structures known as 'pioneer presynaptic MTs' [161]. Microtubules also interact with the components of the active zone via binding to the *Drosophila* homolog of MAP1B, known as Futsch [162, 163]. This interaction promotes MT stability at the presynaptic terminal and supports synaptic growth [164, 165]. Futsch also facilitates the association between MT and the *Drosophila* ELKS homolog, *Bruchpilot*, and calcium channel *Cacophony* [163]. Therefore, through interacting with Futsch, presynaptic microtubules support the stabilization of active zone components and regulate presynaptic physiology.

Microtubules have also been known to interact with synaptic vesicle proteins. Rapidly frozen tissues analyzed by EM demonstrated that microtubule fibers are connected to the SVs at the nerve terminals by thin strands [166], which were later suggested to be single synapsin I molecules [167, 168]. It has been also shown that synatoptagmin-1 interacts with tubulin through its cytoplasmic C2A and C2B domain, which might propose a novel mechanism of how MT associates with the SVs at the presynaptic region [169].

Microtubules have also been observed to invade the dendritic spines during development in an activity-dependent manner [170]. Microtubule plus ends invading the dendritic spine also affects the actin dynamics within the spine and modulates synaptic plasticity [171]. Local calcium transients have also been shown to increase the entry of MT in the spines by upregulating actin polymerization, further implying that spine shape formation by microtubules is affected by synaptic activity [172].

Lastly, microtubules have also been observed to associate with mitochondria in the presynaptic region, and may contribute to proper mitochondria positioning [173, 174, 175, 176].

1.2.2. Actin filaments

Actin filaments (F-actin) are composed of globular actin monomers (G-actin). Much like tubulins, actin monomers also have a nucleotide binding site, which binds to ATP/ADP rather than GTP/GDP. The actin subunits also assemble in a head-to-tail fashion, which leads to distinctly polar actin filaments. Actin filaments are made of two actin protofilaments twisted around each other in a right-handed helix. F-actin dynamics is regulated by numerous actin binding proteins, which control its nucleation, capping, severing and crosslinking [177]. In the axon, actins are generally found in two distinct populations. It has been shown that actin filaments form regularly spaced rings beneath the axonal plasma membrane, providing mechanical support and organizing the membrane proteins in the axon [178, 179]. In addition, in a recent study it was observed that there are 'actin hotspots' within the axon, where the F-actin undergoes constant assembly and disassembly. The authors have suggested that these spots help enrich actin at the presynapse and possibly contribute to synaptic plasticity [180].

1.2.2.1. Actin filaments at the synapse

F-actin is the most abundant cytoskeletal protein at both sides of the excitatory synapse, and its localization becomes more prominent as the neuron matures [179]. From a functional standpoint, there are several studies attributing a variety of roles to F-actin in the presynaptic terminal, including a structural function, facilitating recruitment and positioning of SVs, and regulating both exocytosis and endocytosis [181]. Actin has been shown to be specifically crucial for initial steps of synaptogenesis in *Drosophila* and *C. elegans* [182, 183]. The role of actin filaments during the initial stages of synapse formation is highlighted by the observation that actin depolymerizing agent, latrunculin A, almost completely disrupted the clustering of synaptophysin in culture during the synaptogenesis peak [184].

Another interesting role that has been attributed to F-actin is the coordination of SV and active zone protein clustering. Formation of the N-cadherin-ß-catenin complex triggers downstream signaling cascades which result in increased actin polymerization at synapses. Upon enhanced polymerization of actin filaments, SVs are recruited and

clustered at the presynapse [185]. Synapsin I is also known to interact with actin filaments in a highly regulated manner. Depolarization induces phosphorylation of synapsin I at S566 and S603 by CamKII, which ultimately reduces the synapsin-actin interaction [57, 186, 187]. However, while this process promotes the clustering of SVs, it is not sufficient for the recruitment of active zone proteins. The missing link between actin dynamics and the active zone components might be Piccolo. It has been observed that boutons lacking Piccolo exhibit reduced F-actin polymerization, suggesting Piccolo as a key regulator in actin network assembly at the presynapse [188]. Taken together, it is plausible to think of F-actin assembly as one of the key mechanisms neurons utilize to bring active zone and SV components together at the presynapse.

1.3. Axonal transport in synapse formation

It is generally known that there are two main types of transport in the axons: the fast component and the slow component. Fast axonal transport refers to the delivery of vesicles and organelles at a speed of about 50-400 mm/day, whereas slow axonal component includes the delivery of cytosolic and cytoskeletal proteins moving at a speed of less than 8 mm/day [151]. Both kinesin and dynein motor proteins contribute to intracellular transport in the axons and synapse formation [152].

1.3.1. Anterograde transport by kinesins

Kinesin superfamily proteins (KIFs) are a large group of motor proteins with 45 members in mammals, 38 of which are expressed in the brain [189]. Depending on the motor domain position, kinesins are divided in three groups: the N-terminal motor domain KIFs (N-KIFs), middle motor domain KIFs (M-KIFs), and C-terminal motor domain KIFs (C-KIFs) [190, 189]. N- and C-KIFs are composed of the motor region, which moves on the microtubules with the aid of ATP hydrolysis, the stalk region and a tail domain. Kinesins utilize their tail domain, and occasionally the stalk region, to associate with their cargos [191]. A more recent standardized nomenclature groups kinesins in 14 different subfamilies which have common functional and structural features [192].

1.3.1.1. Kinesin-1 (KIF5)

Kinesin-1 is composed of a dimer of kinesin heavy chains, in addition to a dimer of kinesin light chains (KLCs), which is not always part of the complex [193]. KIF5 heavy chain is expressed in three different isoforms in mammals; KIF5A, KIF5B and KIF5C [189]. All heavy chains form homodimers and/or heterodimers, suggesting some functional redundancy. The main distinction among the isoforms are the localization and expression levels in various neuronal types [194]. In the absence of cargo, kinesin-1 C-terminal tail region folds onto the N-terminal motor domain, thereby keeping the motor in a folded, compact state to avoid unnecessary ATP hydrolysis [195, 196, 197, 198, 199, 200]. Autoinhibition of kinesin-1 is relieved by binding to cargo, which enables the motor protein to hydrolyze ATP and traverse along the microtubules [195, 201, 202, 203]. KLCs are thought to contribute to kinesin activity by regulating KHC autoinhibition, as well as binding to cargos [202, 204, 205].

Cargos of Kinesin-1 in neurons   Kinesin-1 plays a key role in synapse formation by transporting AZ precursors by interacting with syntaxin 1 via syntabulin as a transport adaptor [206]. Interrupting the interaction of syntabulin with KIF5B diminished the axonal flux of PTVs, and led to reduced number of functional presynapses [201]. In addition to syntabulin, FEZ1 also binds to KIF5C and drives the transport of syntaxin 1 along the axons [207]. Kinesin-1 has also been suggested to directly associate with SNAP-25 and facilitate the transport of SNAP-25 containing vesicles to the periphery of the cell, thereby contributing to synaptic fusion [208, 209]. Recently, the kinesin-1 homolog of *C. elegans*, UNC-116, has been shown to mediate the delivery and removal of AMPARs at the synapse, thereby regulating the synaptic strength [210].

Kinesin-1 has also been suggested to contribute to synaptic vesicle transport by numerous studies. Historically, kinesin-1 has been shown to associate with and translocate synaptic vesicles *in vitro* [211], and KIF5A and KIF5B have also been identified on synaptic vesicles [58]. Moreover, functional studies on its homolog in *C. elegans, unc-116,* have suggested that proper localization of synaptobrevin is dependent on this motor [212]. Proper transport of synaptotagmin-1 has also been partially attributed to kinesin-1 through forming a complex with UNC-51/ATG1 and UNC-76 [213].

Another neuronal cargo of kinesin-1 is the amyloid-β precursor protein-containing vesicle, the precursor of the protein that forms the senile plaques observed in Alzheimer's disease [214]. Deficient axonal transport of APP could have implications in progres-

sion of Alzheimer's disease [215, 216]. Specifically, the early axonal transport deficiencies observed in the AD mouse model are suggested to increase the proteolysis of APP resulting in senile plaque formation [217]. It has been suggested that APP-containing vesicles can be either transported as an independent cargo via direct interaction with kinesin-1, or co-transported with c-Jun NH2-terminal kinase-interacting protein 1 (JIP1) in a phosphorylation-regulated manner [218].

Another crucial function of KIF5 is transporting the retrograde motor protein. Dynein-dynactin complex is the only retrograde motor protein in mammals, and it needs to be transported to the distal axon to be able to bind to its cargos [219]. Recently, it has been proposed that dyneins are transported to the distal axon by slow axonal transport via transient interactions with kinesin-1 [220]. This model seems to be in agreement with the previous data where 95% of dynein had been observed to move via either slow axonal transport or with vesicles [221].

1.3.1.2. Kinesin-3 (KIF1)

The kinesin-3 family motor proteins KIF1A and KIF1Bβ are two very similar kinesins, with a pleckstrin homology (PH) domain and a conserved stalk domain. It has been demonstrated that the PH domain is necessary but not sufficient for binding of KIF1A and KIF1Bβ to their cargos [222]. The PH domain has a tendency to bind to phosphatidylinositol 4,5-bis-phosphate (PtdIns(4,5)P$_2$), which is found primarily in the plasma membrane [223]. This motor protein is activated by binding to phospholipids and dimerization [224, 223, 225].

Cargos of kinesin-3 in neurons KIF1A and KIF1Bβ and their homologs in invertebrates, UNC-104 in *C. elegans* and *imac* in *Drosophila*, are mainly responsible for transporting synaptic vesicle precursors (SVPs) and dense core vesicles [224, 226, 227, 228, 229]. It has been shown that overexpression of KIF1A facilitates BDNF-induced synaptogenesis and enhanced learning in the hippocampus [230]. Overexpression of UNC-104 or a gain of function mutation in *unc-104* decreases the capture probability of STVs by stable presynaptic sites, pointing to the role of this motor in proper synapse distribution [104]. An alternatively spliced variant of KIF1Bß, known as KIF1Bα, has been shown to transport mitochondria via interacting with kinesin binding protein (KBP) [231, 232]. Several loss of function studies have shown that deletion of UNC-104 or its adaptors severely affect different aspects of synapse formation. For instance, in *Kif1* knockout mice and *unc-104 C. elegans* mutants, the number of synaptic vesicles was reduced while the active zone

remained normal [224, 233, 234]. In *Drosophila*, mutation of kinesin-3 homolog *imac* led to abnormal synaptic bouton formation and reduced number of synaptic vesicles [228].

KIF1A and KIF1Bβ proteins bind to STVs through association with the adaptor protein DENN/MADD [235]. DENN/MADD is an effector for Rab3, a GTPase abundantly found on synaptic vesicles. The death domain of DENN/MADD binds to the stalk region of KIF1A and KIF1Bβ and the MADD domain interacts exclusively with the GTP-bound form of Rab3 on the synaptic vesicles. Given that the GDP-bound form of Rab3 is unable to bind to the MADD domain, it is speculated that GTP hydrolysis in Rab3 is a mechanism for cargo unloading [235]. Not surprisingly, the size and number of synaptic vesicles are reduced in DENN/MADD knockout mice [236] and deletion of the DENN/MADD homolog in *C. elegans*, *aex-3*, leads to Rab3 mislocalization [237].

Another important adaptor of kinesin-3 for transporting STVs is α-liprin, known as SYD-2 in *C. elegans* [238]. The ultrastructure of the active zone is significantly lengthened in *syd-2 C. elegans* mutants, whereas the number of synaptic vesicles per active zone remained unchanged [239]. Moreover, the net anterograde movement and velocity of UNC-104 is reduced upon *syd-2* mutation in *C. elegans*, suggesting its necessity for motor motility control and transport of cargos [240]. Studies have shown that α-liprin facilitates the clustering of KIF1A monomers, thereby improving its processivity [241, 240].
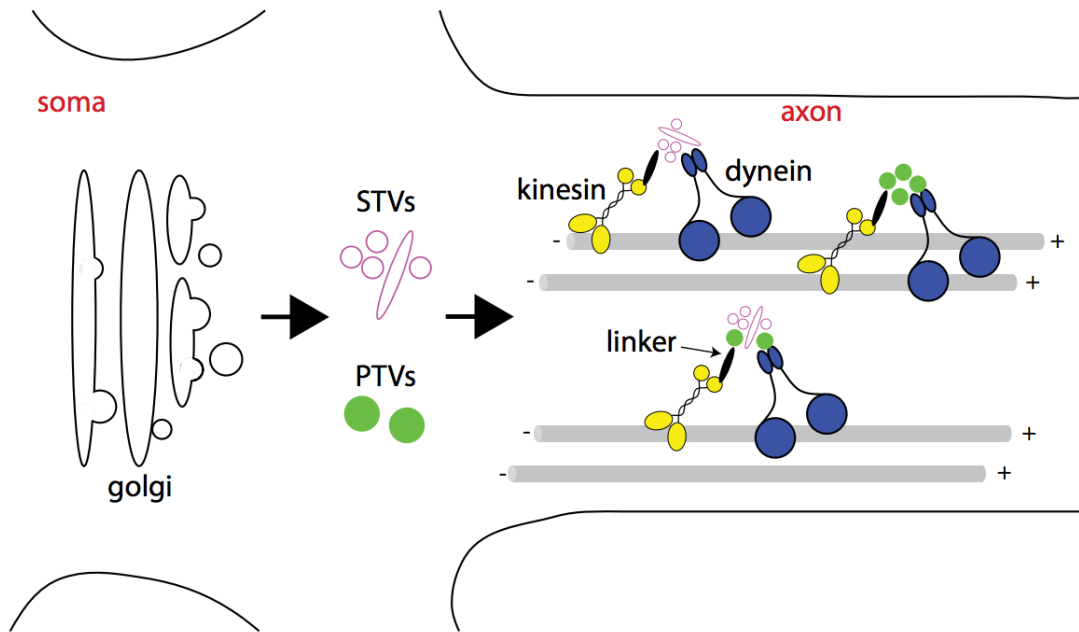
Figure 1.3.1.: Presynaptic cargos are sorted in two distinct trafficking organelles and transported in the axon by kinesins and dyneins. Newly synthesized SV and CAZ proteins are packaged in at least two species of trafficking organelles known as STVs and PTVs, respectively. STVs and PTVs then bind to kinesins either directly or through binding to scaffold or adaptor proteins, and are transported to developing synapses. Retrograde transport occurs by binding to dynein. Illustration adapted from Bury and Sabo, 2016 [242]. Used with permission from SAGE publishing.

1.3.2. Co-trafficking of synaptic vesicle and active zone proteins

As described in 1.1.4.1 and 1.1.4.2, it has been suggested that SV and AZ components are assembled and transported in two distinct trafficking organelles. However, there has been some evidence in support of association between AZ proteins and STVs during transport. Retrospective EM analysis combined with live imaging in cultured neurons have revealed that STVs are found in close proximity to dense core vesicles [96]. Immuno-gold labeling and EM ultrastructural analyses using Piccolo and Bassoon antibodies, in addition to a number of synaptic vesicle proteins has also implicated the assembly of these proteins in multivesicular aggregates [90]. PTVs and STVs have also been shown to co-migrate and pause at the same sites in cultured neurons and in *C. elegans* [103, 104]. The association of SV and AZ proteins during transport may provide a mechanism to co-regulate their assembly and localization in the axon [104].

1.3.3. Dyneins

Dyneins are divided into two main functional groups in eukaryotes.

1. Axonemal dynein is mostly involved in flagellar motility and intraflagellar transport [243, 244, 245].

2. Cytoplasmic dynein is the main retrograde motor protein in the axons and dendrites, facilitating transport of cargos towards the minus end of microtubules [244].

Cytoplasmic dynein is composed of a heavy chain, multiple intermediate chains, light intermediate chains and light chains. The numerous isoforms of each dynein component have diverged to specifically interact and transport a wide variety of cargos, enabling dynein to be the sole retrograde motor in neurons [246, 247]. Additionally, dynactin, a multisubunit protein, binds directly to dynein and is necessary for its motor activity [248]. In addition to well-documented roles of dynein in axonal distribution of vesicles and organelles, there are studies indicating the role of dynein in neuronal morphogenesis. For instance, in the *dandelion clock* (*dlic*) *Drosophila* mutant, in which the dynein light intermediate chain is mutated, the proximal dendritic branching is increased whereas the branching in the distal regions is significantly decreased [249]. The roles of dynein light intermediate chain 2 (dlic 2) and intermediate chain (dic) were later confirmed in this process, in addition to ensuring the uniform microtubule organization in axons [250].

1.3.3.1. Dynein motor in synapse formation

Although presynaptic components move predominantly in the anterograde direction during neuronal development, association of synaptic proteins with a retrograde motor protein is also crucial for moving between neighboring synaptic boutons. For instance, dynein LC8 light chain 1 (DLC1; DynII1) and DLC2 (DynII2) have been shown to directly interact with Bassoon, thereby suggested to facilitate the transport of PTVs between synapses and contribute to synaptic plasticity [251]. Dynein has also been proposed to contribute to postsynaptic plasticity by forming a transport complex with the scaffolding protein Gephyrin, and glycine receptor (GlyR). Gephyrin acts as a transport adaptor in binding of GlyR to dynein DLC1 and DLC2, and is crucial for internalization of glycine receptors [252, 253].

1.3.4. Diseases associated with genetic ablation of motor proteins

The importance of intracellular transport by kinesins is highlighted by the numerous diseases associated with their mutation or deletion.

1.3.4.1. Kinesin-1

Kif5a mutant mice demonstrate loss of large caliber axons and accumulation of neurofilaments in the neurons. In humans, point mutations in KIF5A causes hereditary spastic paraplegia (HSP), which is a neurodegenerative disease characterized by progressive spastic weakness of the lower extremities [254, 255, 256, 257]. These mutations are located in either the neck or the motor domain, the latter reducing the microtubule affinity and/or gliding velocity [258]. Moreover, mutations in KIF5 gene have been implicated in malformations of cortical development (MCD) and severe intellectual disabilities [259]. KIF5B has been proposed to be involved in transporting many crucial organelles, including mitochondria and lysosomes. *Kif5b* knockout mice are embryonically lethal [260]. While *Kif5c* knockout mice are viable, they show a decreased brain size and loss of neurons in brain motor nuclei [194].

1.3.4.2. Kinesin-3

Given that kinesin-3 motor proteins transport synaptic vesicle precursors [235, 226, 261], it is not surprising that there is a wide range of pathologies associated with mutations in either of these motors. *Kif1a* and *Kif1b* knockout mice are both lethal during the perinatal period, and exhibit severe neurological disorders. On a cellular level, neuronal death is increased and the number of synaptic vesicles in the presynaptic area is reduced [234, 261], the latter also observed in *kif1b* mutant zebrafish [262]. Moreover, a functional mutation in the motor domain of KIF1B has been observed in a family with Charcot-Marie-Tooth disease Type 2A, the most common inherited peripheral neuropathy in humans [261, 263]. Lastly, some studies in humans and zebrafish have indicated a role for KIF1B in myelination through affecting the localization of the *mbp* mRNA in the myelinating oligodendrocyte process [262].

1.3.4.3. Dynein

As the major retrograde motor protein, dynein malfunction severely worsens any process that is hinged on proper retrograde signal transduction. Dynein heavy chain

1 (Dync1h1) knockout mice are embryonically lethal, with dispersion of the Golgi and endosome-lysosome system [264]. Dynein dysfunction has been shown to hinder retrograde transport of axonal injury signals such as phosphorylated MAP kinases Erk1 and Erk2 [265], and the activated c-Jun NH2-terminal kinase (JNK) [266]. It also results in premature aggregation of mutant Huntingtin in addition to increased levels of autophagosome marker LC3-II in cell culture and mouse model of Huntington disease [267]. Dynein has also been suggested as a key influencer in development of brain folds and grooves by interacting with LIS1-NDEL complex as its cargo. The LIS1-NDEL complex is crucial for neuronal migration and correct positioning of the nuclei during development [268].

1.3.5. Regulation of directionality in axonal transport

Given the complex architecture of neurons and their vital roles as the building blocks of the nervous system, proper intracellular transport is crucial. Several studies have demonstrated that anterograde and retrograde motors are bound to the cargos simultaneously [269, 270, 271, 272, 273, 274]. There are several models proposed for regulation of transport directionality. In a tug-of-war model, both motors are bound to the cargo, and the direction of movement is eventually determined by the motor applying greater force. Stochastic detachment of the motors from microtubule tracks would result in transport of the cargo by the dominant motor [275]. In reality, this would result in a bidirectional movement of the cargos, punctuated by frequent directional switches. In fact, there is a considerable body of evidence in favor of this hypothesis, including the axonal motility of late endosomes and lysosomes [270].

Alternatively, in a coordination model cargos are often bound to both motors. However, the activity of motor proteins is tightly regulated via post translational modifications or by scaffold and adaptor proteins. The simultaneous binding of antero- and retrograde motor proteins to the cargo can facilitate rapid directional changes to avoid traffic jams and roadblocks, or as a response to local cellular environmental cues [276, 277]. Moreover, this model can also explain the processive movement of cargos in one direction for long distances, despite their simultaneous association with kinesins and dyneins.

1.3.6. Regulation of motor proteins by adaptor proteins

Scaffolding proteins involved in regulation of the motor activities can be found in a complex with the membrane cargo receptors, components of kinesin and dynein

motor proteins and signaling proteins such as kinases and GTPases. They mediate many protein-protein interactions and integrate regulation with the motor protein activity. For instance, KHC motor activity is regulated at the synapse by binding to the Milton/Miro complex in a Ca^{2+}-dependent manner in *Drosophila* [278, 279, 280]. Huntingtin has been shown to act as a molecular switch in the transport of BDNF vesicles. When phosphorylated at serine-421, it recruits kinesin-1 to the dynactin complex on BDNF vesicles, promoting anterograde transport. In contrast, at its non-phosphorylated state, kinesin-1 detaches from BDNF vesicles and they are more likely to be transported retrogradely [281]. JIP1 has also been shown to interact directly with kinesin-1 and dynactin. The p150$^{\text{Glued}}$ subunit of the dynein/dynactin complex binds to JIP1, inhibiting kinesin-1 activation and promoting the retrograde movement of APP-containing vesicles. However, phosphorylation at serine-421 in JIP1 stabilizes the JIP1-kinesin-1 complex and enhances the anterograde transport [282, 283].

1.3.7. FEZ1 is a kinesin-1 adaptor

FEZ1 and FEZ2 are the mammalian homologs of the UNC-76 protein in invertebrates [284, 285]. UNC-76 was found in an analysis of *C. elegans* mutants exhibiting loco-motive defects. Mutations in *unc-76*, along with *unc-34* and *unc-71* genes, caused the axons to end prematurely within the ventral and dorsal nerve cords and also to exit their normal nerve bundles [286, 287, 288]. Locomotion deficiencies were the most severe in *unc-76* mutants. Further analysis of *unc-76* mutants showed that this protein is normally expressed throughout the VNC, DNC and the nerve ring, and seems to play a crucial role in establishment and maintenance of proper axon-axon contacts in nerve bundles [284].

In an attempt to resolve the means through which kinesin-1 associates with its cargos, it was revealed that UNC-76 interacts with the tail domain of KHC in *Drosophila*. Mutations of the *unc-76* gene in flies resulted in progressive paralysis, in addition to abnormal aggregation of syntaptotagmin containing vesicles in the segmental nerves of larvae, phenotypes that closely resembled *khc* and *klc* null mutants. Given that the UNC-76 immunostaining did not show the same punctate pattern observed in syntaptotagmin distribution, the authors speculated that UNC-76 might act as a cargo adaptor for transport of non-vesicular cargos in the axons [289].

It has been shown that FEZ1 binding to kinesin-1 is necessary for activating its motor activity *in vitro* [202]. Recent research has also revealed that FEZ1 is found in a complex with KIF5C, Munc18 and syntaxin-1a. Consistently, *unc-76 C. elegans*

mutants exhibited an abnormal clustering of UNC-64 (syntaxin homolog) in the VNC, which was rescued by restoring the expression of UNC-76 [207].

Previously, it had been shown that phosphorylation of serine-143 in UNC-76 is necessary for associating with and transporting synaptotagmin [213]. The corresponding residue to serine-143 in FEZ1 is serine-58, which has been suggested to be one of the crucial phosphosites, along with S134, S301 and S316, in binding of FEZ1 to KIF5C [207].

1.4. Aims of this study

Previous data from our laboratory and others have shown that FEZ1 acts as an adaptor for kinesin-1 in a phosphorylation-dependent manner and is necessary for its activation [202, 207]. This is particularly intriguing since it introduces another transport adaptor for syntaxin transport, in addition to the previously described syntabulin [206]. Syntaxin 1a is suggested to be transported on the same trafficking vesicles as many other active zone proteins [89, 201]. Therefore, it is plausible to hypothesize that FEZ1 might also contribute to delivery of AZ proteins to the presynapse. This notion appears more likely when one considers the enrichment of synaptic vesicle and active zone components in FEZ1/kinesin-1 immunoisolated vesicles from the rat brain [290].

However, the role of FEZ1 in transporting presynaptic cargo in mammalian neurons has not yet been addressed. This study was initiated in order to investigate the function of mammalian FEZ1 in synapse formation and to answer the following questions:

1. How does the phosphorylation of serine-58 affect FEZ1 movement and transport activity in neurons?

2. What is the role of mammalian FEZ1 in axonal transport and assembly of the presynaptic components?

3. How does FEZ1-mediated transport influence the postsynaptic specializations?

2. Materials and Methods

2.1. Materials

2.1.1. Chemicals

Table 2.1.1.: List of chemicals used in this study.

Chemical	Manufacturer	Catalog/EC-Index number
Boric acid	Sigma-Aldrich	B1934
Sodium tetraborate	Sigma-Aldrich	S9640
Poly-D-Lysine	Sigma-Aldrich	P6407
L-Cysteine	Sigma-Aldrich	30129
D-Glucose	AppliChem PanReac	A0883
$CaCl_2$	Sigma-Aldrich	C1016
NaOH	Merck	109141
$CaCl_2.2H_2O$	Merck	233-140-8
$Na_2HPO_4.2H_2O$	Merck	231-448-7
KCl	Merck	231-211-8
NaCl	Merck	231-598-3
Sodium butyrate	Sigma-Aldrich	205-857-6
$MgCl_2.6H_2O$	Merck	232-094-6
$NaHCO_3$	Merck	205-633-8
Ethanol	Merck	200-578-6
HEPES	Roth	6763.3

Albumin Fraction V	AppliChem PanReac	A1391
Paraformaldehyde	Sigma-Aldrich	P6148
Agarose low EEO (Agarose Standard)	AppliChem PanReac	A2114
Ponceau S	Sigma-Aldrich	P3504
Acetic acid	Merck	200-580-7
2-mercaptoethanol	Sigma-Aldrich	M6250
Triton X-100	Merck	108603

2.1.2. Enzymes

Enzyme	Company	Catalog Number
DNase I from bovine pancreas	Sigma-Aldrich	D5025
Papain	Worthington	LS003126
Trypsin EDTA	Lonza	BE17-161E
FastDigest Esp3l	Thermo Fisher Scientific	FD0454
T4 DNA Ligase	New England BioLabs	M0202
Q5 High Fidelity DNA polymerase	New England BioLabs	M0491
Taq DNA Polymerase	Thermo Fisher Scientific	EP0401

Table 2.1.2.: List of enzymes used in this study.

2.1.3. Antibodies

Table 2.1.3.: List of antibodies used in this study. WB: western blot, ICC: Immunocytochemistry.

1° Antibody	Species	Dilution	Manufacturer	Catalog No.
GFP	rabbit polyclonal	WB: 1:20000, ICC: 1:2000	Synaptic Systems	132002
Cas9	mouse monoclonal	WB: 1:1000, ICC: 1:200	Merck Millipore	MAC133
Bassoon	mouse monoclonal	ICC: 1:400	Enzo Life Sciences	SAP7F407
Bassoon	rabbit polyclonal	ICC: 1:500	Synaptic Systems	141013
Piccolo	guinea pig polyclonal	ICC: 1:500	Synaptic Systems	142104
Synapsin I	rabbit polyclonal	ICC: 1:500	Synaptic Systems	106103
Actin	mouse monoclonal	WB: 1:2000	Synaptic Systems	251011
FEZ1	rabbit polyclonal	WB: 1:1000, ICC: 1:200	Made in-house	-
MAP2	mouse monoclonal	ICC: 1:1000	Sigma-Aldrich	M4403
PSD95	mouse monoclonal	ICC: 1:200	Sigma-Aldrich	P246
VGLUT-1 (C-terminus)	rabbit polyclonal	ICC: 1:200	Generated by Dr. Shigeo Takamori	-

Name	Host	Dilution	Supplier	Catalog
VGAT	mouse	ICC: 1:200	Synaptic Systems	131011
CypHer5E-conjugated synaptotagmin-1	mouse monoclonal	To medium: 1:120	Synaptic Systems	105311CpH
2° Antibody				
IgG (H+L) - HRP conjugate	goat anti-mouse	WB: 1:2000	BioRad	1706516
IgG (H+L) - HRP conjugate	goat anti-rabbit	WB: 1:2000	BioRad	1706515
IRDye® 680RD IgG (H + L)	goat anti-mouse	WB: 1:20000	LI-COR	925-68070
IRDye® 800CW IgG (H + L)	goat anti-rabbit	WB: 1:20000	LI-COR	925-32211
Cy™5-conjugated IgG (H+L)	goat anti-mouse	ICC: 1:400	Jackson ImmunoResearch	115-175-166
Cy™5-conjugated IgG (H+L)	goat anti-rabbit	ICC: 1:400	Jackson ImmunoResearch	111-175-144
Cy™3-conjugated IgG (H+L)	goat anti-mouse	ICC: 1:400	Jackson ImmunoResearch	115-165-166
Cy™3-conjugated IgG (H+L)	goat anti-rabbit	ICC: 1:400	Jackson ImmunoResearch	111-165-144
Alexa Flour 488-conjugated IgG (H+L)	goat anti-mouse	ICC: 1:400	Jackson ImmunoResearch	115-545-003
Alexa Flour 488-conjugated IgG (H+L)	goat anti-rabbit	ICC: 1:400	Jackson ImmunoResearch	111-545-144

2.1.4. Kits

Kit Name	Company	Catalog Number
ProFection® Mammalian Transfection System	Promega	E1200
NEBuilder® HiFi DNA Assembly	New England BioLabs	E5520
Lipofectamine^{TM} 2000	Invitrogen	11668-019
EndoFree Plasmid Maxi Kit	Qiagen	12362
NucleoBond Xtra Midi	Macherey-Nagel	740410
NucleoSpin Plasmid	Macherey-Nagel	740588
NucleoSpin gel and PCR clean-up	Macherey-Nagel	740609
Western lightning plus-ECL	PerkinElmer	NEL104001EA

Table 2.1.4.: List of kits used in this study.

2.1.5. Reagents and Supplements

Reagent	Company	Catalog Number
L-alanyl-L-glutamine	Merck Millipore	K0302
B-27 supplement	Gibco	17504-044
MEM-Vitamin	Biochrom	K0373
Mito+^{TM} serum extender	Discovery Labware	355006
Filtrated bovine serum	PAN Biotech	P90-8500
Goat serum	PAA Laboratories	B11-035
Penicillin-Streptomycin	Lonza	DE17-602E
cOpmlete^{TM}, EDTA-free protease inhibitor cocktail tablet	Roche diagnostics	05056489001
NuPAGE LDS sample buffer (4X)	Invitrogen	NP0008
Mini-PROTEAN TGX gels (4-20%)	BioRad	456-1096
Trans-Blot Turbo^{TM} 5X transfer buffer	BioRad	10026938
Trans-Blot Turbo^{TM}mini-size transfer stacks	BioRad	1704158
GeneRuler 1 kb DNA ladder	Thermo Scientific	SM0314
Blue/Orange Loading Dye (6X)	Promega	G1881
GelGreen Nucleic Acid Gel Stain (10,000X)	Biotium	41005

Table 2.1.5.: List of supplements and reagents used in this study.

2.1.6. Buffers

Buffer	Composition
PBS	2.7 mM KCl, 1.5 mM KH_2PO_4, 137 mM NaCl, 8 mM Na_2HPO_4
TBST	15 mM Tris-HCl, 150 mM NaCl, 0.05 % Tween 20
TAE	20 mM Tris, 10 mM acetic acid, 1 mM EDTA, pH 8.2-8.4
SDS running buffer	25 mM Tris-HCl, 192 mM glycine, 0.1 % SDS
Lysis buffer	50 mM HEPES, 150 mM NaCl, 1 mM EDTA, 1% Triton X-100, pH 7.2
Protease inhibitor	25X solution: 1 tablet of cOpmlete^{TM}EDTA-free protease inhibitor cocktail tablet dissolved in 2 ml ddH_2O
PFA (fixative solution)	Paraformaldehyde 4% (in PBS)
Ponceau S staining solution	0.5% (w/v) Ponceau S, 1% acetic acid
mGBSS	1.5 mM $CaCl_2$, 4.9 mM KCl, 0.2 mM NaH_2PO_4, 11 mM $MgCl_2$, 0.3 mM $MgSO_4$, 130 mM NaCl, 2.7 mM $NaHCO_3$, 0.8 mM Na_2HPO_4, 22 mM HEPES, 5mM D-glucose
HBSS	Lonza, Cat. No. BE10-547F
Sodium borate buffer	25 mM boric acid, 6.3 mM sodium tetraborate
Enzymatic solution	11.39 mM L-Cysteine, 50 mM NaEDTA, 100 mM $CaCl_2$, 3 mM NaOH, 0.1 g/l DNase I, 0.428 g/l papain (in mGBSS)
Inactivation solution	2.5 g/l BSA, 0.1 g/l DNase I (in serum media)

Table 2.1.6.: List of buffers and solutions used in this study.

2.1.7. Cell culture and Bacterial Media

Media/Solutions	Company	Catalog Number
DMEM F-12 Ham	Sigma-Aldrich	D6421
MEM	Sigma-Aldrich	M2414
DMEM	Lonza	BE12-733F
Opti-MEM	Gibco	11058-021

Table 2.1.7.: List of cell culture media used in this study.

Media	Composition
Neuronal plating medium	500 ml DMEM F-12 Ham, 500 µl L-alanyl-L-glutamine (200 mM), 1 ml B27
Serum medium	25 ml of minimum essential media, 95 mg D-glucose, 250 µl L-alanyl-L-glutamine (200 mM), 125 µl MEM-Vitamin, 50 µl Mito+ serum extender, 1.25 ml FBS
D10 medium	500 ml DMEM, 10 % FBS, 4 mM L-glutamine, 250 units Penicillin-Streptomycin
LB medium	1 l LB medium, 10 g tryptone, 5 g yeast extract, 10 g NaCl
LB agar plates	1 l LB medium, 15 g BactoAgar

Table 2.1.8.: List of self-prepared media used in this study.

2.1.8. Primers

Primer	Application	Sequence (5' → 3')
LentiCRISPR_seq_f	Confirmation of gRNA insertion	GGGTTTATTACAGGGGACAGCAGAGATCCAGTTTGG
CRISPR_f_colPCR	Colony PCR to confirm the correct gRNA insertion in lentiCRISPRv2 (forward)	GGTGGAGAGAGACAGAGACAGATC
CRISPR_r_colPCR	Colony PCR to confirm the correct gRNA insertion in lentiCRISPRv2 (reverse)	GCAGGTCCTCTCTGTTCAGCTTC

Table 2.1.9.: List of primers used in this study.

2.1.9. DNA constructs

Plasmid	Insert	Source
LentiCRISPRv2	Cas9, gRNA	Addgene plasmid #52961(Feng Zhang; [291])
LentiCRISPRv2 GFP	Cas9, gRNA and GFP	Addgene plasmid #82416 (David Feldster; [292])
RFP-Bsn95-3938	RFP-tagged Bassoon (amino acids 95-3938)	Eckart D. Gundelfinger [293]
mCherry-syt-1	mCherry-tagged synaptotagmin-1	Camin Dean [294]
FHUGW-GFP	C-terminally GFP-tagged FEZ1 variants (wt, S58A and S58D)	Oleksandr Yagensky
pCMV-VSV-G	Envelope protein for producing lentiviral particles	Addgene plasmid #8454 (Bob Weinberg; [295])
psPAX2	lentiviral packaging plasmid	Addgene plasmid #12260 (Didier Trono)

Table 2.1.10.: List of plasmids used in this study.

2.1.10. Microscopy Equipment

Microscope	Manufacturer	Objective	Lamp/Lasers	Detector	Details
Axiovert 200M	Zeiss	Plan-Apochromat 63×/1.40 Oil DIC	Xenon-short-arc lamp XBO 75	AxioCam MR3	Filter Set 46 (000000-1196-681):BP 500/20, FT 515, BP 535/30 Filter Set 43 (000000-1114-101): BP 545/25, FT 570, BP 605/70 Filter Set 50 (488050-9901-000): BP 640/30, FT 660, BP 690/50
Eclipse Ti-E	Nikon	Plan-Apochromat 60×/1.40 Oil	HBO-100W lamp	Andor X-8536	-
LSM 780, AxioObserver	Zeiss	LCI Plan-Neofluar 63×/1.3 Imm Korr DIC M27 LCI Plan-Apochromat 40×/1.40 Oil DIC M27	Lasers: Argon, DPSS561, HeNe594, HeNe633	PMT	Pinhole 66 µm
TCS SP8	Leica	HC PL APO CS2 63×/1.40 Oil	Lasers: Argon, DPSS 561, HeNe633	PMT, HyD	Pinhole 57.2 µm

Table 2.1.11.: List of microscope setups used in this study.

Equipment/Material	Details	Manufacturer
Glass coverslips	18 mm Ø No. 1	Glaswarenfabrik Karl Hecht GmbH.
Microscope slides	25 × 75 × 1 mm	Thermo Scientific
Immuno-Mount	Mounting medium	Thermo Scientific

Table 2.1.12.: List of imaging equipment used in this study.

2.1.11. Bacterial strains

Strain	Company	Catalog Number
Library efficiency™ DH5α™ *E. coli*	Invitrogen	18263012
One Shot™ Chemically Competent Stbl3™ *E. coli*	Invitrogen	C737303

Table 2.1.13.: List of bacterial strains used in this study.

2.2. Methods

2.2.1. Cloning Procedures

2.2.1.1. Digestion of the lentiCRISPRv2 plasmid

LentiCRISPRv2 plasmid was digested with FastDigest Esp3l for 30 min at 37 °C in the reaction mixture described in table 2.2.1:

LentiCRISPRv2	5 µg
FastDigest Esp3l	3 µl
10X FastDigest Buffer	6 µl
DTT (100 mM)	0.6 µl
ddH$_2$O	up to 60 µl

Table 2.2.1.: Reaction mixture for digestion of lentiCRISPR plasmid.

Digestion of the LentiCRISPRv2 plasmid by Esp3l produced two fragments: a 2-kb 'filler' sequence immediately upstream of the gRNA scaffold, and the 13-kb fragment,

expressing cas9 endonuclease, which was used for ligation. The digestion products were mixed with the loading dye and separated by agarose gel electrophoresis, for which 1% agarose gel containing was prepared in TAE buffer. The gel was run at 100 V for 1 h in TAE buffer and incubated in 0.3% (v/v) GelGreen solution for 30 min to label the DNA fragment. The stained gel was imaged under blue light (Safe Imager, Invitrogen; figure 2.2.1). The 13-kb fragment was extracted from the gel using the NucleoSpin gel and PCR clean-up kit according to the manufacturer's protocol (Table 2.1.4), and used for the subsequent ligation step. The same procedure was performed for digestion of LentiCRISPRv2GFP plasmid.
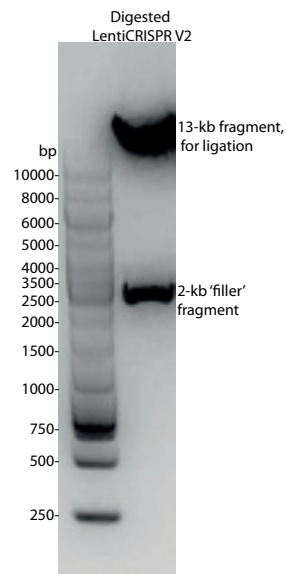
Figure 2.2.1.: Esp3l digestion of LentiCRISPRv2 plasmid excises the 2-kb filler sequence upstream of the gRNA scaffold. Esp3l cuts the lentiCRISPRv2 plasmid at two sites, which results in the excision of a smaller filler sequence, and the 13-kb fragment. The 13-kb DNA fragment, indicated by the upper band, was extracted from the agarose gel and used for ligation to the annealed gRNA oligos.

2.2.1.2. Synthesis and annealing of the gRNA oligos

The online platform provided by Feng Zhang's lab (http://crispr.mit.edu/) was used to design the gRNAs targeting the 2nd exon of the FEZ1 rat gene. According to the protocol by the same lab, the oligos were synthesized with a CACCG at the 5' end of the forward oligo and AAAC at the 5' end of the reverse oligo (Eurofin Genomics, Germany). The addition of the mentioned overhangs was necessary for the insertion of the oligos in Esp3l-digested LentiCRISPRv2 plasmid.

The oligos were mixed according to the reaction mixture described in table 2.2.2,

and annealed by incubating the mixture in thermocycler using the program detailed
in table 2.2.3.

Forward Oligo (100 µM)	1 µl
Reverse Oligo (100 µM)	1 µl
10X T4 ligation buffer	1 µl
ddH$_2$O	7 µl

Table 2.2.2.: Reaction mixture for annealing the gRNAs.

37 °C	30 min
95 °C	5 min, then decreasing to 25 °C at 5 °C/min

Table 2.2.3.: Thermocycler parameters used to anneal the gRNA oligos.

The annealed oligos were diluted at 1:200 ratio with ddH$_2$O.

2.2.1.3. Ligation of the oligos into the lentiviral plasmid

The digested LentiCRISPRv2 plasmid and the diluted, annealed oligos were then
ligated at 25 °C for 1 hour, in the reaction mixture outlined in table 2.2.4.

Esp3l digested plasmid	50 ng
Diluted annealed oligos	1 µl
10X T4 ligase buffer	1 µl
T4 DNA ligase	1 µl
ddH$_2$O	up to total volume of 10 µl

**Table 2.2.4.: Ligation reaction of digested LentiCRISPRv2 and annealed
gRNA oligos.**

2.2.1.4. Transformation of lentiviral plasmids

Stbl3™ chemically competent *E. coli* were briefly thawed on ice. From the ligation reaction, 0.5-1 µl was added to the bacteria and the mixture was incubated for 30 min on ice. The bacteria were then heat-shocked at 42 °C for exactly 45 s, followed by a 2-min incubation on ice. For recovery, 900 µl of the S.O.C. media was added to the bacteria and the cells were then incubated at 37 °C for 1 hour, whilst shaking at 300 rpm. Fifty to 100 µl of the transformed bacteria were plated on LB agar plates supplemented with ampicillin (100 mg/ml).

2.2.1.5. Colony selection

To select the colonies expressing the plasmids with the correct insert, 6-8 colonies were picked from each plate and resuspended in 50 µl ddH$_2$O. The colony PCR reaction mixture was prepared according to table 2.2.5. The colony PCR primers were designed spanning over the 2-kb filler sequence, such that the positive clones yielded a 2102-bp PCR product, and the negative clones resulted either in a 3962-bp PCR product, which was the product of the re-ligated lentiCRISPRv2 plasmid lacking the correct insert, or no product at all (see figure 2.2.2). The resuspended positive colonies were used to inoculate 5 ml LB media supplemented with ampicillin (100 mg/ml) in round bottom tubes, and the cultures were grown overnight at 37 °C while shaking at 150 rpm. The cultures were then centrifuged at 4000g for 10 min. The supernatant was discarded, and the plasmids were extracted from the pellets using the NucleoSpin miniprep kit according to the manufacturer's protocol (See table 2.1.4). The plasmids were verified by sequencing using the 'LentiCRISPR_seq_f' primer (See table 2.1.9).

dNTP (10 mM)	0.5 µl
CRISPR_f_colPCR (10 µM)	0.5 µl
CRISPR_r_colPCR (10 µM)	0.5 µl
DMSO 100%	0.75 µl
25 mM $MgCl_2$	2 µl
Taq DNA polymerase	0.125 µl
Taq $(NH_4)_2SO_4$ buffer	2.5 µl
Resuspended colony (in 50 µl ddH_2O)	3 µl
ddH_2O	up to total volume of 25 µl

Table 2.2.5.: Reaction mixture for colony PCR of lentiCRISPRv2 plasmids to select the positive clones.
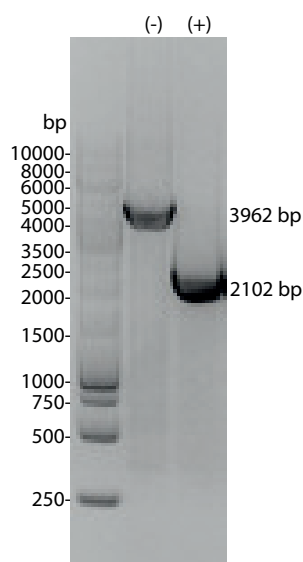
Figure 2.2.2.: Colony PCR product was analyzed by agarose gel electrophoresis. An example of re-ligated lentiCRISPRv2 plasmid, yielding the larger 4-kb PCR product, and the positive colony, resulting in the 2-kb PCR product has been shown.

Liquid cultures were prepared from the positive plasmids by adding 1 ml LB medium to the original culture tubes. The culture was incubated for 3-4 h at 37 °C while shaking at 150 rpm, and then it was used to inoculate 200 ml of LB media. The culture was incubated overnight at 37 °C while shaking at 150 rpm. The plasmids were purified from the culture using the NucleoBond Xtra Midi kit according to the manufacturer's protocol (Table 2.1.4).

The cloning procedure for LentiCRIPRv2GFP plasmid was similar to LentiCRISPRv2. However, since LentiCRIPRv2GFP lacks the 2-kb filler sequence, colony PCR was

not performed to select for the positive colonies. Instead, plasmids were purified from 8 to 10 colonies from each LB plate, and insertion of gRNA was verified by sequencing.

2.2.2. Cell Culture Methods

2.2.2.1. Mammalian cell line maintenance

HEK 293T cells were cultured in D10 medium and maintain in 10 or 15-cm Petri dishes for 3-4 days at 37 °C in 5% CO_2. The cells were passaged when they reached 90% confluency. The cells were initially washed with 8 ml PBS, and incubated with 2 ml Trypsin EDTA for 1 min at room temperature. The trypsin activity was inhibited by adding 8-10 ml of fresh medium. The cells were collected and seeded in new Petri dishes with 10 ml fresh D10 medium. The cells were maintained 37 °C in 5% CO_2. All steps were performed in a sterile condition in a laminal hood.

2.2.2.2. Preparation of hippocampal neuron culture

Prior to preparing the neurons, the coverslips were treated with 1 M HCl overnight, and then by 1 M NaOH for 2 hours. The coverslips were then washed 3 times with 100% ethanol for 10 min, and kept at RT in 100% ethanol. To prepare the culture, the coverslips were briefly flamed and distributed in a 12-well plate. The coverslips were incubated with 600 µl of 0.01 mg/ml Poly-D-lysine solution (in sodium borate buffer) overnight at 37 ºC. Then, the coverslips were washed once with sterile water, air-dried in a sterile condition under the laminal hood, and incubated with 1 ml plating media at 37 °C in 5% CO_2 for 1 hour.

The media and solutions used for neuron culture were freshly prepared (except for the PDL solution), and filtered through 0.2 µm membrane filter (GE healthcare life sciences, USA). The enzymatic and inactivation solutions were incubated in a 15-ml falcon tube with loosely closed lid at 37 °C in 5% CO_2 and the enzymes were added in a subsequent step immediately before adding the hippocampal tissue.

The P0 rat pups were decapitated and the brain was extracted and placed into a 3-cm Petri dish filled with filtered mGBSS solution. The hemispheres were separated and the meninges were removed. Then, the hippocampus was isolated from each hemisphere. The isolated hippocampi were then added to the enzymatic solution and incubated at 37 °C for 30 min, during which the solution was inverted 8-10 times every 10 min. Following the enzymatic dissection, the tissues were allowed to

settle at the bottom of the tube, and the solution was aspirated. The inactivation solution added to the tissues. After a 2-min incubation at RT, the solution was removed, and 1-2 ml of serum media was dispensed in the falcon tube using a fire polished glass Pasteur pipette. The tissue was then triturated in serum media by pipetting up and down. The cell suspension was transferred to a new falcon tube, and centrifuged at 500g for 5 min. Afterwards, the supernatant was discarded, and the cell pellet was resuspended in 3 ml of serum media. To count the cells, 10 µl of the cell suspension was transferred to Neubauer counting chamber. 50,000 neurons were seeded in each well of 12-well plate and maintained at 37 °C in 5% CO_2.

2.2.2.3. Transient transfection of neurons

Neurons were transfected on DIV1-2. The coverslips were transferred to a new 12-well plate containing 750 µl freshly prepared plating media in each well, and incubated at 37 °C for 30 min. The transfection mix was prepared according to table 2.2.6, using the reagents provided in transfection kit from Promega (See table 2.1.4), and incubated at RT for 30 min. 100 µl of the transfection mixture was added drop-wise to each well, and the neurons were incubated with the DNA for 30 min at 37 °C. Afterwards, the neurons were washed briefly with acidified HBSS 4 times (already incubated at 37 °C in 10% CO_2), such that at each washing step, 500 µl of the media was replaced with 500 µl of HBSS to prevent the coverslips from drying. The coverslips were then transferred back to the original plate, and maintained at 37 °C in 5% CO_2. The procedure was entirely performed in sterile condition under a laminal hood.

Endonuclease-free DNA	10 µg
CaCl$_2$	12.6 µl
Endonuclease free water	85 µl
2x HBS	100 µl

Table 2.2.6.: Transfection mixture for mammalian neuron transfection. All reagents were provided in the transfection kit. The amounts shown are sufficient for two wells of a 12-well plate.

2.2.2.4. Lentivirus production

HEK 293T cells were seeded in 15-cm culture dishes (diluted 1:2 from 90-100% confluent 10-cm dishes) and incubated at 37 °C in 5% CO_2 overnight. The cells (now at

40-50 % confluency) were transfected with LentiCRIPSRv2 (or LentiCRISPRv2GFP) plasmid, along with pCMV-VSV-G and psPAX2 plasmids (expressing the envelope and packaging proteins for producing lentiviral particles) at 2:1:1 ratio, respectively. The D10 media was replaced with Opti-MEM supplemented with 10% FBS, and the cells were incubated at 37 °C for 1 h. To transfect one plate, appropriate amounts of the 3 plasmids were diluted in 2 ml Opti-MEM. Lipofectamine 2000 was also diluted in 2 ml Opti-MEM, incubated for 5 min at RT, and added to the plasmid mixture. The transfection reaction mixture is described in table 2.2.7. The transfection mix was subsequently incubated at RT for 1 h, then added drop-wise to the cells. The cells were transferred to the S2-safety level facility, and incubated at 37 °C in 5% CO_2 for 5-6 hours.

Lentiviral plasmid	27 µg	
Envelope plasmid	13.5 µg	diluted in 2 ml Opti-MEM
Packaging plasmid	13.5 µg	
Lipofectamine 2000 reagent	60 µl	diluted in 2 ml Opti-MEM

Table 2.2.7.: Transfection mixture used for lentivirus production in HEK cells. The values are sufficient for one 15-cm dish. The DNA and lipofectamine solutions were prepared separately, then mixed in 1:1 ratio.

The media was then exchanged with DMEM supplemented with 2% FBS and 10 mM sodium butyrate to boost protein production, and the cells were returned to the incubator. After 20-22 h, the viral supernatant was collected, filtered through a 0.4 µm membrane filter (Merck Millipore, USA), and centrifuged at 1000g for 10 min at 4 °C to remove the cell debris. The viral supernatant was collected, and concentrated in Amicon Ultra-15 membrane filters (100 kDa MWCo, Merck Millipore, USA) at 3500g, for 20 min at 4 °C. After discarding the flow-through, the concentrated viral supernatant was collected from the column using a 23 G syringe needle (B. Braun, Germany), and diluted with DMEM F-12 Ham. To keep the virus titration consistent, the concentrated supernatant from each 15-cm dish was diluted up to total volume of 1 ml. The lentivirus was aliquoted and flash-frozen in liquid nitrogen, and kept at -80 °C.

2.2.2.5. Infection of neurons

Neurons were infected on DIV1. Lentiviruses were thawed at RT immediately before infection, and 50-75 µl of virus was added drop-wise to each well of the 12-well culture dishes. The volume of virus used for control and knockdown conditions were similar.

Neurons were maintained at 37 °C in 5% CO_2. Infection and maintenance of neurons were carried out in the S2-safety level facility.

2.2.2.6. Immunocytochemistry of fixed neurons

Neurons were initially washed with PBS, then fixed by incubating with 4% PFA in PBS for 15 min at RT. Afterwards, the neurons were washed 3 times with PBS, and then permeabilized with 0.3% Triton X-100 in PBS for 5 min. The coverslips were then washed 3 times with PBS, and then incubated with blocking buffer (10% NGS in PBS) for 1 h at RT. Primary antibodies were diluted in the appropriate ratio (See table 2.1.3) in blocking buffer, and incubated on the coverslips for 1 h at RT. The coverslips were subsequently washed 3 times with PBS. Fluorescent dye-conjugated secondary antibodies were diluted in blocking buffer in the suitable ratio and applied to the coverslips for 1 h at RT. The coverslips were washed 3 times with PBS, mounted on the microscopy glass slides using mounting medium, and stored at 4 °C for the mounting medium to solidify.

2.2.2.7. Labeling synaptic vesicles for release experiments

On DIV14, 300 µl of the old medium on neurons were transferred to a new 12-well plate. The coverslips were then transferred to the new culture dish, and 2.5 µl of the 1 mg/ml CypHer5E-conjugated syt-1 antibody solution was added to each well. The neurons were then incubated at 37 °C in 5% CO_2 for 45 min to 1 h. The cells were subsequently washed 3 times with Tyrode's solution and transferred back to the original plate. The procedure was performed in a sterile condition under a laminal hood.

2.2.3. Biochemical Methods

2.2.3.1. Sample collection from neuron cultures

The media was replaced by 1 ml of ice-cold sterile PBS, and the neurons were scraped off from the coverslips. The cell suspension was then transferred to 1.5-ml eppendorf tubes, and centrifuged at 13000g for 15 min at 4 °C. The supernatant was discarded and the pellet was resuspended in 7.5 µl lysis buffer supplemented with protease inhibitor solution. Then, 7.5 µl of 2X LDS sample buffer supplemented by 5% ß-mercaptoethanol was added to the the resuspended pellet. Samples were boiled at 95 °C for 5 min and analyzed by SDS-PAGE.

2.2.3.2. SDS-PAGE and Western blotting

To analyze the efficacy of the knockdown, 15 µl of sample (collected typically from two wells of neuron culture) prepared as described in section 2.2.3.1 was loaded on 4-20% Mini-Protean TGX stain-free gels, a pre-cast polyacrylamide gel. Electrophoresis was performed in the running buffer described in table 2.1.6 for 30 min at 200 V. For Western blotting, separated proteins were transferred from the gel to nitrocellulose membrane (BioRad, USA) using the 'Mixed MW (Turbo)' protocol on Trans-Blot Turbo$^{\text{TM}}$ transfer system (BioRad, USA). This pre-programmed protocol is designed to transfer proteins with the molecular weight of 5-150 kDa, and is performed at 1.3 A, up to 25 V for 7 min. Afterwards, the membrane was briefly stained by Ponceau S staining solution to ensure the efficiency of protein transfer. The membrane was then washed with distilled water, and blocked with 5% skim milk powder in TBST for 1 h at RT. The primary antibody was diluted in blocking buffer and incubated with the membrane overnight at 4 °C. The membrane was then washed with TBST 3 times for 10 min, and then incubated with HRP-conjugated secondary antibodies diluted in blocking buffer for 45 min at RT. The membrane was subsequently washed 3 times with TBST for 10 min and then covered with 1:1 mixture of ECL. After a 1-min incubation period, the membrane was visualized by the chemiluminescence detector on LumiImager (Boehringer Ingelheim, Germany). In the event of using fluorescent secondary antibodies, the blots were scanned using the Odyssey® imaging system (LI-COR, USA).

2.2.4. Image Acquisition

Immunocytochemistry on fixed neurons Images from the fixed neurons were acquired using Axiovert 200 epifluorescence microscope or AxioObserver confocal laser scanning microscope (Zeiss, Germany).

Tracking of axonal cargos in living neurons Mobility of RFP-Bassoon and mCherry-syt-1 in neurons were tracked using SP8 confocal microscope (Leica, Germany). The time lapse experiments were carried out for 120 frames, at a rate of 0.5 fps.

FRAP experiments The FRAP experiments were performed on AxioObserver confocal laser scanning microscope (Zeiss, Germany). The FEZ1 wt demonstrated a stronger signal and therefore was imaged at 1% laser power, while the FEZ1 S58A and S58D mutants were visualized using the laser at 5-6 % power. The bleaching was

performed at 100% laser power, for 35 iterations and lasted no longer that 60 seconds for each neuron. For every experiment, 15 frames were acquired before bleaching, followed by 105 frames during the recovery period, at a rate of 0.5 fps.

Synaptic release measurement Neurons were imaged at 37 °C in 5% CO_2 in an OKOLab cage incubator system (OKOLab, Italy) assembled on a Ti-E (Nikon, Japan). The coverslip was covered with Tyrode's solution, and the electrodes were installed on top. The neurons were imaged for a duration of 5 min, acquiring images at the rate of 0.5 fps. The neurons were stimulated at two time-points during the acquisition period: 60 action potentials were applied at 20 Hz after 60 s, to induce the exocytosis of the readily releasable pool. The second stimulation was applied after 90 s of the beginning of the experiment, for which 600 action potentials were applied to the neurons at 20 Hz, to release the entire releasable population of synaptic vesicles. To correct for acquisition bleaching in the analysis procedure, each coverslip was also imaged once for the same duration without the stimulations.

Electron microscopy Neurons grown on ACLAR®–Fluoropolymer film (Science Services, Germany) were fixed on DIV14 by immersion using 2% glutaraldehyde in 0.1 M cacodylate buffer at pH 7.4 overnight at 4°C. After post-fixation in 1% osmium tetroxide and pre-embedding staining with 1% uranyl acetate, tissue samples were dehydrated and embedded in Agar 100. Thin sections (80 nm) were examined using a Philips CM 120 BioTwin transmission electron microscope (Philips Inc, The Netherlands). Images were taken with a TemCam F416 CMOS camera (TVIPS, Germany). Statistics of bound synaptic vesicles were performed using the iTEM software (Olympus Soft Imaging Solutions). The number of bound vesicles were counted and normalized by the length of the presynaptic density. Image acquisition and analysis was kindly done by Dr. Dietmar Riedel (facility for electron microscopy, Max Planck Institute for Biophysical Chemistry, Göttingen, Germany).

2.2.5. Image Analysis

All images were converted to 8-bit TIFF files using Fiji before analysis [296].

2.2.5.1. Quantification of Western blots

The protein bands were quantified relative to the loading control in the same lane. A region of interest was selected around the protein of interest, with the minimum

area covering the entire protein band. The same ROI was used to select the loading control and the background in each lane. The background was selected from an area of the blot without stains or protein bands. A separate background region was selected for the protein of interest and the loading control. Then, the signal intensities were obtained using the measurement function in Fiji. The measured values were then inverted (subtracted from 255). To obtain net values, the inverted value for the protein of interest and the loading controls were subtracted from their corresponding inverted background value. Relative amount of protein was calculated by dividing the net value of protein to the net value of the loading control. The obtained ratio from the negative control (LUC gRNA) was scaled to 100%, and the relative protein in the knockdown samples were calculated accordingly.

2.2.5.2. Puncta density quantification

To analyze the puncta density, a MATLAB script (Mathworks, USA) was kindly provided by Dr. Andrew Woehler (Berlin Institute for Medical Systems Biology, Berlin, Germany), which is generated based on a multiresolution algorithm [297]. The image was loaded in MATLAB. A line was drawn manually along the neurite of interest. To limit the spot detection to the area of interest, a distance threshold was defined from the center of the drawn line. The script created sub-images centered on detected spots. The background for each spot was locally defined as the mean intensity of neighboring pixels with the lowest intensity, and subtracted from the integrated intensity of the detected spot. The number of detected spots were divided by the length of the drawn line in µm to quantify the puncta density. The area of the spots were quantified and provided as a matrix. The script for spot detection has been included in the appendix.

2.2.5.3. Spine density quantification

Quantification of dendritic spines was carried out using a semi-automatic method with Fiji [296, 298]. The images were binarized using the thresholding function, then converted to the skeleton of the neurite with the skeletonize function. The binary function 'close' was applied to the skeletonized image, followed by another round of skeletonization, to remove the overlaying and the short branches. The image was then analyzed by the skeleton analysis function, and the number of skeleton endings were obtained. Adjustments were made accordingly in case of obtaining more than one skeleton from a single neurite due to low signal to noise ratio.

2.2.5.4. Time-lapse imaging

Mobility of Bassoon and syt-1 were tracked using the TrackMate plug-in available through Fiji [299, 296]. To detect the spots, the DoG detector (an approximation of the LoG operator by *d*ifferences of *g*aussian) was used, and the estimated spot diameter was set to 1 µm. After the initial automated detection of the spots by TrackMate, the spots were manually examined, and the quality threshold was adjusted so that falsely detected spots outside of the axon due to low signal to noise ratio were omitted. To track the movement of spots, the 'linear motion LAP tracker' method was selected, and the 'initial search radius' and 'search radius' were both set to 1 µm. The detected tracks were filtered such that only the tracks with at least 5 detected spots were selected. To ensure the accuracy of detected tracks, all were manually examined. Lastly, the detected tracks were sorted based on the direction of movement (anterograde vs. retrograde movements) and filtered according to the number of consecutive frames in which they were detected, total length of displacement and average speed using a MATLAB script (Mathworks, USA). The spots detected in at least 5 consecutive frames, demonstrating a minimum displacement of 0.5 µm and minimum speed of 0.2 µm/s were considered mobile.

2.2.5.5. FRAP experiments

Image analysis of FRAP experiments were carried out using multiple MATLAB function kindly provided by Prof. Dr. Silvio Rizzoli (Department of Neuro- and Sensory Physiology, University Medical Center Göttingen, Göttingen, Germany). To generate FRAP curves, circles with a radius of 20 pixels were drawn along the bleached region until the entire FRAP area was covered. Each of the circles have been referred to as 'segments' in the results. The mean intensity of each circle was quantified and normalized to the average intensity of the same area in the 15 prebleaching frames. The FRAP curves were plotted using the normalized intensity from each segment against time, and these values were subsequently fitted to an exponential curve in MATLAB with the following equation:

$$y = A(1 - e^{-\tau t})$$

A represents the mobile fraction, while τ is the time constant of recovery, indicative of the mobility rate of the protein. The half-maximum was then calculated using the following formula:

$$\tau_{1/2} = \frac{ln0.5}{-\tau}$$

2.2.5.6. Synaptic release

The average intensity of the entire field of view over time was quantified using the Time Series Analyzer V3, a plug-in available through Fiji [296]. Data analysis was performed using a MATLAB script kindly provided by Sven Truckenbrodt (Department of Neuro- and Sensory Physiology, University Medical Center Göttingen, Göttingen, Germany). The values obtained from the bleaching experiments were normalized to the average intensity of the first frame, and subsequently scaled to 100%. The normalized, scaled bleaching curves from each condition were averaged, and used to correct for the acquisition bleaching of the coverslips from the same condition. The same procedure was performed to normalize and scale the experimental data. Subsequently, the experimental values at each time point were divided by the corresponding value in the average bleaching curve. The average curves were then generated in Origin (OriginLab, USA).

2.2.5.7. Sholl analysis

Sholl analysis was performed on images using the Sholl analysis plug-in available through Fiji [300, 296].

2.2.6. Statistical analysis

All statistical analyses in this study were performed using Origin (OriginLab). The bar graphs in this study represent the average from the indicated number of cells, and the error bars represent the standard error of the mean (SEM). All values reported in the results are the mean $\pm$ standard error of the mean (SEM). Statistical significance was determined using the Kruskal-Wallis ANOVA test, and the p-values for significant differences have been indicated in the figure legends. P-values below 0.05 were considered statistically significant.

3. Results

3.1. FEZ1 is mobile in neurons and mobility is regulated by its phosphorylation

Previous reports have indicated that FEZ1 is involved in microtubule plus-end transport by functioning as an activator and adaptor of kinesin-1 [289, 202, 207]. It has also been shown that phosphorylation of serine-58 in FEZ1, one of its four phosphosites, is necessary for binding to kinesin-1 [207, 301, 302], thereby directly influencing its mobility. However, the dynamics of FEZ1 movement itself in neurons has not yet been directly addressed. To confirm that mammalian FEZ1 is similarly involved in axonal transport, I began by analyzing the movement of FEZ1 and its S58 mutants in cultured neurons. The two phosphomutants were generated by replacing serine-58 to alanine (S58A) or aspartate (S58D). There were two main issues to be addressed:

1. How does the mobility of FEZ1 change in correlation to the phosphorylation state of S58?

2. Considering that FEZ1 is an adaptor facilitating the anterograde movement, is there a directional bias in the movement of FEZ1 in axons, and how is it affected by phosphorylation state of S58?

FEZ1, a soluble protein, is widely expressed throughout the neuron. While endogenous FEZ1 demonstrates punctate staining over a strong diffuse background (as shown in figure 3.1.1), overexpression of this protein leads to a completely diffuse localization. Therefore, to track the movement of FEZ1 and its phosphomutants within the axon, fluorescence recovery after photobleaching (FRAP) experiments were performed [303]. Neurons were transiently transfected with C-terminally GFP-tagged FEZ1 variants (wt, S58A and S58D) one day after plating and FRAP experiments were carried out on DIV7. To track the movement with sufficient temporal resolution, a 60-70 µm segment of the axon was bleached. The proximal edge of the bleached area was never farther than 50-60 µm from the cell body. As demonstrated in figure 3.1.2, bleaching was achieved with very high efficiency.
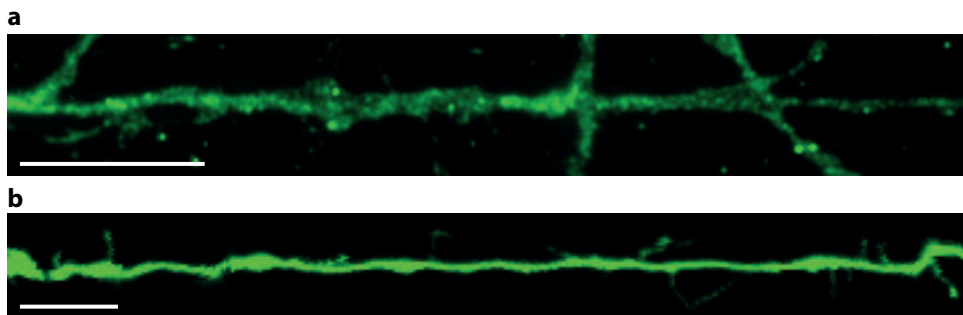
Figure 3.1.1.: Endogenous vs. overexpressed FEZ1 in neurons on DIV7.
(**a**) Endogenous FEZ1 shows a punctate staining overlaying a strong diffuse background. (**b**) Overexpression of FEZ1 shows a completely diffuse localization. Scale bar = 10 µm.

For the analysis, the bleached area was divided into 20-pixel longitudinal segments (yielding either 7 or 8 segments per bleached region). The segments located closest to the cell body are indicated as 'proximal' segments, and the ones located farthest from the cell soma are indicated as 'distal' segments. The segments were numbered, starting from the segment closest to the FRAP edge. To gain a complete overview of FEZ1 dynamics in anterograde and retrograde directions, three neighboring segments at either end of the FRAP region were analyzed (Figure 3.1.3.a). The FRAP curves were normalized against the mean fluorescent intensity of the pre-bleach frames (frames 1-15). The normalized curves were then plotted against time.

In figure 3.1.3.b, c and d, the average recovery curves of the 1st, 2nd and 3rd proximal segments are shown, respectively. The average recovery curves of the 1st, 2nd and 3rd distal segments have been depicted in figure 3.1.3.e, f and g, respectively. In each segment, average recovery of FEZ1 wt reaches the highest extent in comparison to both FEZ1 S58A and FEZ1 S58D.

To better demonstrate this observation, the recovery curves of individual neurons were plotted and fitted to exponential curves. The exponential fit yields the mobile fraction, which is the fraction of the protein that contributes to recovery. In figure 3.1.4.a, b and c, the mobile fraction of each FEZ1 variant has been calculated and compared in the 1st, 2nd and 3rd proximal segments, respectively. The mobile fractions of FEZ1 variants in the 1st, 2nd and 3rd distal segments are shown in figure 3.1.4.d, e and f. As summarized in the table in figure 3.1.4.g, substitution mutations at S58 reduce the mobile fraction significantly in all segments analyzed, implying that both mutant variants lead to an overall decreased mobility. Specifically, FEZ1 S58A demonstrates the least mobility, while FEZ1 S58D exhibits an intermediate
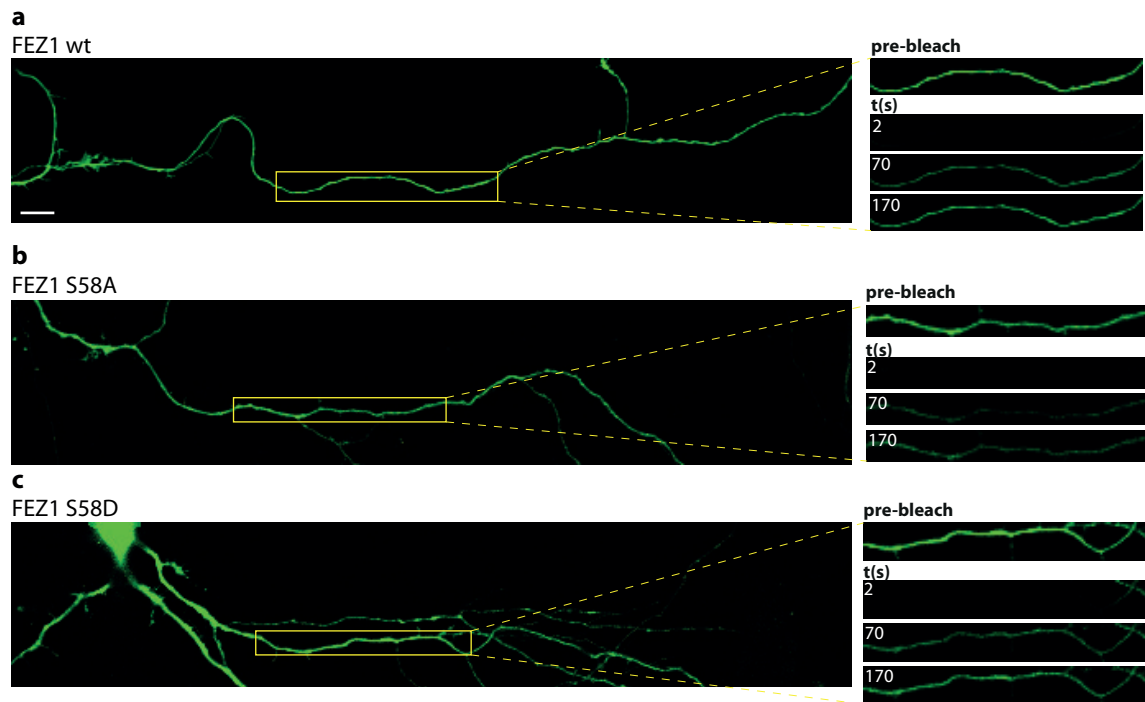
Figure 3.1.2.: Representative images of the FRAP experiments performed on neurons overexpressing FEZ1 wt (a), FEZ1 S58A (b), and FEZ1 S58D (c). The field of view is shown on the left with the bleached region indicated by the yellow box. The bleached region is shown at four time points, indicating (from top to bottom) the region before bleaching, immediately after bleaching and the start of recovery (time = 2 s) and two time points during recovery (time = 70 and 170 s). Scale bar = 10 µm.

behavior. FEZ1 S58A is unable to bind to and activate kinesin-1 [207]. Therefore, diminished mobility of this mutant is not surprising and agrees with previous research where FEZ1 binding to kinesin-1 increased the number of motile events *in vitro* [202]. The fact that FEZ1 S58D, the variant with supposedly the highest association with kinesin-1, shows less mobility than FEZ1 wt is somehow surprising [207, 302]. Overexpression of FEZ1 S58D leads to upregulated binding of this protein to kinesin-1, resulting in a larger population of activated motors. *In vitro* assays have suggested that increasing the concentration of kinesins above a critical value can lead to jamming and reduced velocity [304]. Therefore, hampered mobiliy of FEZ1 S58D might be a result of a crowding effect in the axon.
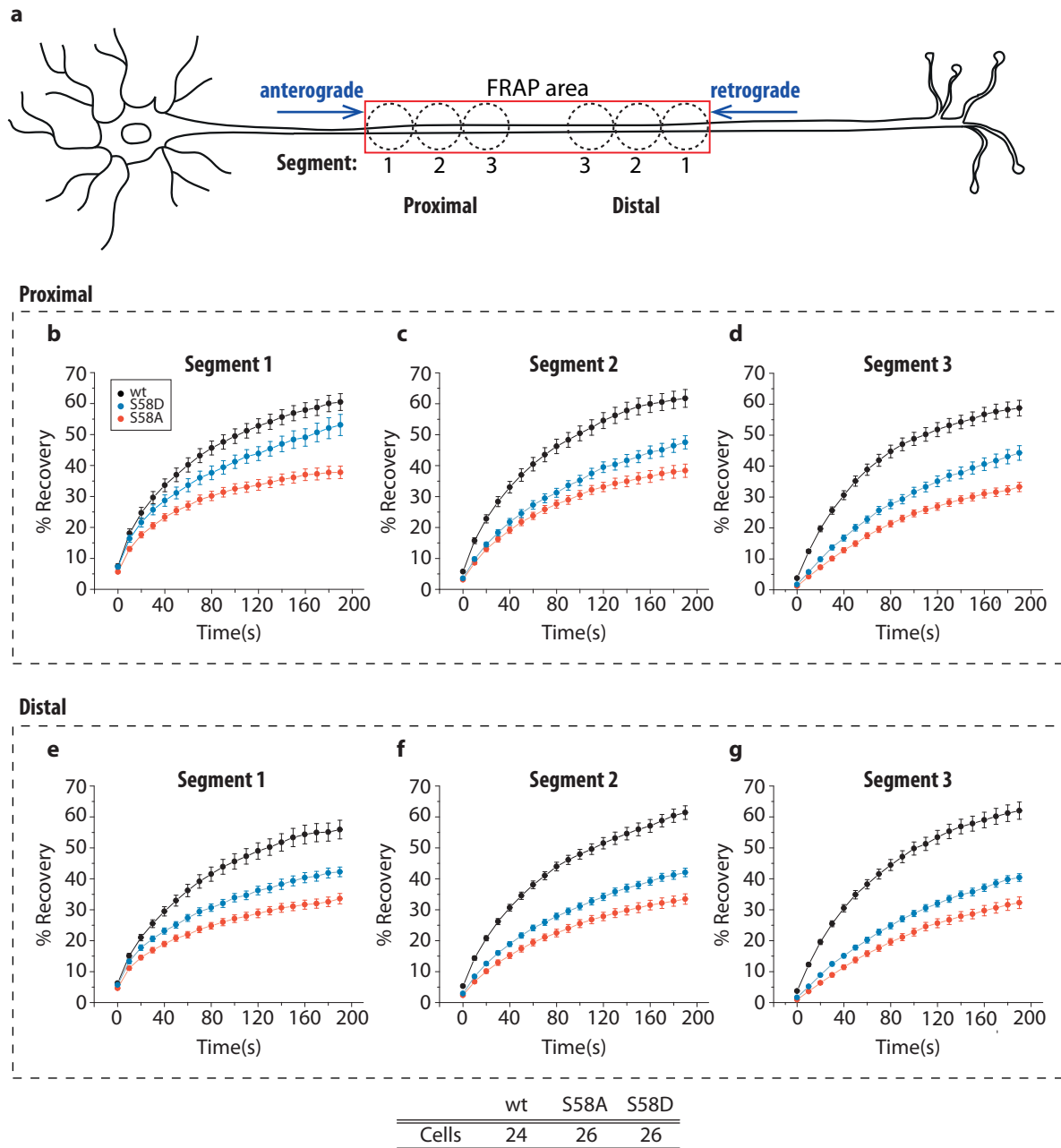
Figure 3.1.3.: FRAP experiments were performed on DIV7 neurons over-expressing GFP-tagged FEZ1 wt, FEZ1 S58A and FEZ1 S58D to investigate the movement of FEZ1 variants. (**a**) The axon segments used for acquisition and analysis are schematically shown. The bleached area was divided into 7 or 8 20-pixel segments for analysis. The segments were numbered in such a way that the 1st segment always refers the one closest to the FRAP edge. The three segments closest to and farthest from the cell soma are referred to as proximal and distal segments, respectively. Signal recovery in the proximal segments would indicate an anterograde movement, whereas recovery in the distal segments is a result of retrograde movement of the protein. (**b-d**) Recovery curves for the proximal segments in the bleached region. (**e-g**) Recovery curves for the distal segments in the bleached region. The number of cells analyzed for each condition are shown on the bottom table.

g		wt	S58A	S58D
Segment 1	Proximal	62.3 ± 2.6	37.7 ± 2.0	49.7 ± 2.4
	Distal	56.9 ± 3.3	32.4 ± 1.6	41.8 ± 1.6
Segment 2	Proximal	63.8 ± 2.9	41.8 ± 2.5	51.1 ± 2.4
	Distal	62.7 ± 2.4	41.1 ± 2.7	47.1 ± 2.3
Segment 3	Proximal	60.5 ± 2.5	44.5 ± 2.8	54.1 ± 3.2
	Distal	64.7 ± 3.0	40.8 ± 2.7	53.2 ± 2.5
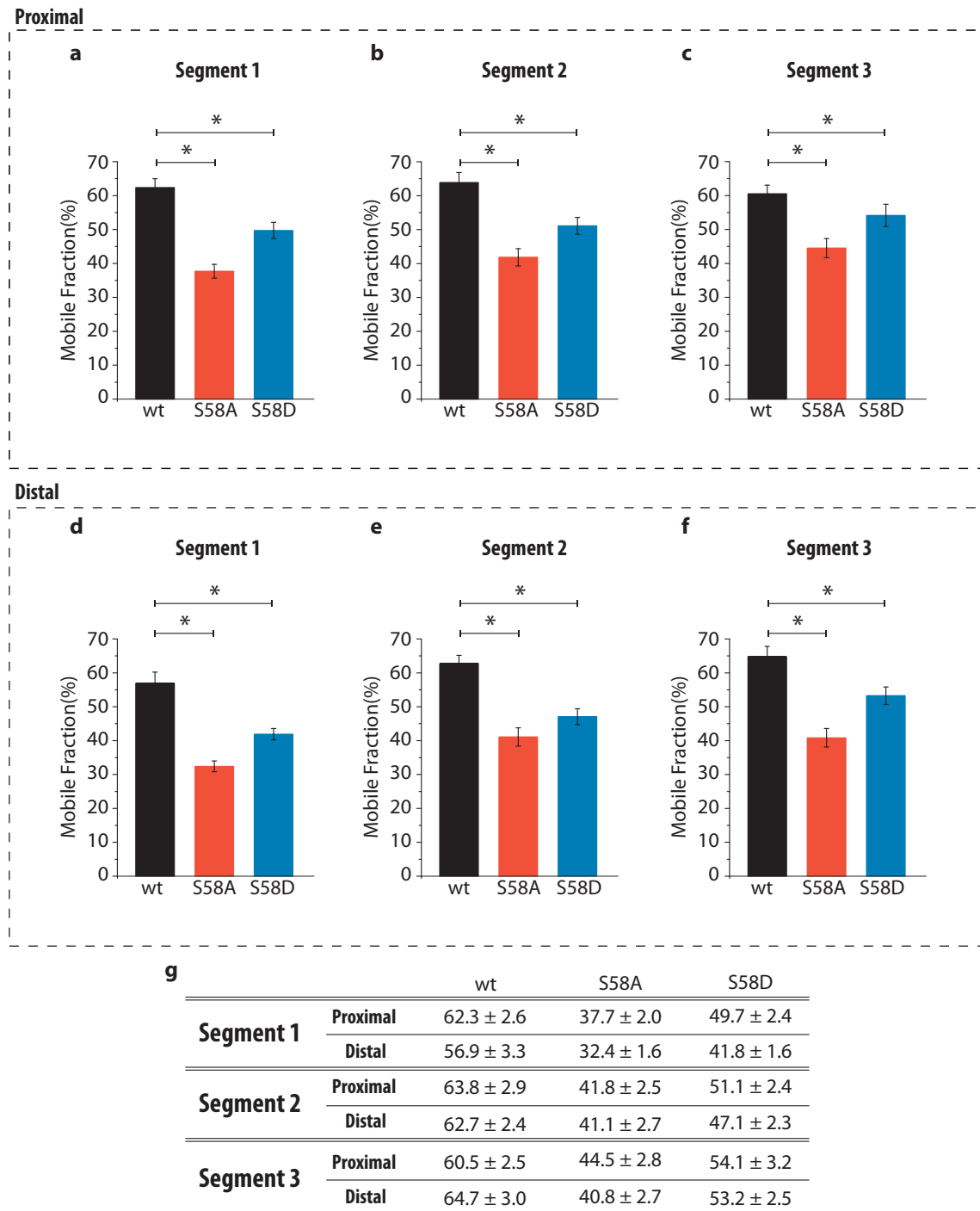
Figure 3.1.4.: Mobile fractions of FEZ1 variants in segments 1- 3 at the proximal (a-c) and distal (d-f) sides. (a) p-value$_{\text{wt vs. S58A}}= 10^{-7}$, p-value$_{\text{wt vs. S58D}}= 10^{-3}$.**(b)** p-value$_{\text{wt vs. S58A}}= 7\times10^{-6}$, p-value$_{\text{wt vs. S58D}}= 2\times10^{-3}$.**(c)** p-value$_{\text{wt vs. S58A}}= 10^{-4}$, p-value$_{\text{wt vs. S58D}}= 0.02$. **(d)** p-value$_{\text{wt vs. S58A}}= 10^{-7}$, p-value$_{\text{wt vs. S58D}}= 3\times10^{-4}$. **(e)** p-value$_{\text{wt vs. S58A}}= 10^{-6}$, p-value$_{\text{wt vs. S58D}}= 2\times10^{-5}$.**(f)** p-value$_{\text{wt vs. S58A}}= 10^{-4}$, p-value$_{\text{wt vs. S58D}}= 0.02$. All p-values were calculated using the Kruskal-Wallis ANOVA test. **(g)** Calculated mobile fractions are summarized.

Next, the speed of movement in FEZ1 variants was investigated. To this end, the time
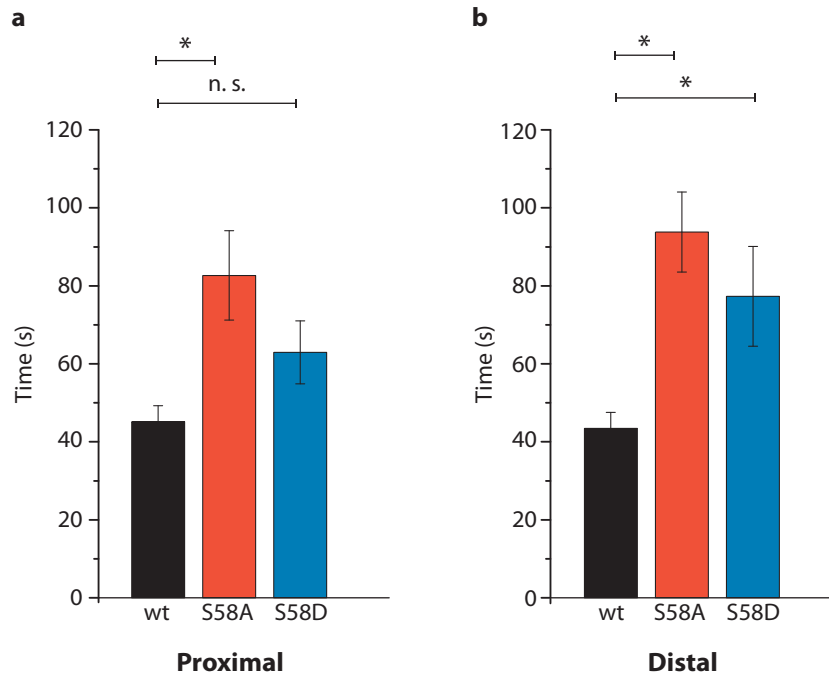
Figure 3.1.5.: The time to reach half of maximum recovery observed in the wild type for FEZ1 mutants in the first segment. (**a**) p-value$_{\text{wt vs. S58A}}$= 0.003. (**b**) p-value$_{\text{wt vs. S58A}}$= 6 ×10^{-6}, p-value$_{\text{wt vs. S58D}}$= 6 ×10^{-4}. P-values were calculated using the Kruskal-Wallis ANOVA test.

it took for FEZ1 mutants to reach half of the maximum recovery observed in normal condition (i.e. in FEZ1 wt) was analyzed in the 1$^{\text{st}}$ proximal and distal segments. Half of maximum recovery at each segment for FEZ wt was estimated by dividing the FEZ1 wt value for mobile fraction by 2 (31.15% in the proximal segment, and 28.45% in the distal segment). The time to reach this value was then calculated and compared for each FEZ1 mutant (Figure 3.1.5). On the proximal side, FEZ1 S58A showed the slowest movement with time of recovery of 82.66 ± 11.45 s while FEZ1 S58D showed an intermediate recovery time of 62.93 ± 8.04 s. The S58A mutant showed a significant deviation from the wt condition though the effect was less severe for S58D. The same trend could be observed on the distal side, where FEZ1 S58A took 93.78 ± 10.27 s to reach half the fluorescence recovery present in the wild type, while this value was 77.30 ± 12.77 s for FEZ1 S58D. These data show that FEZ1 S58A moves at the slowest speed in the axon, while the speed of FEZ1 S58D falls intermediate between wt and S58A. Nevertheless, the differences observed between the rate of recovery of FEZ1 S58A and S58D did not reach statistical significance.

Another purpose of this experiment was to determine if FEZ1 is in fact an adaptor facilitating the anterograde movement, and whether this function is influenced by the phosphorylation state of S58. To this end, the mobile fraction and half life ($\tau_{1/2}$) of

the closest segments to the accessible protein reservoir for recovery (i.e. segment 1 in either proximal or distal region) was calculated and compared for each FEZ1 variant (Figure 3.1.6). The hypothesis was that a significant increase in the rate of recovery (indicated by a shorter $\tau_{1/2}$) or the mobile fraction in the proximal region would hint at directional preference in the anterograde direction, while faster recovery or higher mobility in the distal region would implicate a preferential retrograde movement.

As shown in figure 3.1.6.a, FEZ1 wt did not demonstrate a significant difference in the rate of recovery between the 1st proximal and distal segments (41.7 $\pm$ 3.1 s in the proximal segment vs. 38.9 $\pm$ 1.6 s in the distal segment). Comparing the distal and proximal $\tau_{1/2}$ of FEZ1 S58A and FEZ1 S58D demonstrated the same behavior (29.8 $\pm$ 2.9 s in proximal vs. 32.6 $\pm$ 1.8 s in the distal region for S58A, and 36.4 $\pm$ 2.7 s in proximal vs. 37.4 $\pm$ 2.6 s in distal region for S58D). Similarly, the proximal and distal mobile fraction of FEZ1 wt were not significantly different (62.37 $\pm$ 2.61% in proximal vs. 56.93 $\pm$ 3.30% in distal region), and the same phenomenon was observed in mobility of S58A and S58D mutants (36.85 $\pm$ 1.93% in proximal vs. 32.40 $\pm$ 1.61% s in distal region for S58A, and 47.61 $\pm$ 2.11% in proximal vs. 41.89 $\pm$ 1.68% in distal region for S58D). The observation that FEZ1 wt is equally mobile and recovers at the same speed at either side of the FRAP area implies that this protein is moving similarly in the anterograde and retrograde direction. This phenomenon is also observed for FEZ1 S58A and FEZ1 S58D, which means that the phosphorylation state of serine-58 does not seem to affect the directional preference of FEZ1.

In summary, FEZ1 wt is very dynamic in the neurons, and the phosphorylation state of its serine-58 residue influences its mobility and speed of movement significantly. This phosphorylation however does not appear to affect the directional preference of FEZ1 movement.
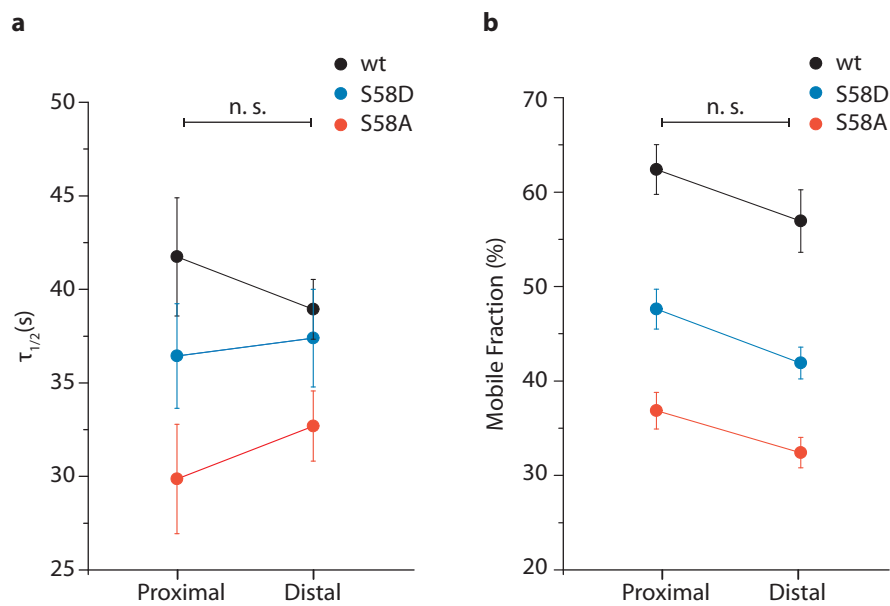
Figure 3.1.6.: Comparison of recovery rate and mobile fraction at the 1st segment of the distal and proximal FRAP area suggests symmetrical movement in either direction for all FEZ1 variants. The average $\tau_{1/2}$ (a) and the mobile fraction (b) of the 1st segment at proximal and distal ends of the bleached area for FEZ1 wt, FEZ1 S58A and FEZ1 S58D have been derived and plotted. The Kruskal-Wallis ANOVA test was performed on the data.

3.2. Acute knockdown of FEZ1 in cultured neurons by CRISPR/cas9

Previous work in our lab had shown that mutation of UNC-76 in *Caenorhabditis elegans* impairs axonal transport, leading to aggregation of syntaxin (UNC-64) in axons. The irregular clustering of syntaxin in the ventral nerve cord of *C. elegans* was rescued by expressing the UNC-76 mammalian ortholog, FEZ1 [207]. Clustering of syntaxin-1a had also been observed upon knockdown of syntabulin, another kinesin-1 transport adaptor in young neurons [206]. Moreover, later studies showed that synaptobrevin puncta appear enlarged or disorganized in *unc-76* mutants of *C. elegans,* implying a defective synapse formation [290]. Taken together, these data suggest a key role for FEZ1 in delivering synaptic components and establishing functional presynaptic terminals. To extend the relevance of these findings to mammalian neurons, I took advantage of the CRISPR/cas9 knockdown system and designed three different guide RNAs (gRNA) targeting the FEZ1 gene in *Rattus norvegicus.* FEZ1 gene is comprised of 10 coding exons, which yields a 1683-nucleotide mRNA, and is eventually translated into a 393-amino-acid protein (Figure 3.2.1). The gRNAs were designed using the online CRISPR design tool provided by Feng Zhang's laboratory (http://crispr.mit.edu/) and targeted the second exon of the FEZ1 gene. Three gRNAs targeting the FEZ1 gene were selected based on the scoring system provided by the design platform, such that the function of their possible off-target genes had the least probability of interfering with any neuronal processes. As negative control, one gRNA was designed to target the luciferase gene (See table 3.2.1). The gRNAs were then cloned into two lentiviral plasmids: One co-expressing cas9 endonuclease and the gRNA, and another with the same backbone with the puromycin selection marker replaced by a GFP tag (LentiCRISPRv2 No. 52961 from addgene, and LentiCRISPRv2GFP, No. 82416 from addgene). The GFP tag helps select for the infected neurons during the imaging experiments. For all experiments in this study, the lentiviral plasmid co-expressing cas9, gRNA and GFP was used, unless noted otherwise.

To evaluate the ability of the gRNAs to eliminate FEZ1 expression, dissociated P0 rat hippocampal neurons were infected with lentiviruses encoding either control or FEZ1 gRNAs one day after plating. Immunoblot analyses of neurons infected with lentiviruses encoding either FEZ1a or FEZ1b (but not FEZ1c) gRNA on DIV7
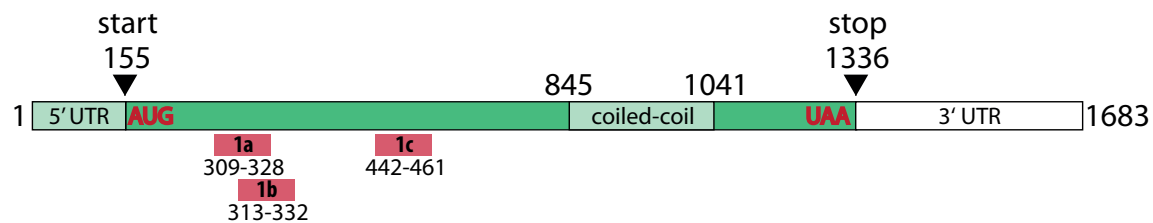
Figure 3.2.1.: Schematic of the rat FEZ1 transcript and the relative position of CRISPR/cas9 gRNAs targeting regions. The FEZ1 gene in rat encodes a 1683-nucleotide transcript, which is subsequently translated into the 393-aa FEZ1 protein. FEZ1 CDS is indicated by the green box (the sequence from position 155 to 1336). The regions targeted by the gRNAs are indicated by the red boxes. The coiled-coil domain of FEZ1 is shown.

gRNA	Forward	Reverse
FEZ1a	GGACTTGAAGCTGATTATTT	AAATAATCAGCTTCAAGTCC
FEZ1b	AATCAGCTTCAAGTCCATGG	CCATGGACTTGAAGCTGATT
FEZ1c	GGAGGAGACTCTTCGGGATG	CATCCCGAAGAGTCTCCTCC
LUC	CCGGGCTTTAACGAATATGA	TCATATTCGTTAAAGCCCGG

Table 3.2.1.: Designed gRNA sequences targeting the FEZ1 gene and luciferase gene as the negative control.

showed a marked reduction in endogenous FEZ1 levels. This was not observed in control neurons infected with a non-targeting gRNA (LUC). In comparison, neurons infected with FEZ1c lentivirus did not display any change in FEZ1 expression over control neurons (Figure 3.2.2). These results demonstrated the effectiveness of the gRNAs FEZ1a and FEZ1b, but not FEZ1c, to ablate FEZ1 expression in neurons.
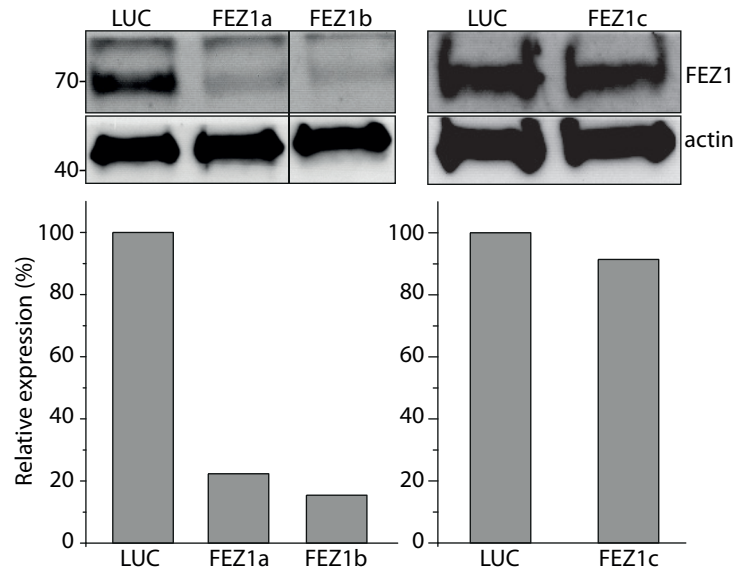
Figure 3.2.2.: Infection of DIV1 hippocampal neurons using FEZ1 specific gRNAs ablates expression of FEZ1. Knockdown efficiency of FEZ1 gRNAs in cultured hippocampal neurons was assessed by Western blotting. Neurons were lysed 6 days after infection, and the expression of FEZ1 was analyzed by SDS-PAGE. Actin was used as the loading control. Samples analyzed on separate gels are quantified and shown separately. Replicates of the experiment are shown in the appendix.

3.3. Investigating the effect of FEZ1 deletion on transport of presynaptic components

Previous studies have shown that *unc-76* mutation in *Drosophila* leads to abnormal aggregation of synaptotagmin-positive vesicles [289]. As mentioned previously, we have also observed that *unc-76* mutants of *C. elegans* exhibit abnormal clustering of syntaxin-1a and synaptobrevin in the axons, suggesting an impaired axonal transport [207, 290]. It is important to note that the clogging phenotypes observed in *unc-76* mutants imply transport deficiency in two primary populations of transport packets, namely STVs and active zone protein containing vesicles. Consistent with this notion, it was also shown that both synaptic vesicle and active zone proteins are associated with FEZ1/kinesin-1 vesicles [290]. Collectively, these data suggest that FEZ1, through linking the kinesin-1 heavy chain to presynaptic cargos, plays an important role in presynaptic development. However, the functional relevance of this phenomenon in mammalian neurons has not been clarified. To this end, the effect of FEZ1 deletion on motility of Bassoon and synaptic vesicles was analyzed in living neurons. Cultured neurons were co-transfected with the lentiviral plasmid co-expressing cas9, FEZ1a gRNA (or LUC gRNA for control) and GFP, along with

either RFP-tagged Bassoon (amino acids 95-3938, Bsn95-3938) or mCherry-tagged synaptotagmin-1 on DIV1. Bassoon and synaptotagmin-1 had both been identified as FEZ1/kinesin-1 associated cargos in the brain [290]. The migration of these two markers was then tracked using confocal microscopy at a time point when the synapses were beginning to form, which is around DIV8 in our cultures. Imaging was performed on a 80-100 µm section of the main axonal shaft, no farther than 60-70 µm from the cell body.

3.3.1. Mobility of Bassoon is reduced upon FEZ1 knockdown

RFP-Bsn95-3938 can be observed as mobile puncta in transfected neurons. This N-terminally truncated Bassoon construct has been extensively characterized and shown to fully represent all the properties of full-length Bassoon, including presynaptic localization and juxtanuclear concentration. The advantage of using this Bassoon variant rather than the full-length protein is that it does not produce diffuse fluorescence caused by tag cleavage in neurons [293, 93]. However, the fluorescence level of overexpressed RFP-Bassoon per cell was low, causing a relatively poor signal to noise ratio (Figure 3.3.1.a, b). This is possibly due to the large size of Bassoon that could have hampered the delivery of the plasmid into neurons and also on its expression once delivered.

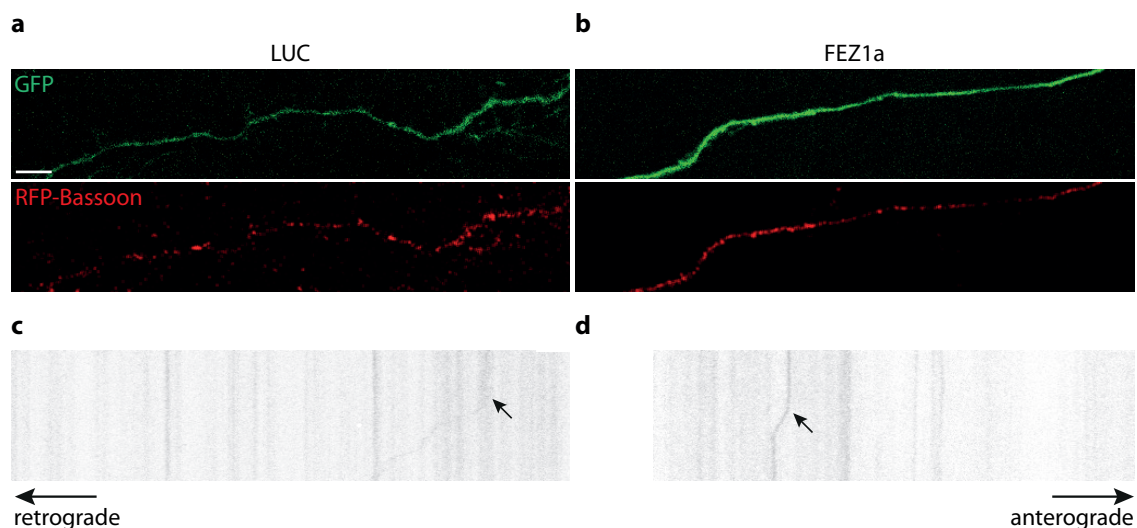**Figure 3.3.1.: Time lapse microscopy of RFP-Bsn95-3938 in control and FEZ1 knockdown neurons on DIV8. (a,b)** Representative images of control (a) and FEZ1a knockdown (b) neurons co-transfected with lentiviral plasmid and RFP-Bassoon. Scale bar = 5 µm. (**c,d**) Kymographs displaying movement of RFP-Bassoon in time. Examples of movement of Bassoon are indicated with arrows.

3.3 Investigating the effect of FEZ1 deletion on transport of presynaptic components

Mobile vesicles containing Bassoon were tracked displaying an average anterograde displacement of 2.58 ± 0.05 µm in control neurons and 2.42 ± 0.05 µm in FEZ1 knockdown neurons. The retrograde displacement of Bassoon puncta varied from an average of 2.50 ± 0.05 µm in control to 2.53 ± 0.05 µm in FEZ1 knockdown neurons (Figure 3.3.2.a). These values are in agreement with the previously reported run lengths of Bassoon in neurons [251]. The comparison of net displacement in either direction between control and knockdown neurons suggested no significant effect of FEZ1 ablation in the distance traversed by Bassoon containing trafficking packets.

The average anterograde speed of Bassoon puncta was 0.275 ± 0.002 µm/s in control, and 0.266 ± 0.002 µm/s in FEZ1 knockdown neurons. The observed speed of retrograde movement was 0.271 ± 0.002 in control and 0.266 ± 0.002 µm/s in knockdown neurons (Figure 3.3.2.b). The observed average speed of RFP-Bassoon is within the same range as observed in previous research (between 0.1 and 0.3 µm/s on DIV8 as reported by [201], and [76]). Similar to displacement measurements, these values imply that the effect of FEZ1 depletion was negligible on the average transport speed of Bassoon puncta in either direction, except for a slight decrease in the anterograde movement of these particles.

Interestingly, when the total number of mobile particles was quantified in each condition, it was observed that the mobile pool of Bassoon puncta was diminished in FEZ1 knockdown neurons (Figure 3.3.2.c). The percentage of mobile Bassoon puncta decreased significantly from $58.64 \pm 2.95\%$ in control to $43.99 \pm 3.68\%$ in FEZ1 deletion neurons. *In vitro* motility assays have shown that addition of FEZ1 to kinesin-1 is accompanied by the activation of the motor and a significant increase in the number of motile events [202]. This finding is in agreement with the marked reduction of mobile Bassoon puncta upon FEZ1 knockdown. This phenotype points to a smaller population of available FEZ1 to bind to and activate kinesin-1, which in turn leads to a lower number of Bassoon containing vesicles being transported. Considering that the acute knockdown of FEZ1 does not diminish its presence entirely, the remaining pool of the protein remains available to associate with kinesin-1 and mediate the transport of Bassoon to the length and at a speed similar to the wild type condition. Furthermore, the unchanged run length and speed of Bassoon movement can be partially explained by the presence of syntabulin, which is also known to transport Bassoon [206, 201]. Overall, these data suggest that FEZ1 plays an important role in the axonal transport of Bassoon, and possibly the cohort of other active zone proteins found within the same trafficking packet, to the presynaptic terminals.
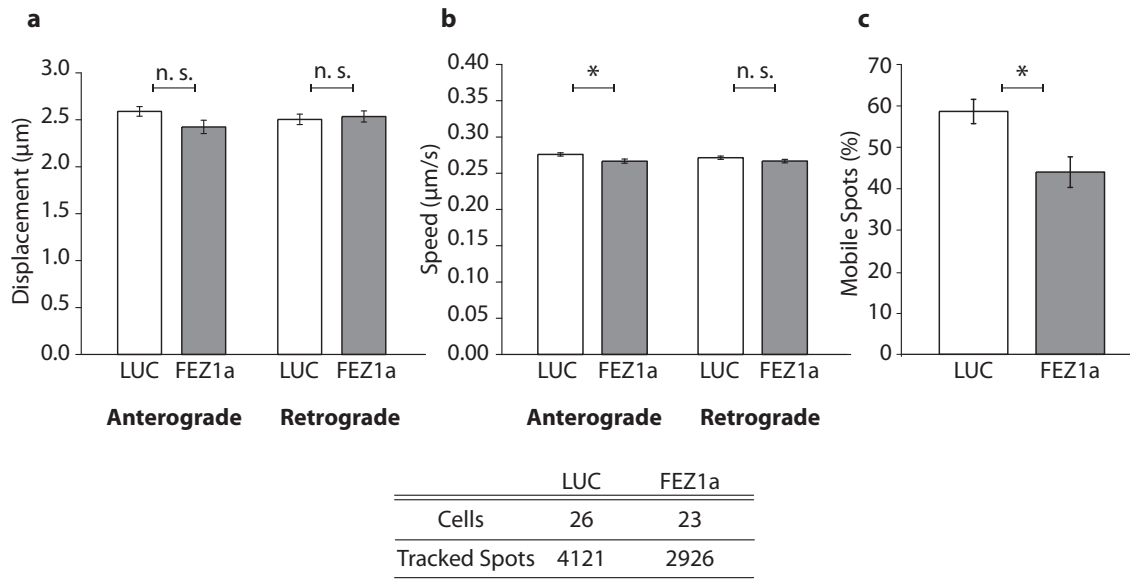
Figure 3.3.2.: FEZ1 knockdown does not affect the distance and speed of individual Bassoon puncta in the axons, but it reduces the mobile Bassoon population. (**a**) Displacement of Bassoon in the proximal axon does not change significantly upon FEZ1 deletion. (**b**) Speed of Bassoon movement in proximal axon does not change significantly in FEZ1 knockdown neurons. p-value$_{\text{LUC vs. FEZ1a KD(ant)}}$= 0.01. (**c**) The percentage of mobile Bassoon puncta in total number of tracked spots. p-value = 0.003. The number of cells and tracked puncta are indicated on the table. Error bars = SEM. P-values are derived from Kruskal-Wallis ANOVA test. The results are from 4 independent experiments.

3.3.2. Transport of synaptic vesicle precursors are also affected in FEZ1 knockdown

Our previous data also indicated the presence of subpopulations of SV proteins in FEZ1/kinesin-1 transport vesicles [290]. To determine if FEZ1 could indeed play a role in transporting these proteins (which has been conventionally attributed to kinesin-3 [224, 226, 261, 227]), the effect of FEZ1 depletion on delivering synaptic vesicle precursors was investigated by co-transfecting DIV1 neurons with mCherry-tagged synaptotagmin-1, as a marker for synaptic vesicles, and lentiviral plasmid co-expressing cas9, GFP, and gRNAs targeting either LUC or FEZ1 gene. The neurons were then imaged on DIV8. The co-transfection efficiency and the signal to noise ratio of both plasmids were sufficiently high (Figure 3.3.3).

While the average anterograde displacement of synaptotagmin remains unchanged upon FEZ1 knockdown (4.07 ± 0.38 µm in control vs. 4.98 ± 1.07 µm in FEZ1 knockdown), the vesicles appear to travel longer distances in the retrograde direction in the knockdown compared to the control neurons (5.1 ± 0.34 µm in control vs. 7.16
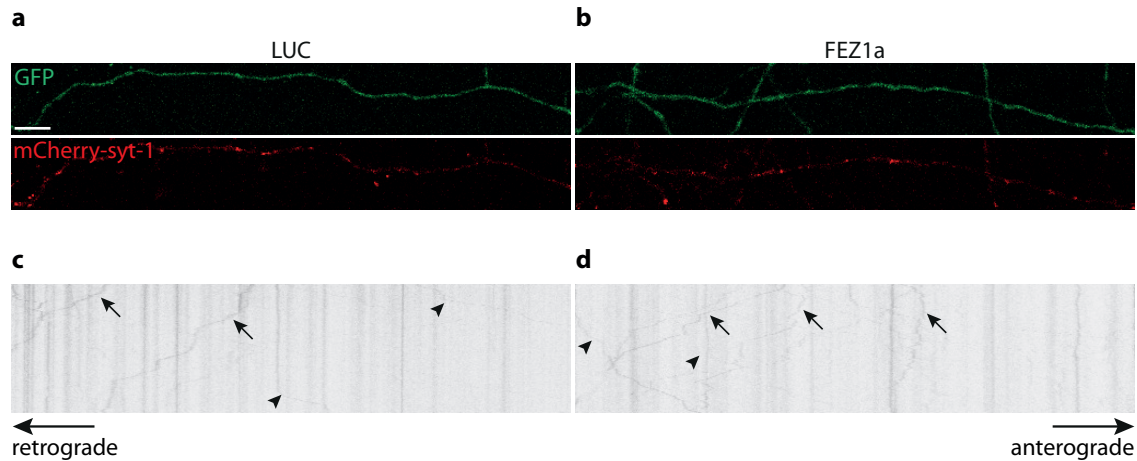
Figure 3.3.3.: Time lapse microscopy of mCherry-synaptotagmin-1 in control and FEZ1 knockdown neurons on DIV8. (**a,b**) Representative images of control (a) and FEZ1a knockdown (b) neurons co-transfected with lentivirus plasmid and mCherry-syt-1. Scale bar = 5 µm. (**c,d**) Kymographs displaying movement of mCherry-syt1 in time. Examples of retrograde and anterograde movements of synaptotagmin-1 are indicated with arrows and arrowheads, respectively.

± 0.73 µm in FEZ1 knockdown, figure 3.3.4.a). Overall, these values are comparable to the observed run lengths of STVs in mammalian neurons in previous research [103, 240]. Syt1-containing vesicles move at an anterograde speed of 0.286 ± 0.010 µm/s in the FEZ1 knockdown, which is not a significant deviation from their speed of 0.279 ± 0.006 µm/s in the control condition. However, in the retrograde direction, synaptic vesicles travel at a speed of 0.301 ± 0.007 µm/s in the FEZ1 knockdown, which is significantly faster than that of control cells (0.276 ± 0.004 µm/s, figure 3.3.4.b). While the range of STV speed observed in this study is within the same range as reported in mammalian neurons [103, 240], it is slower compared to studies on isolated vesicles *in vitro* [223] and on synaptic markers in *C. elegans* [305, 306]. This discrepancy might be due to the different model systems used. When the percentage of mobile syt-1 vesicles was quantified, no significant change was observed caused by FEZ1 deletion (18.47 ± 2.09% in control vs. 17.77 ± 2.17% in knockdown neurons, figure 3.3.4.c).

Our results indicate that FEZ1 scarcity in neurons leads to an exaggerated retrograde STV motility with regards to both speed and distance. So far, there has been no report on a direct interaction between FEZ1 and kinesin-3, although components of synaptic vesicles, including syt-1, have been identified in the kinesin-1/FEZ-1 transport vesicles [290]. The observed phenotype might be due to the transport of at least a fraction of STVs by FEZ1/kinesin-1 vesicles. Alternatively, FEZ1 might also interact directly with kinesin-3 in a yet unknown mechanism. Furthermore, most

axonal cargos are bound simultaneously to anterograde and retrograde motors [270, 269, 271, 307]. Lack of sufficient FEZ1 as a promoter of anterograde movement, might indirectly lead to higher processivity of dynein-mediated transport by diminishing its opposing force. Therefore, this phenotype might further emphasize the role FEZ1 plays as a kinesin adaptor.

	LUC	FEZ1a
Cells	27	22
Tracked Spots	2664	1720
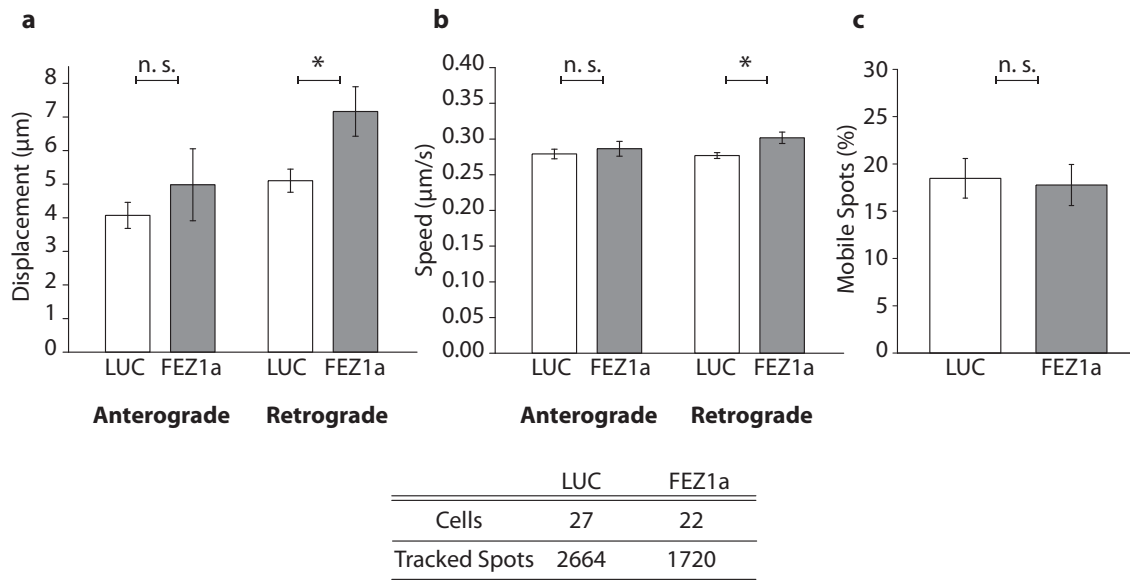
Figure 3.3.4.: FEZ1 knockdown promotes the speed and length of syt-1 retrograde transport, while it has no effect on the ratio of the motile STV population. (**a**) Retrograde displacement of syt-1 in the proximal axon is increased following FEZ1 knockdown. p-value$_{\text{LUC vs. FEZ1a KD (ret.)}}$ = 0.01. (**b**) Speed of syt-1 movement in proximal axon is increased slightly but significantly in the retrograde direction. p-value$_{\text{LUC vs.FEZ1a KD (ret.)}}$ = 5×10^{-4}. (**c**) The percentage of mobile syt-1 vesicles remains unchanged in FEZ1 knockdown. The results are from 3 independent experiments.

3.4. Effect of ablation of FEZ1 expression on synapses

The importance of FEZ1 in axonal transport in living neurons has been established. To further characterize the phenotypes caused by FEZ1 knockdown, the distribution of synaptic vesicle and active zone markers was analyzed using immunocytochemistry in control and FEZ1 knockdown neurons.

3.4.1. FEZ1 knockdown leads to reduction of presynaptic sites

First, the localization of synapsin I was analyzed. Synapsins are one of the most abundant phosphoproteins present at most synapses in the vertebrate CNS [308, 309, 310, 311]. These soluble proteins have been found to co-purify with synaptic vesicles, and at 8.3 copies per vesicle are among the most abundant SV-associated proteins [57, 58]. Microscopy studies have demonstrated that synapsin I highly colocalizes with mobile VAMP2 and synaptophysin vesicles, suggesting their co-transportation during presynapse assembly [96, 312]. Synapsin I has also been suggested to keep STVs at their pausing sites along the axons during initial stages of synaptogenesis [95], which is consistent with its documented role in tethering SVs to the actin cytoskeleton at the synaptic boutons [309, 313, 314]. Taken together, these studies presented synapsin I as a suitable marker for investigating the effect of FEZ1 knockdown on the formation of presynaptic specializations.

To ablate the FEZ1 expression, cultured P0 hippocampal neurons were transduced with lentiviruses expressing either the LUC or FEZ1a gRNA with GFP on DIV1. The neurons were then fixed and immunostained on DIV7. The density of synapsin I puncta along axons was assessed by automatically detecting and counting the number of puncta and dividing this number by the neurite length. As can be appreciated from figure 3.4.1.a, FEZ1 ablation leads to partial loss of synapsin I puncta and dispersion of its signal. Quantification results of puncta density in control neurons revealed the synapsin I density to be 0.73 ± 0.03 per µm, while it was decreased to 0.57 ± 0.04 per µm when FEZ1 expression was suppressed (Figure 3.4.1.b). The reduced density of synapsin I puncta highlights abnormalities in the formation of the presynapse.
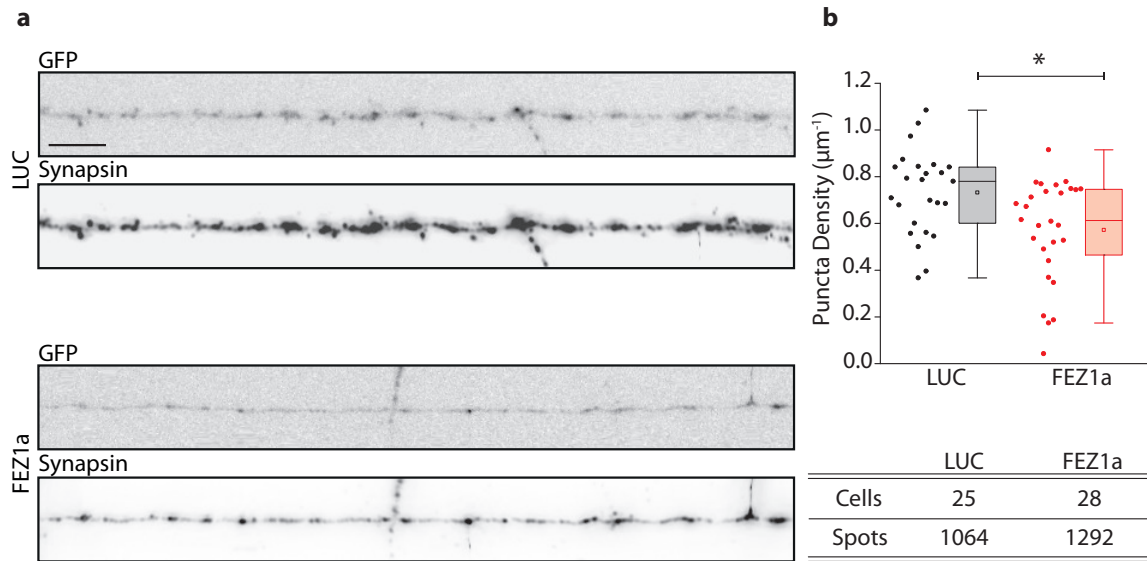
Figure 3.4.1.: Density of synapsin I puncta is reduced in FEZ1 knockdown. (a) Representative images of synapsin I immunostaining on DIV7. Scale bar = 5 µm. (**b**) Quantification of synapsin I puncta density (number of puncta/µm). The number of analyzed cells and puncta in each condition is indicated. p-value (derived from Kruskal-Wallis ANOVA test) = 0.006. The results are from 3 independent experiments.

It is generally accepted that the presynaptic components are transported from the cell soma into axons in two biochemically and morphologically distinct populations of transport packets [96, 315, 99, 95, 90, 316]. The assembly of presynaptic terminals requires the presence of both species of transport vesicles at the same site [94]. Indeed, there are a number of studies suggesting a correlation between the transport of STVs and PTVs. Microscopy of living neurons have shown that STVs and PTVs tend to pause at the same sites within the axons [103], and immunolabeling of electron micrographs have indicated that numerous SV markers, such as VAMP and SV2, are found in the proximity of vesicular structures containing Piccolo and Bassoon [90]. Furthermore, we had previously observed that syntaxin 1 transport is heavily impacted in *unc-76* mutants of *C. elegans* [207], and syntaxin 1 has been shown to co-migrate with the transport vesicles containing Bassoon and Piccolo [89, 76, 201]. Therefore, following the observed decrease in synapsin I density, to gain more insight into FEZ1 roles in presynapse formation, densities of Bassoon and Piccolo puncta were quantified.

To knock down FEZ1 expression, DIV1 neurons were transduced with lentiviruses expressing either cas9, FEZ1a gRNA with GFP, or cas9 and FEZ1b gRNA (without GFP). Control and FEZ1 knockdown neurons were fixed and immunostained on DIV7 (Figure 3.4.2.a, b). As shown in figure 3.4.2.c, density of Bassoon puncta was

significantly decreased from 0.81 ± 0.04 per µm in control to 0.59 ± 0.03 per µm in the knockdown when FEZ1a gRNA was used, and 0.51 ± 0.03 per µm when FEZ1b gRNA was used.

Staining for Piccolo also showed a significant decrease in puncta density in FEZ1a knockdown, from 0.89 ± 0.03 per µm in control to 0.61 ± 0.04 per µm in knockdown neurons (Figure 3.4.3.b). The aberrant clustering and significant decrease in puncta density of Bassoon and Piccolo upon deletion of FEZ1 points to a defect in active zone formation. Moreover, the puncta not only seemed to aggregate abnormally, but they also appeared slightly enlarged (specially observed in Bassoon staining). To confirm this, the area size of Bassoon and Piccolo puncta were also quantified. The area size of the Bassoon puncta was indeed increased significantly in FEZ1 knockdown, while this increase was less severe in the case of Piccolo (Figure 3.4.4). The increased size of Bassoon puncta can be explained by the hampered mobility and clustering of Bassoon containing vesicles within the axon, which leads to enlarged puncta. This is also in line with previous research pointing to the role of UNC-76 in normal presynaptic organization [317].

a

GFP

LUC

Bassoon

GFP

FEZ1a

Bassoon

b

Control

FEZ1b

c

	LUC	FEZ1a	FEZ1b
Cells	42	27	30
Spots	1795	1152	834
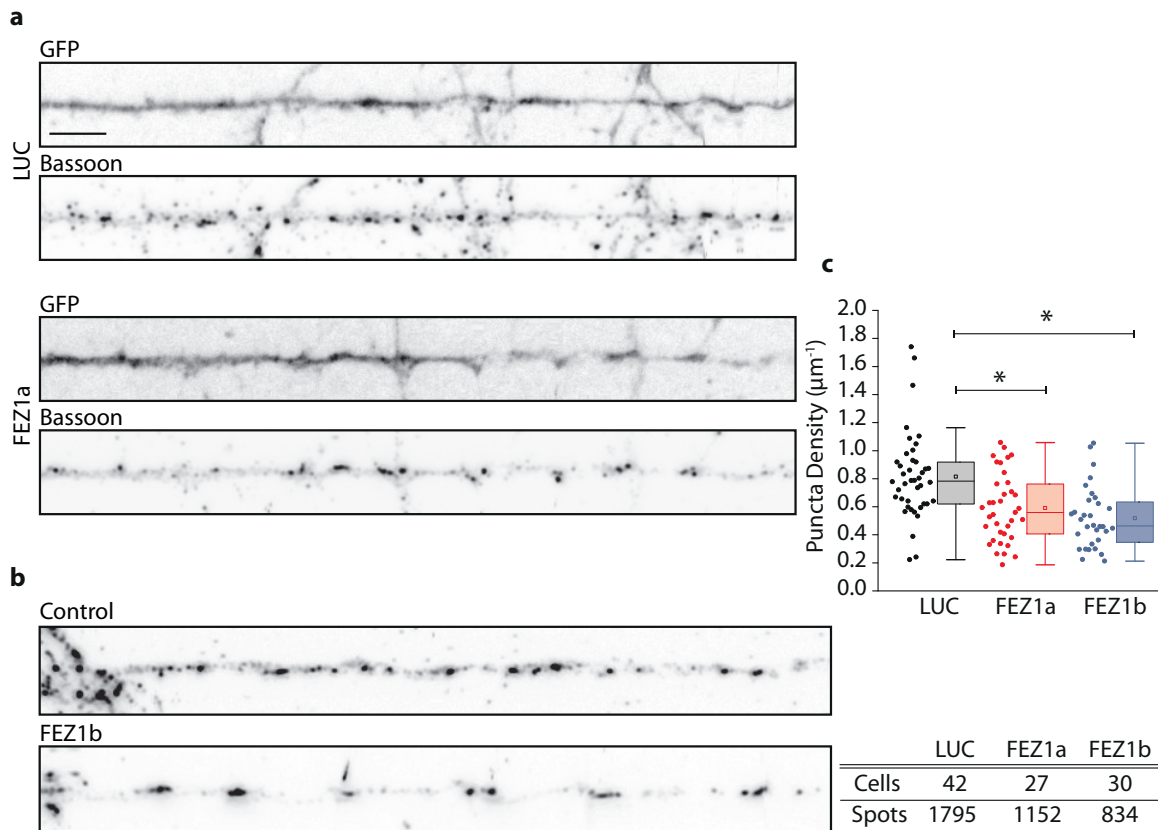
Figure 3.4.2.: Density of Bassoon puncta is reduced in FEZ1 knockdown.
(**a**) Control and FEZ1a knockdown neurons were immunostained for Bassoon. The FEZ1a gRNA was expressed by the lentiviral plasmid along with GFP. Scale bar = 5 µm. (**b**) Control and FEZ1b knockdown neurons were immunostained for Bassoon. The lentiviral plasmid expressing the FEZ1b gRNA did not have the GFP tag. Neurons were co-stained with cas9 antibody to select for the infected cells (not shown). Scale bar = 5 µm. (**c**) Comparison of Bassoon puncta indicated a significant reduction in density in FEZ1 knockdown. p-value$_{\text{LUC vs. FEZ1a}}$ = 7 $\times 10^{-4}$, p-value$_{\text{LUC vs. FEZ1b}}$ = 7.3 $\times 10^{-6}$. The number of cells and puncta in the analysis are indicated in the table below. The results are from 3 independent experiments for FEZ1a, and 2 independent experiments for FEZ1b. All p-values are derived from the Kruskal-Wallis ANOVA test.
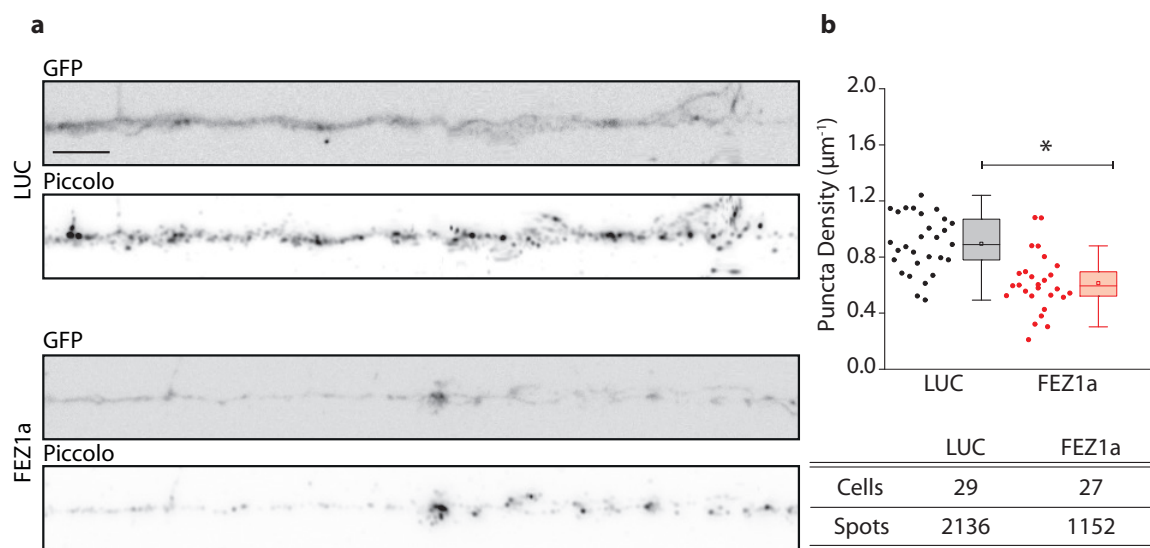
Figure 3.4.3.: Density of Piccolo puncta is reduced in FEZ1 knockdown.
(**a**) Control and FEZ1a knockdown neurons were immunostained for Piccolo.
Scale bar = 5 µm. (**b**) Density of Piccolo puncta was quantified. p-value =
4×10^{-6}(derived from the Kruskal-Wallis ANOVA statistical test). The number of
cells and puncta in the analysis are indicated in the table below. The results are
from 3 independent experiments.
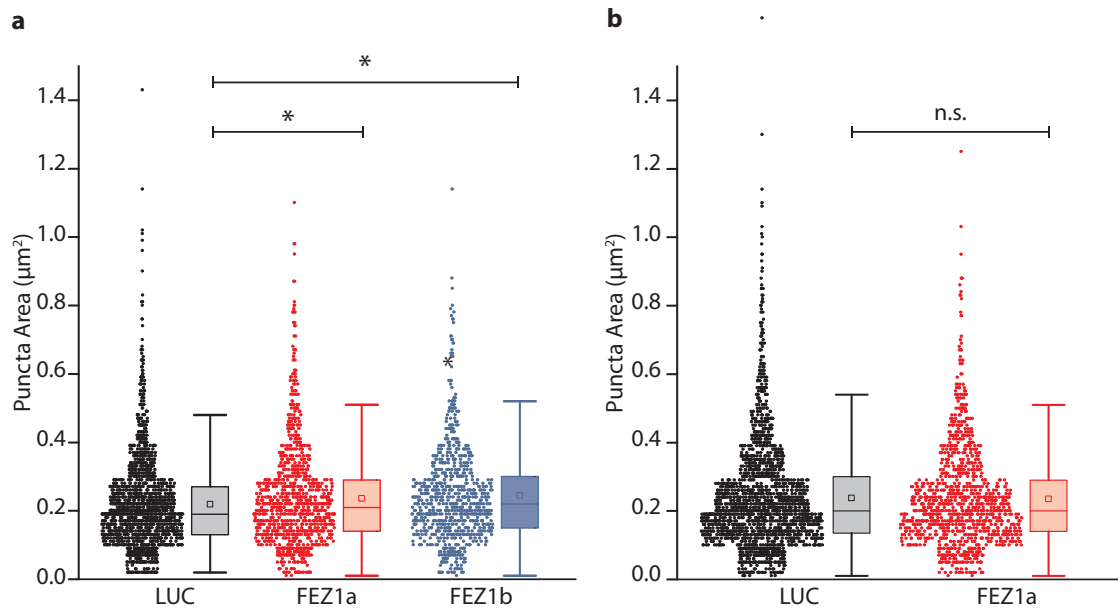
Figure 3.4.4.: Puncta area of Bassoon is increased in FEZ1 knockdown, while this increase is less significant in Piccolo staining. (**a**) Area size of Bassoon puncta in control and FEZ1 knockdown neurons were measured. p-value$_{\text{LUC vs. FEZa}}$ = 0.005 , p-value$_{\text{LUC vs. FEZ1b}}$ = 4×10^{-7}. All p-values are derived from the Kruskal-Wallis ANOVA statistical test. The results are from 3 independent experiments for FEZ1a, and 2 independent experiments for FEZ1b. (**b**) Area size of Piccolo puncta in control and FEZ1 knockdown neurons was measured, and did not show a significant shift. The results are from 3 independent experiments. The number of analyzed cells and puncta are the same as Bassoon and Piccolo puncta density quantifications.

To determine if the defects observed in the early synaptogenesis might persist as neurons further develop, the puncta density of Bassoon was also quantified on DIV14-15. Morphologically, the Bassoon puncta density did not appear starkly different between control and knockdown on DIV14-15 (Figure 3.4.5.a), which was also confirmed by measured puncta density of 1.88 ± 0.1 per µm in control vs. 1.96 ± 0.11 per µm in FEZ1 knockdown neurons (Figure 3.4.5.b). Considering that the difference between these values was not statistically significant, the effect of early impairment in axonal transport and reduced puncta density of Bassoon appears to be alleviated at a later stage during development in neurons that survive.

In order to determine if the effect of FEZ1 ablation acts preferentially on subtypes of presynapses, the densities of excitatory and inhibitory presynaptic sites, two major types of synapses in hippocampal neurons were quantified. Excitatory presynapses were labeled using vesicular glutamate transporter-1 (VGLUT-1), while inhibitory presynapses were marked using gamma-aminobutyric acid (GABA) transporter (VGAT) antibodies. Interestingly, it was observed that FEZ1 knockdown has
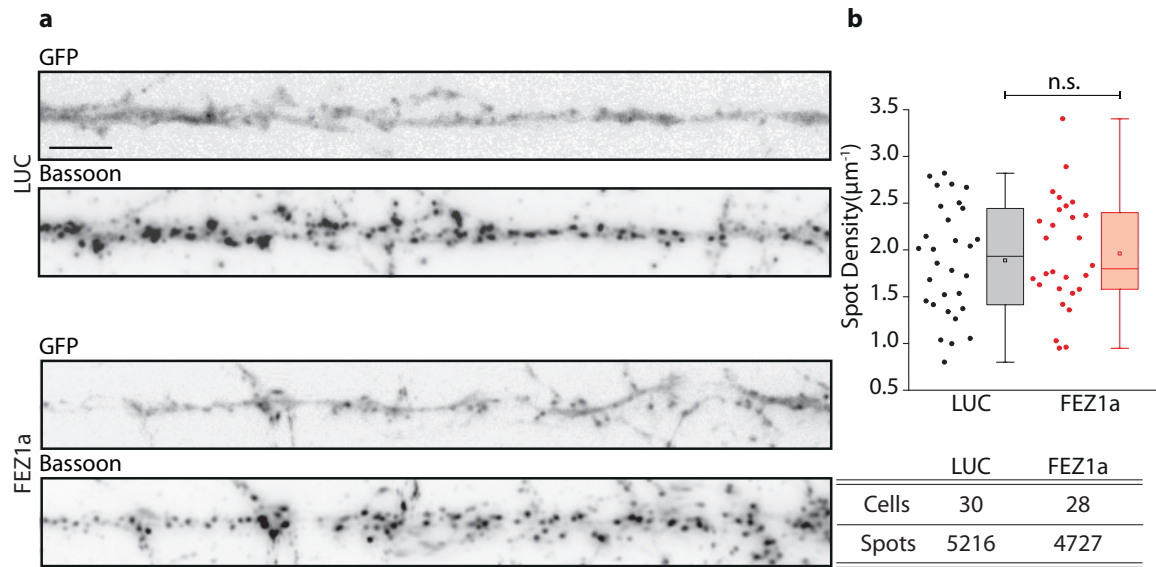
Figure 3.4.5.: Density of Bassoon puncta on DIV14-15 in FEZ1 knock-down remained the same in comparison to control neurons. (a) Representative images of Bassoon immunostaining are shown from control and FEZ1 knockdown neurons. Scale bar = 5µm. **(b)** Quantification of puncta density of Bassoon on DIV14-15. Clustering of the Bassoon puncta was alleviated as neurons matured. Results are from 3 independent experiments, and the number of cells quantified is indicated on the table below.

a more severe effect on VGAT rather than VGLUT-1 distribution (Figure 3.4.6). While the density of VGLUT-1 puncta did not change dramatically from control (1.49 ± 0.07 per µm) to knockdown neurons (1.42 ± 0.07 per µm), VGAT puncta density exhibited a slight but significant reduction from control (1.11 ± 0.04 per µm) to knockdown (0.97 ± 0.05 per µm) condition. The marked reduction of VGAT staining upon deletion of FEZ1 suggests that FEZ1 might be, directly or through transport of active zone components, more involved in trafficking of components of inhibitory synapses.
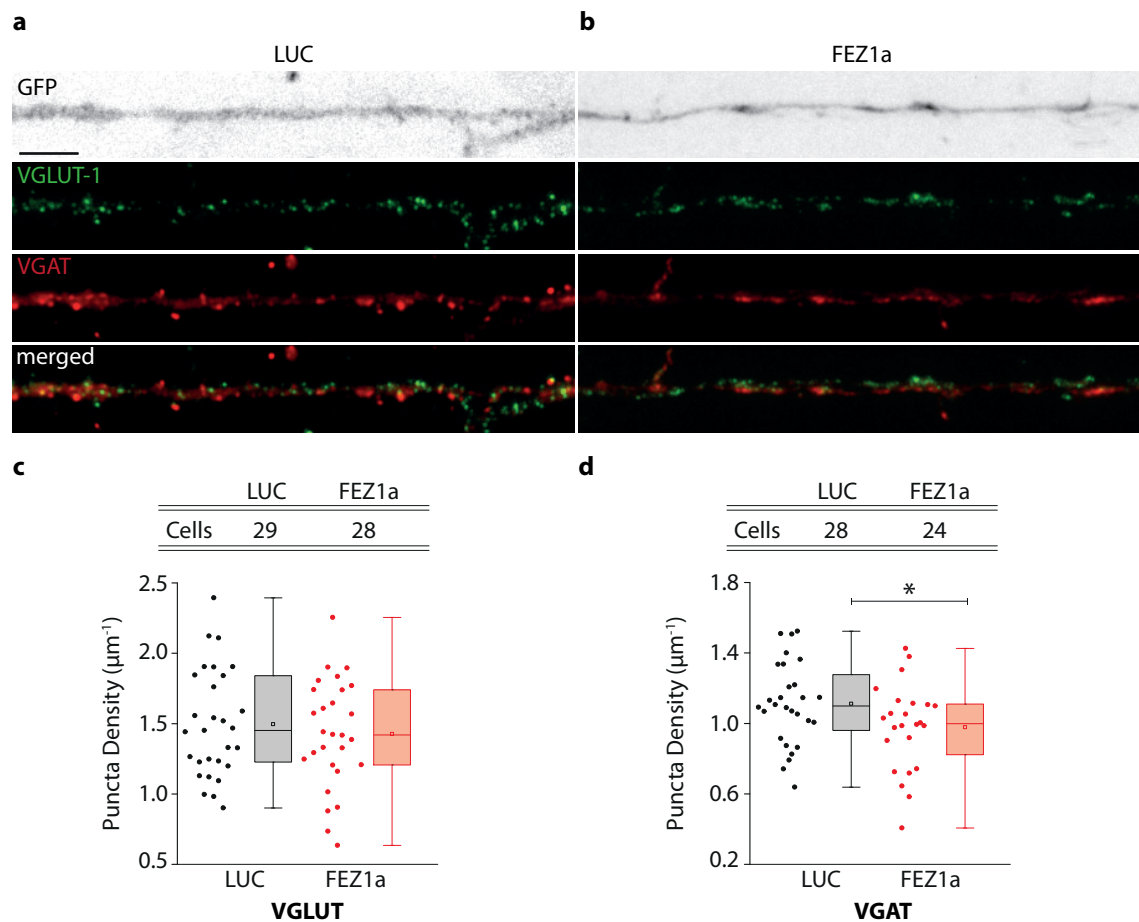
Figure 3.4.6.: FEZ1 knockdown leads to a more severe reduction in puncta density of inhibitory rather than excitatory synaptic vesicles. (a,b) Infected control (a) and FEZ1 knockdown (b) neurons were distinguished by GFP expression by the lentivirus, and stained for VGLUT-1 and VGAT. Merging of the VGLUT-1 and VGAT channels demonstrates little to no colocalization between the two transporters. **(c,d)** Quantification of VGLUT-1 puncta density shows no significant difference between the control and knockdown neurons, while FEZ1 knockdown causes a slight but significant drop in density of the VGAT puncta. The results are from 3 independent experiments. p-value (Kruskal-Wallis ANOVA) = 0.04. Scale bar = 5 µm.

3.5. Effect of FEZ1 ablation on the ultrastructure of presynaptic terminals

Although FEZ1 knockdown impaired the distribution of active zone and synaptic vesicles in young neurons, analysis of the puncta density of Bassoon on DIV14 suggested that this phenotype is less severe as neurons mature. However, immunofluorescence staining of neurons cannot address the morphological deficiencies in individual synapses. Therefore, the ultrastructure of the presynaptic terminals on DIV14 was analyzed using electron microscopy. As before, cultured P0 hippocampal neurons were transduced with lentiviruses targeting either the FEZ1 gene, or the LUC gene as the control. Neurons were fixed on DIV14, and electron microscopy images were acquired from the synapses (kindly done by Dr. Dietmar Riedel, facility for electron microscopy, Max Planck institute for biophysical chemistry).

FEZ1 knockdown neurons demonstrated a slight but significant reduction of the number of docked synaptic vesicles at the active zone (Figure 3.5.1). This observation might be a result of the impaired formation of the active zone as a result of diminished transport of AZ components. It has been shown that the simultaneous deletion of Bassoon and Piccolo in mice leads to a severe reduction in the number of synaptic vesicles in the 150-nm proximity of the active zone and the number of docked vesicles per synapse [54]. Moreover, ultrastructural and functional studies have shown that deletion of Bassoon reduces the number of membrane-proximal vesicles and impairs vesicle replenishment [49, 48, 51]. These data emphasize the importance of Bassoon presence for clustering and docking of SVs. While the overall localization of Bassoon appears normal in FEZ1 knockdown neurons on DIV14, it is possible that the quantity of this protein at individual synapses is reduced due to deficient axonal transport. Therefore, the recruitment of synaptic vesicles to the synapse might be negatively affected by FEZ1 ablation. Nevertheless, these results have to be confirmed by replicates.
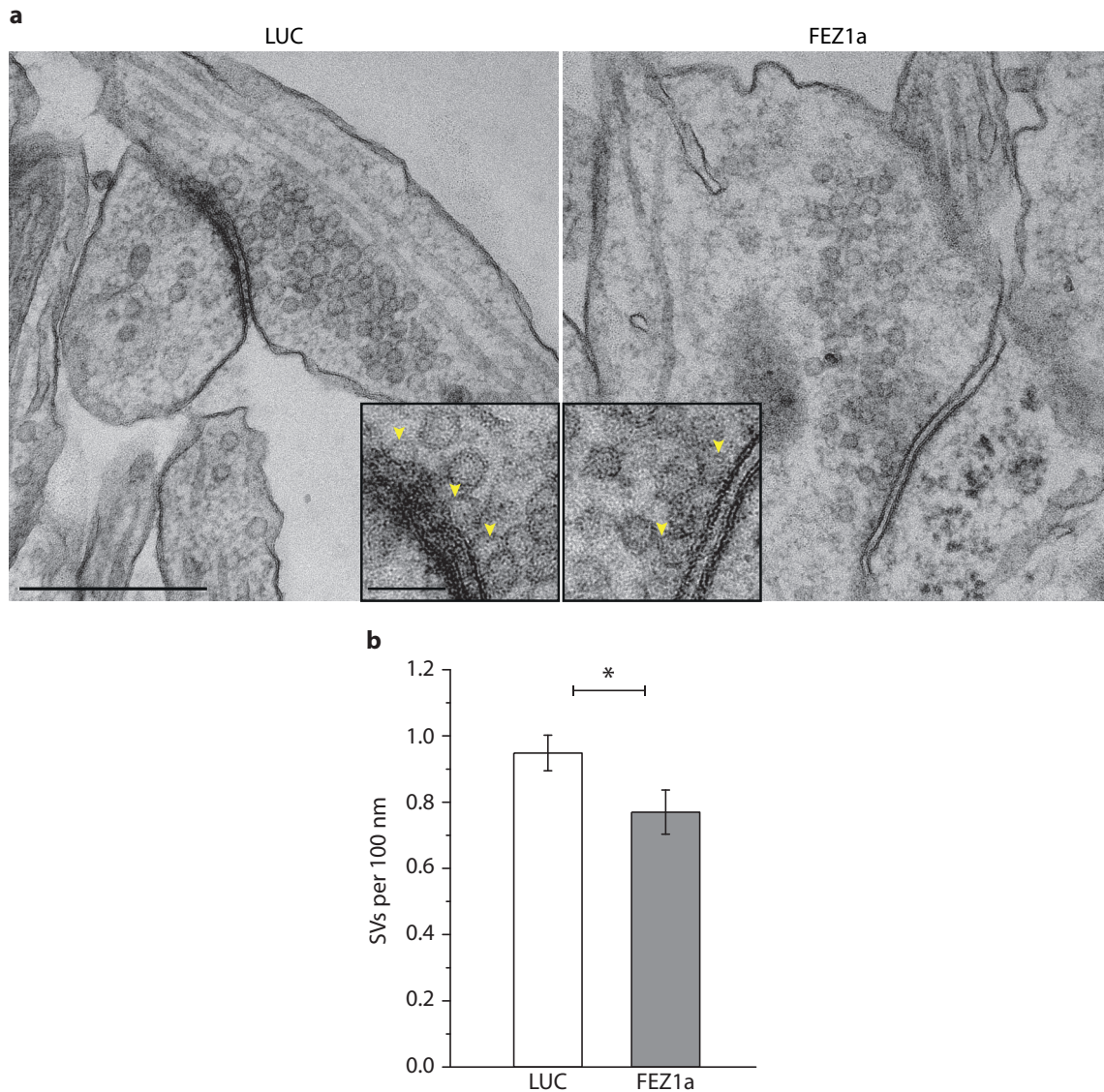
Figure 3.5.1.: Analysis of the electron microscopy images of FEZ1 knockdown neurons shows a significant decrease in the number of docked synaptic vesicles. (**a**) Representative images of synapses in control and FEZ1 knockdown neurons on DIV14 are shown. Examples of docked vesicles are indicated by arrowheads in the inset. Scale bar (entire image) = 500 nm, scale bar (inset) = 100 nm. (**b**) The number of docked vesicles per 100 nm are shown. p-value (Kruskal-Wallis ANOVA) = 0.04. Results are from one experiment. Imaging and analysis was kindly done by Dr. Dietmar Riedel.

3.6. Effect of FEZ1 ablation on the postsynaptic specializations

In order for a synapse to fully mature, after axo-dendritic contact, the presynaptic and postsynaptic elements have to come together at the opposing sides of the synapse. There have been numerous studies showing a correlation between the positioning of pre- and postsynapse in developing neurons at sites of synaptogenesis [318, 319, 320, 321]. In cultured neurons, it has indeed been observed that the axonal accumulation of synaptic vesicles precedes formation of PSD95 clusters in the postsynaptic neurons [322]. Moreover, it has also been demonstrated that neuroligin-1-containing PSD clusters can in fact recruit synaptic vesicles on the presynaptic side, which leads to formation of synapses capable of release [115]. These data suggest that irregular presynapse formation might lead to aberrant postsynaptic localization.

So far, the experiments have shown that FEZ1 knockdown causes defects in presynaptic specializations. To investigate whether the presynaptic impact of FEZ1 knockdown also influences the postsynaptic densities, the density of PSD95 puncta, and the colocalization of Bassoon and PSD95 were assessed in cultured neurons on DIV14-15. This time point was selected to give the synapses sufficient time to fully mature. As shown in figure 3.6.1, there was no significant difference in the distribution of PSD95 between control and FEZ1 knockdown neurons (2.95 $\pm$ 0.16 per µm in control vs. 3.01 $\pm$ 0.18 per µm in FEZ1 knockdown neurons). Moreover, Pearson's coefficient indicating the colocalization of Bassoon and PSD95 did not change significantly from 0.54 $\pm$ 0.02 in control to 0.56 $\pm$ 0.03 in FEZ1 knockdown (Figure 3.6.2). These data collectively suggest that FEZ1 knockdown does not affect the apposition of pre- and postsynaptic sites.

a   **b**

GFP

LUC PSD95

GFP

FEZ1a PSD95
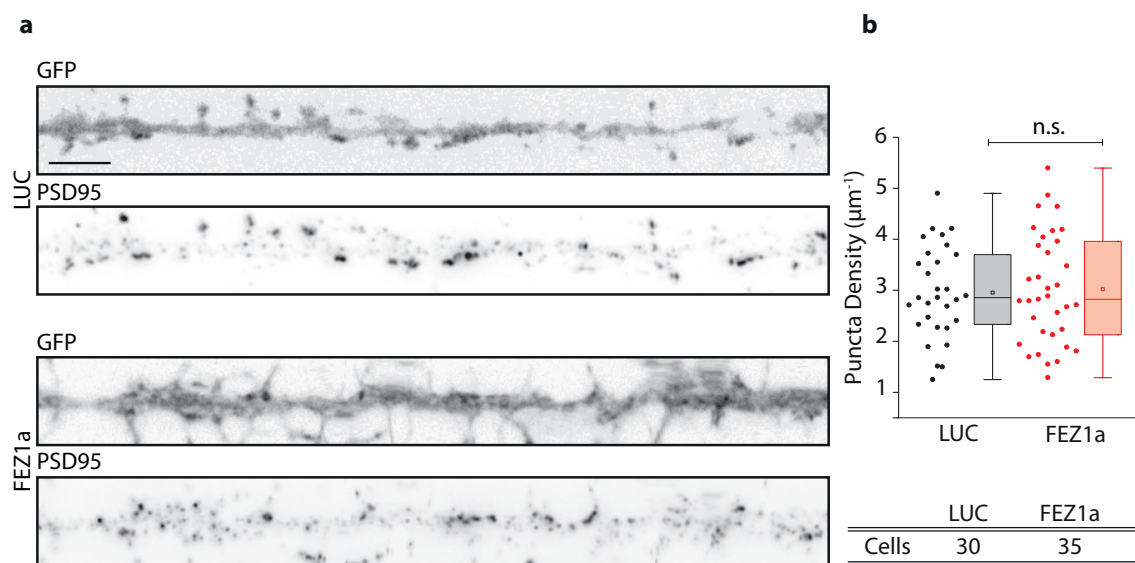
Figure 3.6.1.: Ablation of FEZ1 expression did not affect the density of PSD95 puncta on DIV14-15. (**a**) Representative images of PSD95 staining are shown in control and FEZ1 knockdown neurons on DIV14-15. Scale bar = 5μm. (**b**) Quantification of PSD95 puncta density in dendrites. The number of cells quantified are indicated. Results are from 3 independent experiments.
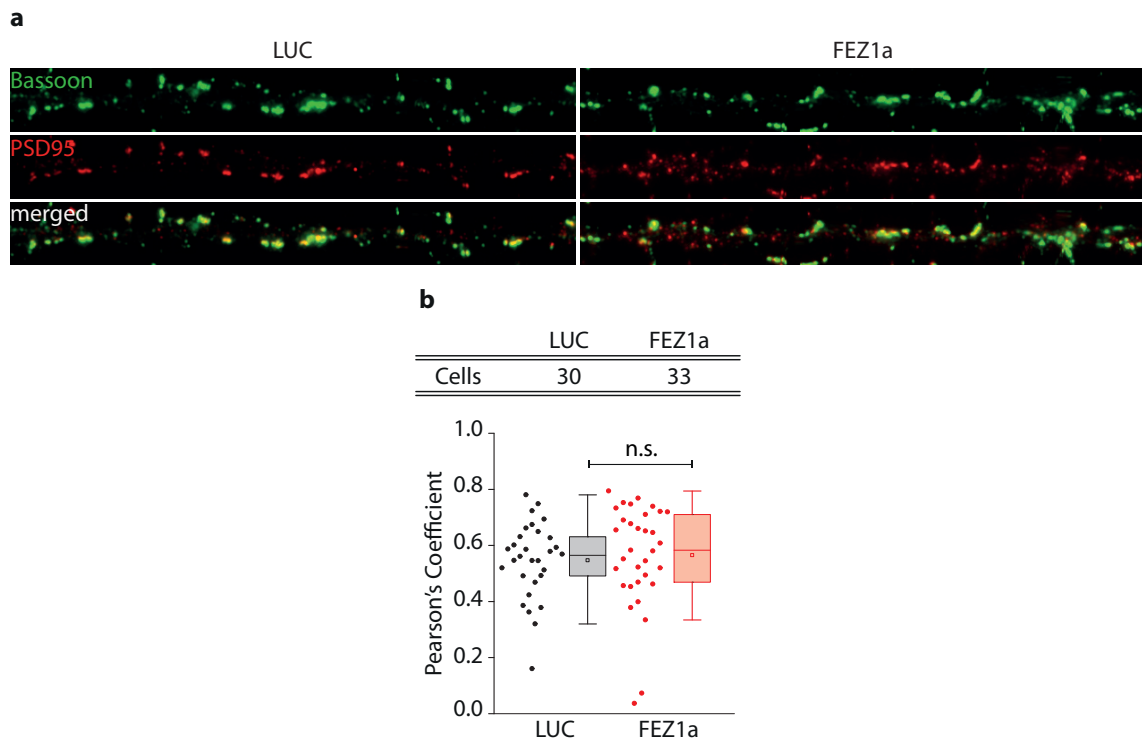
Figure 3.6.2.: Ablation of FEZ1 expression did not influence the colocalization of Bassoon and PSD95 on DIV14-15. (**a**) Representative images from control and FEZ1 knockdown neurons, stained for Bassoon and PSD95 are shown. The merged image has been shown to depict the colocalization of the two proteins. (**b**) The number of cells quantified are indicated, and the Pearson's coefficient was calculated to assess the colocalization of Bassoon and PSD95. Results are from 3 independent experiments.

3.7. FEZ1 affects the morphology of dendritic spines

FEZ1 deletion in mature neurons did not affect the density of postsynaptic special-izations along the axons, or the juxtaposition between the pre- and postsynaptic sites. However, examining the morphology of neurons on DIV14 showed a stark distinction between the dendritic protrusions in control and FEZ1 knockdown (Fig-ure 3.7.1). To confirm, neurons were categorized based on the morphology of their dendritic protrusions: the ones showing mostly mushroom spines, and the ones with mostly filopodial protrusions. While 80.00% of control neurons demonstrated mostly mushroom spines in the dendrites, this population was reduced to 39.28% in FEZ1 knockdown neurons (Figure 3.7.2.a).

Moreover, quantification of spine density in each category showed that the spine density in the dendrites of the filopodial group remained similar between the control and knockdown neurons (0.08 ± 0.01 in control, vs. 0.09 ± 0.01 in FEZ1 knockdown, per 10 µm dendritic length). However, FEZ1 deletion reduced the spine density of the mushroom category from 0.14 ± 0.01 in control to 0.09 ± 0.01 in the knockdown (Figure 3.7.2.b).
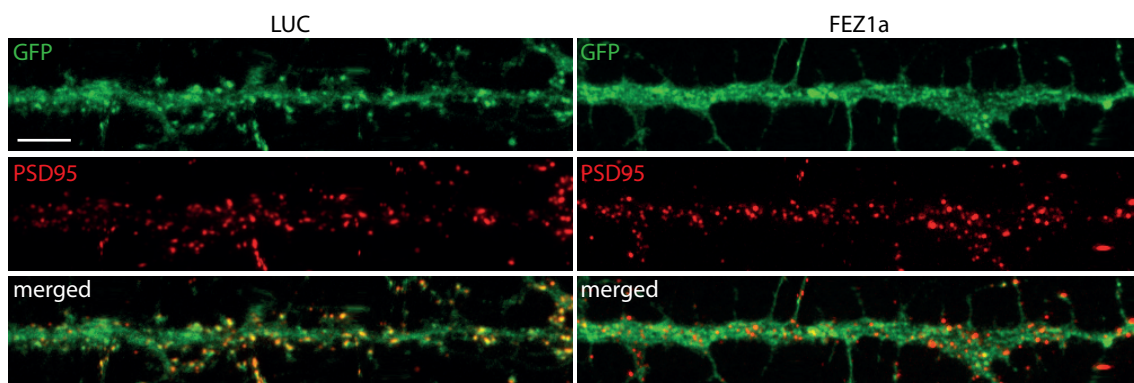
Figure 3.7.1.: FEZ1 knockdown induces a shift from mostly mushroom spines to filopodial protrusion in dendrites. Representative images of GFP signal and PSD95 immunostaining are shown. Neurons were infected on DIV1 and imaged on DIV7. Scale bar = 5 µm.

It is known that during development, dendritic spines first appear as filopodia search-ing for synaptic terminals, and eventually turn into mature spines [100]. Dendritic spines are highly dynamic, and can disappear or change their shape in response to a variety of stimuli. Therefore, their morphology is a crucial means for structuring synaptic interactions and plasticity [323, 324, 325, 326, 327, 328, 329, 330]. There are numerous psychiatric and neurological disorders associated with aberrant spine morphology and number, including mental retardation [331], schizophrenia [332, 333]
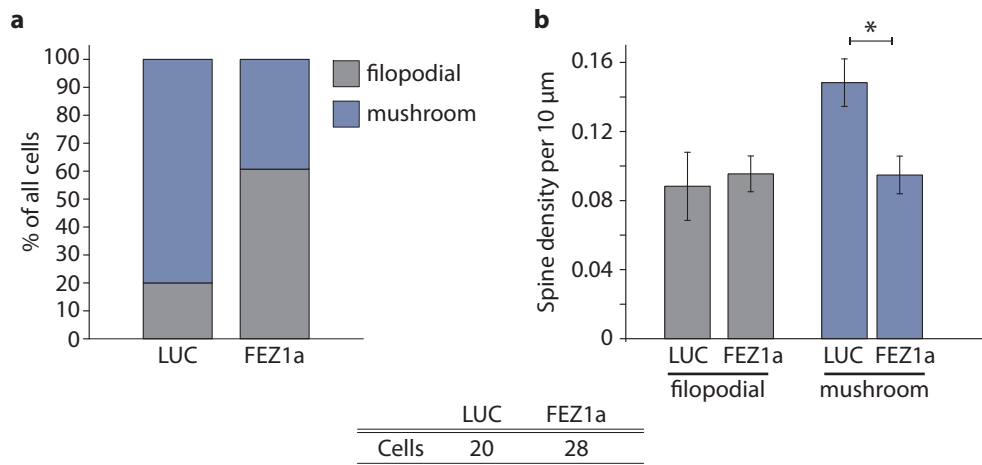
Figure 3.7.2.: Categorization of neurons based on the morphology of dendritic spines, and quantification of the spine density in each category. (**a**) A larger population of control neurons demonstrate mostly mushroom spines, while the spines on FEZ1 knockdown neurons are mostly filopodial. (**b**) Quantification of spine density in each group shows that FEZ1 knockdown leads to a significant reduction in the mushroom group. p-value = 0.005. Numbers of analyzed cells are indicated on the table below. The results are from 3 independent experiments.

and autism [334]. Presence of thin filopodial dendritic protrusions in mature neurons has been long associated with mental retardation. First observed in a study on children with non-specific mental retardation [335], it has also been observed in fragile X syndrome, an inheritable form of mental retardation, where spines tend to be long and thin [336]. Individuals with Down syndrome also exhibit decreased spine density [337, 338, 339, 340].

FEZ1-dependent transport deficiencies observed thus far pointed to an important role of this protein in presynaptic assembly. The fact that the FEZ1 knockdown leads to a transition from mature, mushroom spines to filopodial spines on dendrites suggests that this protein might also play a key role in postsynapse development. This task might be accomplished by influencing the postsynapse formation through presynaptic transport, or by directly associating with postsynaptic cargos [290].

3.8. Effect of FEZ1 knockdown on dendritic development

FEZ1 has recently been shown to participate in adult neurogenesis of the mouse dentate gyrus. Knockdown of FEZ1 expression in newborn neurons led to soma en-

largement accompanied by a dramatic increase in dendritic complexity and length. This phenotype was enhanced upon concurrent knockdown of FEZ1 and its interaction partner, Disrupted-in-Schizophrenia-1 (DISC1) [341]. Moreover, suppression of FEZ1 in the subgranular zone (SGZ) of postnatal mice (P6) was followed by an increase in the dendritic complexity as revealed by Sholl analysis two weeks after manipulation. This study also suggests FEZ1 to be a negative regulator of dendritic development in the early postnatal stage of development in young neurons [342]. Consistent with studies in mice, the interaction between FEZ1 and DISC1 was shown to be upregulated during neuronal differentiation in PC12 cells, and disruption of this interaction inhibited neurite outgrowth. However, overexpression of DISC1 in PC12 cells was followed by enhanced neurite outgrowth, suggesting a facilitating role for DISC1 during early stages of neuronal development [343].

To investigate whether FEZ1 also plays a role in early neuronal development, dendritic morphology was studied in FEZ1 knockdown neurons. Cultured neurons were transfected with lentiviral plasmids co-expressing cas9 and FEZ1 targeting gRNAs along with GFP on DIV1. The effect of FEZ1 deletion on dendritic development was investigated by Sholl analysis on DIV7 [344]. This method measures the complexity of dendritic arborization by drawing concentric circles around the cell body and counting the number of their intersections with the neurites. Remarkably, as depicted in figure 3.8.1, a significant decrease in dendritic complexity was observed in FEZ1 knockdown. The phenotype was similar using either FEZ1a or FEZ1b gRNAs.

The observed phenotype in primarily pyramidal neurons of the hippocampal cultures suggests that FEZ1 suppression has a negative effect on dendritic development at an early postnatal stage. The contrast between our results and the previous studies might lie within the fundamental differences between adult neurogenesis in the dentate gyrus and early postnatal neuronal development. Moreover, the enhanced dendritic complexity in FEZ1 knockdown at the postnatal stage was observed in 3-week-old mice [342], which is in comparison at a significantly more mature stage. It might be plausible to speculate that FEZ1 plays a bi-modal role during neuronal development, where its sufficient expression is crucial during initial neurite outgrowth in young neurons, whereas later it might have a ceiling effect on dendritic arborization, and its suppression leads to exaggerated outgrowth in dendrites.
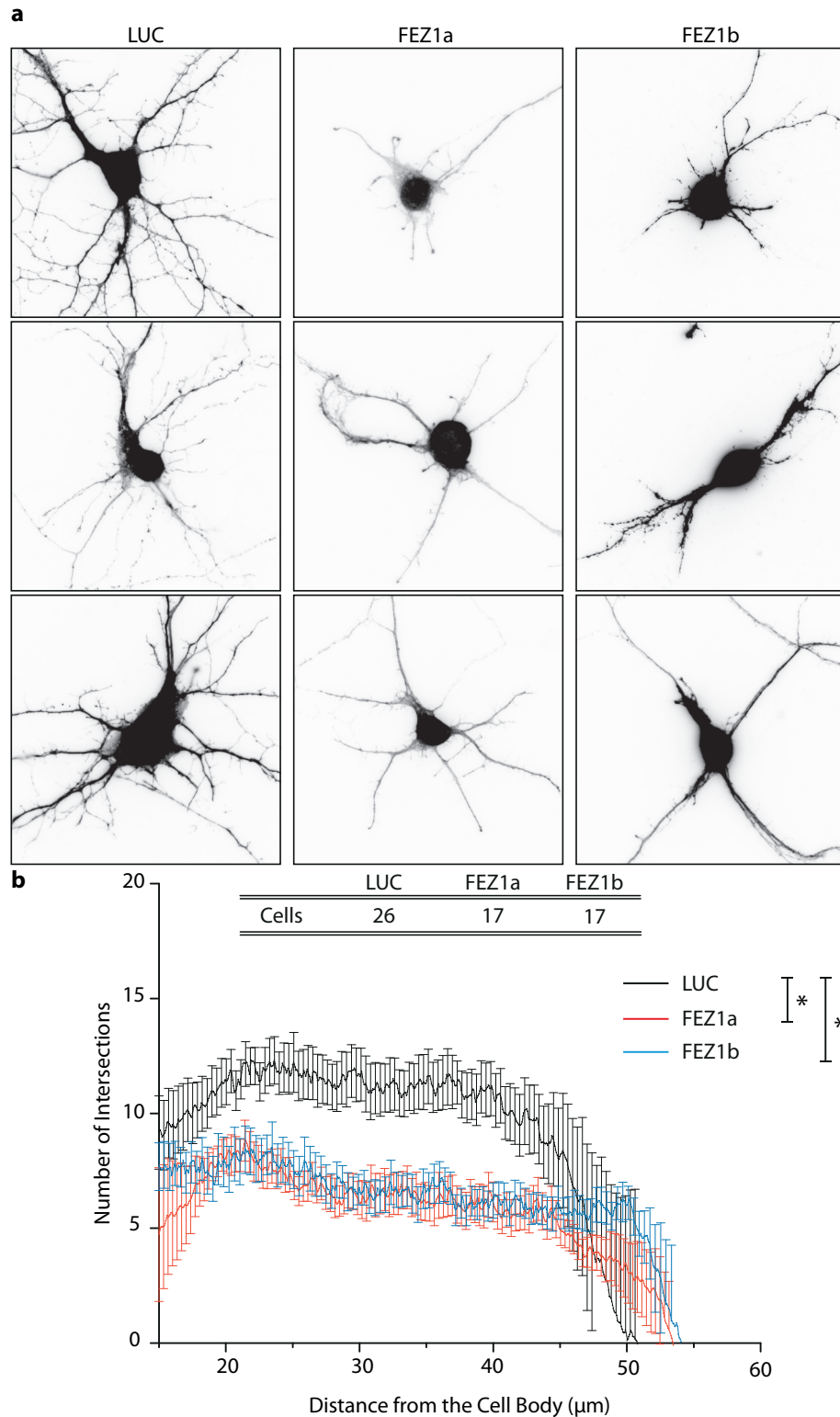
Figure 3.8.1.: FEZ1 suppression decreases dendritic complexity in cultured hippocampal neurons. (**a**) Representative images of neurons transfected with the lentiviral plasmid concurrently expressing either control (LUC), FEZ1a or FEZ1b gRNA and GFP. The images show the GFP expressed in the lentiviral plasmid. (**b**) Dendritic complexity was reduced in the absence of FEZ1 as revealed by Sholl analysis. The Kruskal-Wallis ANOVA test was performed on the area under the curves. p-value$_{\text{LUC vs. FEZ1a}} = 2{\times}10^{-4}$, p-value$_{\text{LUC vs. FEZ1b}} = 0.004$. The results shown are from 2 independent experiments. Error bars = SEM.

3.9. The effect of FEZ1 deletion on neurotransmission

So far, it was concluded that FEZ1 deletion impacts the axonal movement of presynaptic components, including synaptic vesicle precursors and active zone proteins. Moreover, it was also shown that FEZ1 deletion seems to reduce the number of docked vesicles. These data confirm the role of FEZ1 in presynapse formation, however it was yet unclear whether it influenced synaptic activity. To address the role of FEZ1 in synaptic release, neurons were transduced by lentiviruses co-expressing Cas9, GFP and either LUC or FEZ1a gRNA, and synaptic transmission was measured by using a pH-sensitive dye, CypHer5E, conjugated to an antibody against the lumenal domain of syt-1 on DIV14 [345].

The neurons were stimulated by 60 (stimulation 1) and 600 (stimulation 2) action potentials at 20 Hz to induce the exocytosis of vesicles in the readily releasable pool and the entire releasable SV pool, respectively. Images were acquired every 2 seconds, for a total of 5 minutes. The fluorescence recovery of CypHer5E was subsequently corrected for acquisition bleaching and plotted against time.

As depicted in figure 3.9.1, the fluorescent signal drop followed by stimulation 1 averaged to $1.36 \pm 0.23\%$ in control and $2.18 \pm 0.43\%$ in knockdown neurons. In stimulation 2, the fluorescence signal was reduced by $1.81 \pm 0.43\%$ in control and $2.64 \pm 0.77\%$ in knockdown neurons. As can be appreciated from the overlap and the large error bars seen in the traces, the bleaching or the recovery behavior of the two conditions did not show any difference. The signal loss observed after the second stimulation (to release to entire releasable SV pool) appears to be similar to that of stimulation 1, which was not expected. Nevertheless, FEZ1 depletion does not seem to dramatically affect the release of synaptic vesicles, at least at the time point and with the procedure used in our measurements.
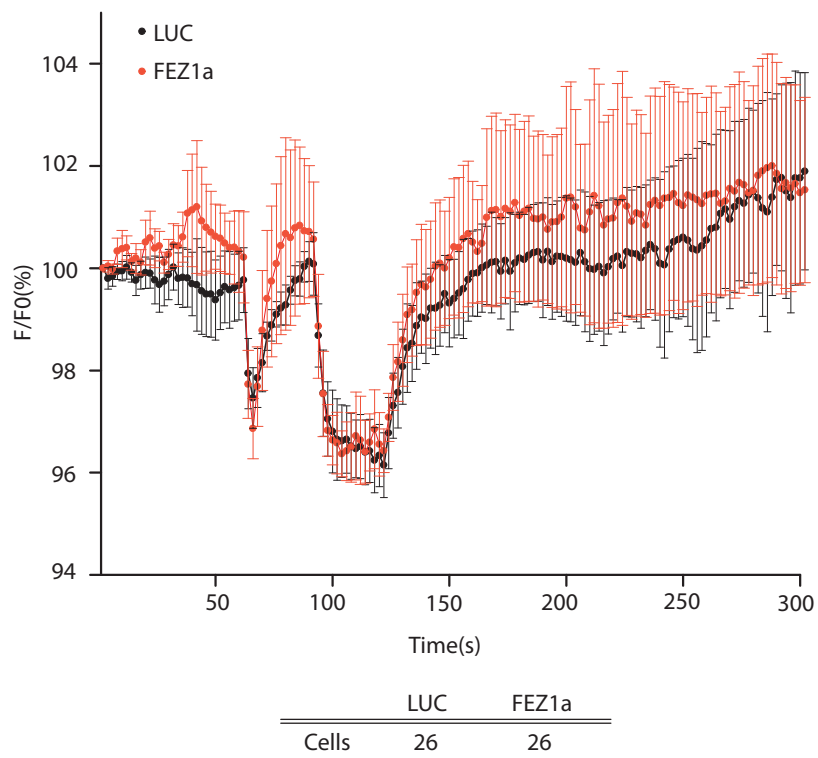
Figure 3.9.1.: FEZ1 knockdown does not impact synaptic release. The numbers indicated on the table are the number of experiments carried out for each condition. Results are from 3 independent biological replicates.

4. Discussion

In this study, I characterized the mobility of a kinesin-1 transport adaptor known as UNC-76 in invertebrates and FEZ1 in mammalian neurons. I also investigated the function of FEZ1 in formation of presynaptic terminals by studying the movement of active zone and synaptic vesicle precursors following FEZ1 deletion. My results show that neuronal FEZ1 is highly mobile, and its movement is dependent on serine-58, a phospho-site previously shown to be crucial in its binding to kinesin-1 [207]. FRAP experiments on FEZ1 variants demonstrated that saturating the system with FEZ1 phosphomimetic (S58D) or abundance of phosphorylation-deficient variant of FEZ1 (S58A) lead to axonal stalling of this protein, and possibly of its cargos. Furthermore, FEZ1 was shown to be involved in transport of active zone precursors, indicated by diminished mobility observed in Bassoon puncta upon FEZ1 loss. FEZ1-mediated anterograde transport was further highlighted by an exaggerated retrograde transport observed in synaptotagmin-1. Overall, ablation of FEZ1 expression resulted in disorganization of presynaptic markers. Finally, abnormal branching of dendrites in young neurons, in conjunction with an unexpected predominance of filopodial spines observed in mature neurons suggests an important role for FEZ1 in development and formation of postsynaptic specializations.

4.1. FEZ1 mobility is regulated by serine-58 phosphorylation

FEZ1 has been shown to transport syntaxin by biochemical and functional studies in worm [207], and is suggested to be associated with the components of active zone and synaptic vesicles [289, 290]. Transport function of FEZ1 can be regulated on two levels: either by modulating its association with the cargo, or alternatively via regulating its binding to the motor. The latter has been suggested by the necessity of serine-58 phosphorylation for binding to kinesin-1 in previous studies [207, 302].

My FRAP experiments addressed the mobility of mammalian FEZ1 variants for the first time. The results helped clarify the regulatory role of serine-58 on two important

parameters of FEZ1 dynamics: mobility and speed.

Based on my results, the transport activity of FEZ1 is regulated by maintaining a balanced association with kinesin-1 through the phosphorylation on serine-58. Replacing this residue with alanine hampers FEZ1 mobility and speed, likely by interrupting its association with kinesin-1 as evident from previous reports [207, 302]. The drastic reduction of FEZ1 S58A mobile fraction and recovery speed immediately in the segments closest to FRAP edge shows that presence of functional FEZ1 is in fact crucial for efficient delivery of its cargos. This is in agreement with previous research where it was observed that FEZ1-activated kinesin-1 displays a higher number of motile events *in vitro* [202].

Mutation of serine-58 to aspartate also diminishes FEZ1 mobile fraction and speed in the neuron. Overexpression of FEZ1 S58D may saturate the system by activated kinesin-1, which leads to axonal clogging or traffic jams. This phenomenon has been observed *in vitro*, where increasing the motor concentration leads to increased flux of motor protein to the microtubule plus end, creating a high density region. This crowding effect in turn results in lower speed of motor movement [304]. A similar scenario can by speculated for the movement of kinesin upon overexpression of its activator FEZ1 S58D. Due to the phosphomimetic mutation, FEZ1 S58D does not dissociate from kinesin-1, keeping it in an active state. Subsequently, this might lead to overpopulating the MT with kinesin-1 and axonal clogging.

Lack of a significant difference between the mobility and speed of movement of FEZ1 wt in either direction suggests FEZ1 flux in the anterograde and retrograde directions are largely identical. This phenomenon could be partially explained by FEZ1 association with the retrograde motor protein, dynein (Butkevich et al. 2016), which exhibits a similar speed to kinesin motor proteins in vivo (Ma and Chisholm 2002). Alternatively, FEZ1 might be passively associated with the cargos that are now traveling retrogradely. Nevertheless, the role of FEZ1 as a specific anterograde transport adaptor was not clear from these experiments.

Some adaptor proteins participate in both anterograde and retrograde movements. This bi-modal behavior is modulated by post translational modifications, such as phosphorylation on serine-421 in JIP1 [283], or the modification on serine-421 in Huntingtin [281]. Therefore, directional regulation of FEZ1 movement by its phospho-site was an intriguing possibility, specially considering the identification of dynein on FEZ1-associated vesicles [290]. However, our results show that phosphorylation of serine-58 does not affect the directionality of FEZ1, and its influence appears to be predominantly limited to mobility, and marginally on speed.

One intriguing follow-up experiment is to study the movement of FEZ1-associated

cargos in the presence of overexpressed phosphomutants. It would be interesting to investigate how the displacement or the speed of movement of, for instance, Bassoon or synaptic vesicle proteins, is affected in presence of FEZ1 phosphomutants. These experiments can provide additional mechanistic details of how FEZ1 phosphorylation regulates its association with the cargo, rather than the motor protein.

4.2. FEZ1 is involved in presynaptic assembly

Motility of Bassoon, one of the earliest proteins to arrive at the active zone [102, 89], was studied in FEZ1 knockdown neurons. The role of FEZ1 in transport of AZ components, thereby in assembly of the active zone was investigated by monitoring changes in Bassoon movement. My experiments in living neurons showed that the run length of Bassoon is unaffected by FEZ1 deletion. This suggests that the processivity of kinesin-1, the main motor protein for transport of AZ components [201], does not diminish by FEZ1 scarcity. This observation is contradictory with *in vitro* studies [202], where it was shown that binding of FEZ1 to kinesin-1 increases the motor processivity. This discrepancy may be due to the different model systems used.

Similarly, FEZ1 deletion did not reduce the speed of Bassoon puncta movement in either direction, which suggests that binding of FEZ1 does not affect the speed of kinesin-1 motor protein. This closely resembles the observations in FEZ1-activated kinesin-1 motor protein *in vitro* [202]. Together, these observations suggest that reduced expression of FEZ1 does not affect the trafficking parameters of individual motor-cargo complexes. It is however important to note, that AZ proteins are being transported by, at least, another parallel mechanism, via using syntabulin as the adaptor protein [206, 201]. Therefore, the quantified parameters are indicative of both transport alternatives. It is possible that the effect of FEZ1 knockdown is partially masked by the syntabulin-mediated transport. Considering that approximately 40% of Piccolo has been observed to colocalize with syntabulin in DIV8 neurons [201], the effect of syntabulin-mediated transport on my observations cannot be overlooked.

Nevertheless, the contribution of FEZ1 to mobility of AZ precursors is emphasized by the significant reduction in the mobile pool of RFP-Bassoon. This dramatic decrease in trafficking of AZ components has also been observed in syntabulin knockdown neurons [201]. Moreover, FEZ1 has also been shown to activate and induce motile events in kinesin-1 [202]. Taken together, these results attribute a considerable fraction of AZ precursor transport to FEZ1/kinesin-1 complex, and define a role for FEZ1 in the assembly of active zone in mammalian neurons.

Tracking the movement of syt-1, as the synaptic vesicle precursor marker in FEZ1 knockdown demonstrated that FEZ1 does not diminish the anterograde trafficking of synaptic vesicle proteins. Interestingly, FEZ1 deletion increases retrograde run length in these vesicles, which suggests a higher processivity in the transport towards the cell soma. Similarly, the speed of retrograde movement appears slightly higher in FEZ1 knockdown. This phenomenon can be interpreted in a few different scenarios.

It is known that synaptic vesicle precursors are mainly transported by kinesin-3 (or KIF1) [224, 226, 227]. However, there are a number of studies suggesting a possible role for kinesin-1 in transport of these vesicles. Stalling of vesicles in larval segmental nerves has been reported in *khc Drospholia* mutants [346]. Kinesin-1 has also been implicated in transport of synaptic vesicle proteins synaptotagmin and synaptobrevin [212, 213]. Consistently, kinesin heavy chains KIF5A and KIF5B have been identified on synaptic vesicles [58]. Lastly, in a recent study by our lab components of synaptic vesicles were identified in mass spectrometry of FEZ1/kinesin-1 trafficking vesicles in the rat brain [290]. Therefore, it is possible that kinesin-1 also contributes to transport of synaptic vesicle precursors in a FEZ1-mediated manner.

It is known that most cargos are simultaneously bound to both anterograde and retrograde motors, and the net movement is accomplished by the motor that exerts the dominant force [270, 269, 271, 307]. FEZ1 deletion leads to a reduced population of activated kinesin-1 [202]. This might in turn lead to higher probability of retrograde motors winning in a tug-of-war mechanism [275]; hence the longer retrograde run lengths in FEZ1 knockdown neurons.

Another possibility is the influence of FEZ1 on movement of STVs through its role in trafficking of AZ proteins. It has been shown that transport of AZ trafficking packets and synaptic vesicle precursor proteins are coordinated [201, 103]. Therefore, the observed upregulation of retrograde movement might be an indirect result of FEZ1 function in transport of AZ precursor proteins.

Although there have been no reports so far on direct interaction of FEZ1 with kinesin-3, the possibility of this interaction cannot be entirely ruled out. Switching to retrograde movement of synaptobrevin have been also observed when the kinesin scaffolding protein, SYD-2, is unable to bind to the motor in *C. elegans* [240]. Therefore, adaptor activity of FEZ1 for kinesin-3 can also be speculated, though it has to be verified by follow-up experiments.

4.3. FEZ1 deletion leads to presynaptic disorganization

Consistent with the reduced trafficking of AZ precursors, Bassoon and Piccolo, two major active zone proteins [14], were abnormally distributed. The clustering of Bassoon as a result of its deficient transport had been also reported in syntabulin knockdown [201]. Furthermore, this phenomenon also closely resembles the clustering behavior of syntaxin-1 in *unc-76 C. elegans* mutants [207]. Since syntaxin-1a, Bassoon and Piccolo, in addition to other active zone components, have been shown to be present on the same kinesin-1 associated transport packets [201, 76, 89], simultaneous disorganization of these proteins upon FEZ1 knockdown is not surprising. Trafficking in living neurons and the localization of AZ proteins in immunostained FEZ1 knockdown neurons collectively suggest that FEZ1 is largely involved in transport and distribution of AZ components, and affects the active zone assembly.

The abnormal dispersion of synapsin I puncta in FEZ1 knockdown further suggests an important role for FEZ1 in proper distribution of STVs. This observation is in line with the reduced number of synaptophysin puncta along the axons observed in syntabulin knockdown. Although SV proteins were not immunoisalated on syntabulin-associated membranous vesicles, it was shown that the axonal density of synaptophysin was reduced in syntabulin knockdown [201]. Synapsin I has been identified in the FEZ1/kinesin-1 associated vesicles [290]. Therefore, FEZ1 might be directly involved in transport of synapsin I containing STVs (as described in [96]). Moreover, partial loss of synapsin I puncta in FEZ1 knockdown could be explained by deficient transport of N-cadherin, present on Bassoon and Piccolo transport packets [89, 201]. This in turn leads to reduced recruitment and clustering of synaptic vesicles to the presynaptic sites [347, 348]. Overall, dispersion of synapsin I puncta points to a direct or indirect influence of FEZ1 in its proper distribution.

4.4. FEZ1 in dendritic morphology

Axonal density of Bassoon in FEZ1 knockdown in older neurons appeared similar to normal condition. This suggests that at least some of the neurons were able to eventually compensate for the loss of FEZ1 by upregulating other transport pathways of AZ precursors, for instance by increasing the expression of syntabulin [206]. It is also possible that FEZ1-mediated transport is more crucial in the earlier developmental stages of neuron. Consistently, the density of postsynaptic specializations was not

significantly different between FEZ1 knockdown and control neurons on DIV14-15. This is in agreement with several studies that suggest a correlation between clustering of presynaptic and postsynaptic proteins [322, 320, 321].

Although the density of PSDs remained normal, FEZ1 knockdown led to a shift from mushroom spines to filopodia-like protrusions. The presence of mostly filopodial protrusions in dendrites of older neurons has important implications on the role of this protein in synapse development. Dendritic spines exhibit a highly dynamic and experience dependent morphology [349, 350]. A number of neurological diseases exhibit abnormal spine size, shape or number as common symptoms. Specifically, reduced spine density and appearance of thin dendritic spines have been long associated with mental retardation [335, 351, 352, 337, 353]. A larger number of filopodium-like spines accompanied by a reduction in mushroom and stubby spines, with an overall decrease in spine density have also been observed in individuals with Down syndrome [354]. Decreased spine density has also been observed in schizophrenia [332, 333].

FEZ1 can induce this change either by directly participating, or lack thereof in FEZ1 knockdown, in transport of presynaptic cargos. While transport of various cargos in the spine by actin based myosin motor proteins has been extensively studied [355, 356, 357, 358], entry of microtubules into dendritic spines has been a recent topic of research [359, 171, 360]. Presence of MT in the dendritic spines implies possible roles of kinesin-mediated transport in spinogenesis. For instance, it has been recently shown that kinesin-3 (KIF1A) is trafficked into the spines, and its loss leads to a reduced spine density, along with an increase in dendritic filopodia. The abnormal spine morphology is speculated to be a result of interrupted transport of cargos into the spines [361]. It is therefore plausible to hypothesize that FEZ1 deletion also influences dendritic morphology through interrupting proper transport of its cargos. Although this does not coalesce with the preliminary observation that Bassoon is normally distributed in FEZ1 knockdown in mature neurons, more elaborate characterizations of the synaptic markers at this time-point might reveal other presynaptic abnormalities.

On the other hand, FEZ1 immunoisolated traffic vesicles have shown to contain post-synaptic material, such as Gephyrin and Shanks [290]. Therefore, FEZ1-mediated transport of postsynaptic cargos into the spines is also an intriguing possibility. The postsynaptic phenotype also ties in with the decreased dendrite complexity observed upon FEZ1 knockdown. Dendrite arborization and branching is an important process during neuronal development and is regulated by various intrinsic and environmental cues[362, 363]. Simultaneous deficiencies in dendrite branching and reduced spine density have been shown in neurological disorders associated with intellectual dis-

abilities, such as Down syndrome [364, 365, 366, 367] and Coffin-Siris syndrome [368]. These phenotypes together suggest a role for FEZ1 in overall neural network connectivity. Analysis of postsynaptic compartment in FEZ1 knockdown reveals exciting implications of this protein in development of neurons and possibly in neurological diseases.

4.5. FEZ1 does not alter the synaptic release

Synaptic boutons in FEZ1 knockdown neurons responded similarly to normal condition when stimulated by different action potential trains. Previously, it has been shown that neurons on DIV14-21 exhibit an approximate 5% signal loss of CypHer5E-syt1 in response to 50 APs at 20 Hz [345], which is comparable to what I observe in both control and knockdown neurons. However, stimulating with 600 APs should induce the exocytosis of the entire releasable SV pool, indicated by a larger reduction in the CypHer5E fluorescent intensity [345]. This is not observed in my CypHer5E experiments in neither control nor knockdown neurons. Considering that this trend was persistent in all three repetitions, it is possible that neurons are not properly stimulated at this time-point. Performing release assays at a later stage in neurons could reveal more details on possible effects of FEZ1 loss in neurotransmission. Loss of function of syntabulin has been shown to decrease FM dye uptake by the presynaptic boutons, in addition to reduced amplitude of PSCs [201]. Moreover, preliminary ultrastructure analysis of synapses in FEZ1 knockdown suggests that there is a slight but significant reduction in the number of docked SVs to the active zone. There are a number of studies supporting a model where readily releasable pool and docked vesicles are positively correlated [369, 20, 22, 370, 371]. Therefore, collecting more data on EM analysis of the synapses in FEZ1 knockdown, and perhaps investigating neurotransmitter release by an alternative electrophysiological method (e.g. using a different marker for release or performing the experiments at a different developmental stage) are interesting routes to follow up.

A. Appendix

A.1. Confirmation of FEZ1 knockdown efficacy by Western blotting

To ensure that the designed gRNAs efficiently knocked down the expression of FEZ1 in neurons, during this study neuron lysates were analyzed multiple times by SDS-PAGE. Actin was used as the loading control, and the protein bands were visualized by using fluorescent labeled secondary antibodies (Figure A.1.1.a). The expression of synaptophysin and PSD95 were also assessed, to verify that the expression of synaptic proteins are not affected by FEZ1 gRNA (Figure A.1.1.b).
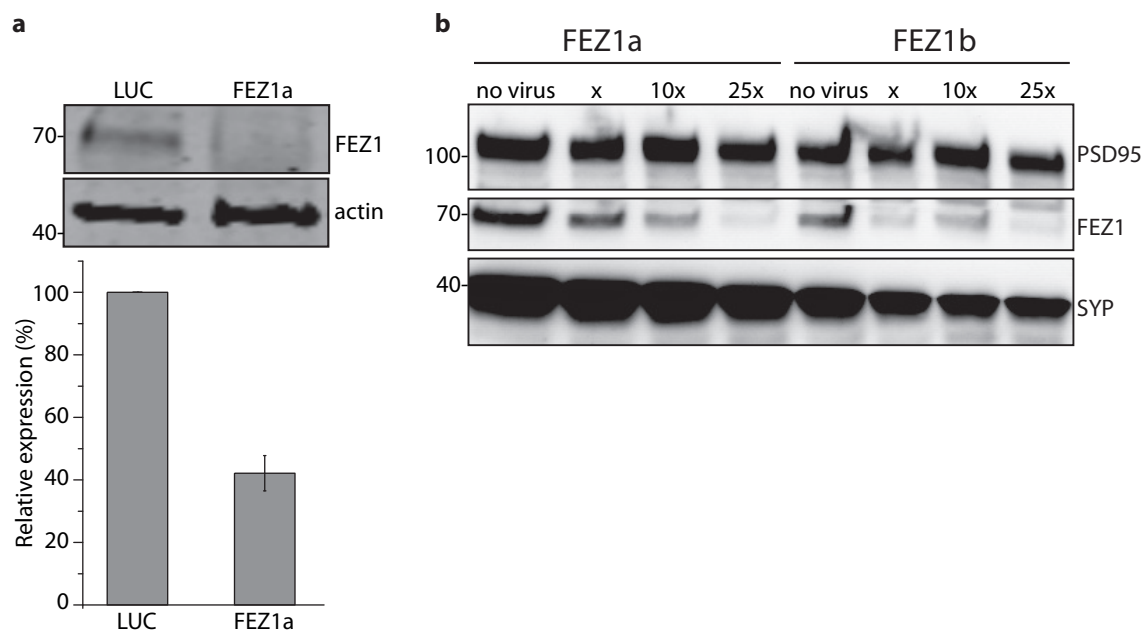
Figure A.1.1.: The efficiency of FEZ1a and FEZ1b gRNAs were confirmed by Western blotting. (**a**) Neurons were infected with lentiviruses expressing gRNAs targeting either LUC or FEZ1 gene (FEZ1a) on DIV1 and lysed on DIV7. The blot was probed by fluorescent labeled antibodies, and the signal intensity was quantified. The results are from 2 independent experiments. (**b**) Neurons were transduced by increasing amounts of lentiviruses expressing FEZ1a or FEZ1b gRNA on DIV1, and the expression of FEZ1, in addition to synaptophysin and PSD95 on DIV14. The expression of FEZ1 remains effectively ablated in mature neurons, while the expression of synaptic markers is unaffected.

A.2. Immunocytochemistry of FEZ1 knockdown neurons

The efficacy of gRNAs was further assessed by immunostaining for endogenous FEZ1 in infected neurons. Control neurons exhibited localization of FEZ1 in the cell soma as well as the neurites. However, the presence of FEZ1 signal, specifically in the neurites, was marginally reduced in neurons infected with either FEZ1a or FEZ1b (Figure A.2.1). FEZ1 signal was not entirely abolished upon acute knockdown in neurons due to the early onset of FEZ1 expression during the embryonic period [372].
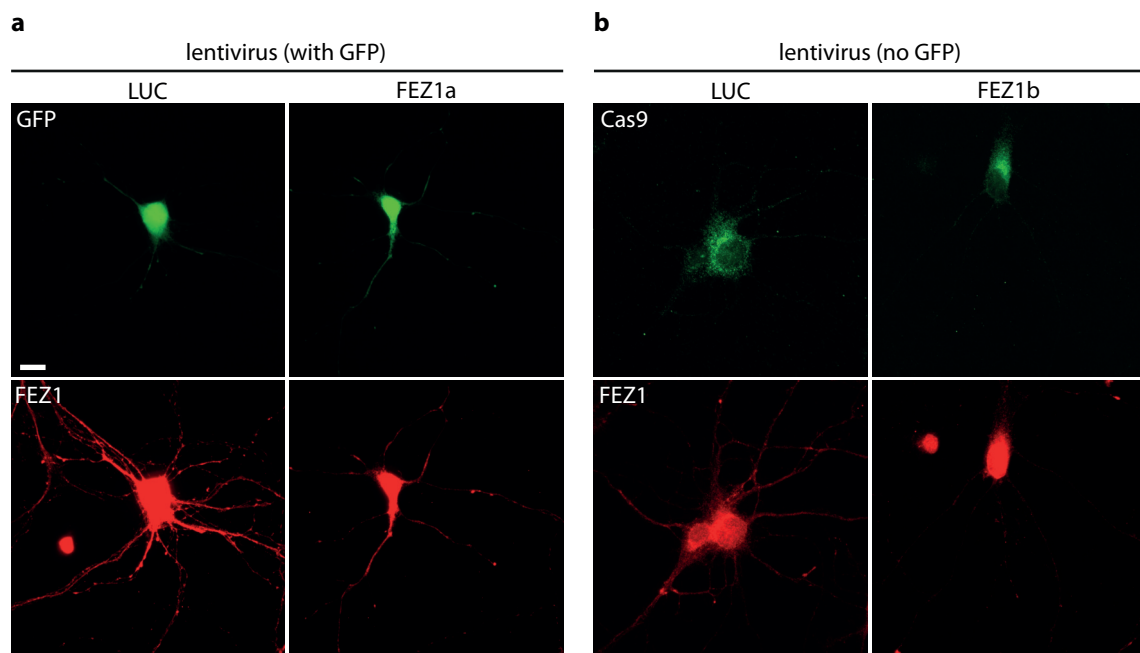
Figure A.2.1.: Immunocytochemistry of FEZ1 knockdown neurons. (a) Neurons were infected with lentiviruses expressing either LUC or FEZ1a gRNA along with GFP. (**b**) Neurons were infected with viruses expressing either LUC or FEZ1b gRNA with no GFP. The infected neurons were detected by immunostaining with cas9 antibody. Scale bar = 10 µm.

A.3. MATLAB code for spot detection

```matlab
% [frameInfo imgDenoised] = detectSpotsWT(img, S, dthreshold,
    postProcLevel)
%
% Performs detection of local intensity clusters through a
    combination of
% multiscale products and denoising by iterative filtering
    from
% significant coefficients:
% Olivo-Marin, "Extraction of spots in biological images using
    multiscale products," Pattern Recoginition 35, pp.
    1989-1996, 2002.
% Starck et al., "Image Processing and Data Analysis," Section
    2.3.4, p. 73
%
% INPUTS:   img               : input image (2D array)
%           {S}               : postprocessing level.
%           {dthreshold}    : minimum allowed distance of
    secondary maxima in large clusters
%           {postProcLevel} : morphological post processing
    level for mask

% Parts of this function are based on code by Henry Jaqaman.
% Francois Aguet, March 2010

function [frameInfo imgDenoised] = spotDetector(img, S,
    dthreshold, postProcLevel)

if nargin<2
    S = 4;
end
if nargin<3
    dthreshold = 5;
end
if nargin<4
    postProcLevel = 1;
end


```

```matlab
30  maxI = max(img(:));
31  minI = min(img(:));
32  [ny nx] = size(img);
33
34  %=====================================================
35  % Iterative filtering from significant coefficients
36  %=====================================================
37  imgDenoised = significantCoefficientDenoising(img, S);
38
39
40  res = img - imgDenoised; % residuals
41  sigma_res0 = std(res(:));
42
43  delta = 1;
44  while delta > 0.002
45      resDenoised = significantCoefficientDenoising(res, S);
46      imgDenoised = imgDenoised + resDenoised; % add significant
              residuals
47      res = img - imgDenoised;
48      sigma_res1 = std(res(:));
49      delta = abs(sigma_res0/sigma_res1 - 1);
50      sigma_res0 = sigma_res1;
51  end
52
53  %=====================================================
54  % Multiscale product of wavelet coefficients
55  %=====================================================
56  % The support of the objects is given by the multiscale
      product in the wavelet domain.
57  W = awt(imgDenoised, S);
58  imgMSP = abs(prod(W(:,:,1:S),3));
59
60
61  %=====================================================
62  % Binary mask
63  %=====================================================
64  % Establish thresholds
65  [imAvg imStd] = localAvgStd2D(imgDenoised, 9);
66
67  mask = zeros(ny,nx);
```

```matlab
68  mask((imgDenoised >= imAvg+0.5*imStd) & (imgDenoised.*imgMSP
        >= mean(imgDenoised(:)))) = 1;

69

70

71  % Morphological postprocessing
72  mask = bwmorph(mask, 'clean'); % remove isolated pixels
73  mask = bwmorph(mask, 'fill'); % fill isolated holes
74  mask = bwmorph(mask, 'thicken');
75  mask = bwmorph(mask, 'spur'); % remove single pixels 8-
        attached to clusters
76  mask = bwmorph(mask, 'spur');
77  mask = bwmorph(mask, 'clean');

78

79  if postProcLevel >= 1
80      mask = bwmorph(mask, 'erode');
81      if postProcLevel == 2
82          mask = bwmorph(mask, 'spur');
83      end
84      mask = bwmorph(mask, 'clean');
85      mask = bwmorph(mask, 'thicken');
86  end

87

88

89  % rescale denoised image
90  imgDenoised = (imgDenoised-min(imgDenoised(:))) * (maxI-minI)
        / (max(imgDenoised(:))-min(imgDenoised(:)));

91

92  imgDenoised = mask.*imgDenoised;
93  localMax = locmax2d(imgDenoised, [9 9]);

94

95  %====================================================
96  % Process connected components
97  %====================================================
98  [labels, nComp] = bwlabel(mask, 8);

99

100 area = zeros(nComp, 1);
101 totalInt = zeros(nComp, 1);
102 nMaxima = zeros(nComp, 1);
103 xmax = zeros(nComp, 1);
104 ymax = zeros(nComp, 1);
```

```matlab
105  xcom = zeros(nComp, 1);
106  ycom = zeros(nComp, 1);
107  labelVect = zeros(nComp, 1);
108
109  xmax2 = cell(nComp, 1);
110  ymax2 = cell(nComp, 1);
111  area2 = cell(nComp, 1);
112  totalInt2 = cell(nComp, 1);
113  labelVect2 = cell(nComp, 1);
114
115  % Compute area and center of mass for each component
116  stats = regionprops(labels, imgDenoised, 'Area', '
         WeightedCentroid', 'PixelIdxList');
117
118  % component labels of local maxima
119  maxLabels = labels .* (labels & localMax >0);
120  maxCoords(1:nComp) = struct('PixelIdxList', []);
121  mc = regionprops(maxLabels, 'PixelIdxList');
122  maxCoords(1:length(mc)) = deal(mc);
123
124
125  for n = 1:nComp
126      %[yi,xi] = find(labels == n); % coordinates of nth
             component
127      [yi,xi] = ind2sub([ny nx], stats(n).PixelIdxList);
128      [ym,xm] = ind2sub([ny nx], maxCoords(n).PixelIdxList);
129      area(n) = stats(n).Area;
130      com = stats(n).WeightedCentroid;
131      xcom(n) = com(1);
132      ycom(n) = com(2);
133
134      values = imgDenoised(stats(n).PixelIdxList);
135      totalInt(n) = sum(values);
136
137      nMaxima(n) = length(xm);
138      if nMaxima(n)==1
139          xmax(n) = xm;
140          ymax(n) = ym;
141          nMaxima(n) = 1;
142          labelVect(n) = labels(ym,xm);
```

```matlab
143    elseif nMaxima(n)==0 % no maximum was detected for this
            cluster
144        maxValueIdx = find(values == max(values));
145        xmax(n) = xi(maxValueIdx(1));
146        ymax(n) = yi(maxValueIdx(1));
147        nMaxima(n) = 1;
148        labelVect(n) = labels(ymax(n), xmax(n));
149    else % resolve multiple maxima cases
150        maxValues = localMax(sub2ind(size(localMax), ym, xm));
                % highest local max
151        maxIdx = find(maxValues == max(maxValues));
152        xmax(n) = xm(maxIdx(1));
153        ymax(n) = ym(maxIdx(1));
154        labelVect(n) = labels(ymax(n), xmax(n));
155
156        % remove highest max from list
157        xm(maxIdx(1)) = [];
158        ym(maxIdx(1)) = [];
159
160        % compute distance of secondary maxima to primary
161        dist2max = sqrt((xmax(n)-xm).^2 + (ymax(n)-ym).^2);
162        dist2com = sqrt((xcom(n)-xm).^2 + (ycom(n)-ym).^2);
163        mindist = min(dist2max,dist2com);
164
165        % retain secondary maxima where mindist > threshold
166        idx2 = find(mindist > dthreshold);
167        if ~isempty(idx2)
168            xmax2{n} = xm(idx2);
169            ymax2{n} = ym(idx2);
170            nSecMax = length(idx2);
171            nMaxima(n) = nSecMax+1;
172
173            % split area
174            area2{n} = area(n)*ones(nSecMax,1)/nMaxima(n);
175            area(n) = area(n)/nMaxima(n);
176            labelVect2{n} = labels(sub2ind(size(labels), ymax2
                {n}, xmax2{n}));
177
178            %intensity values
```

```matlab
179              totalInt2{n} = totalInt(n)*ones(nSecMax,1)/nMaxima
                    (n);
180              totalInt(n) = totalInt(n)/nMaxima(n);
181          end
182       end
183  end
184
185  xmax2 =  vertcat(xmax2{:});
186  ymax2 = vertcat(ymax2{:});
187  totalInt2 = vertcat(totalInt2{:});
188  area2 = vertcat(area2{:});
189  labelVect2 = vertcat(labelVect2{:});
190
191  % assign results to output structure
192  frameInfo.xmax = [xmax; xmax2(:)];
193  frameInfo.ymax = [ymax; ymax2(:)];
194  frameInfo.xcom = [xcom; xmax2(:)];
195  frameInfo.ycom = [ycom; ymax2(:)];
196  frameInfo.totalInt = [totalInt; totalInt2(:)];
197  frameInfo.area = [area; area2(:)];
198
199  frameInfo.nMaxima = nMaxima; % maxima per component
200  frameInfo.labels = [labelVect; labelVect2(:)];
201  frameInfo.nComp = nComp;
202
203  frameInfo.maxI = maxI;
204  frameInfo.minI = minI;
205
206
207  % prepare fields for tracker
208  nObj = length(frameInfo.xmax);
209  frameInfo.amp = zeros(nObj,2);
210  frameInfo.xCoord = zeros(nObj,2);
211  frameInfo.yCoord = zeros(nObj,2);
212
213  frameInfo.amp(:,1) = frameInfo.totalInt;
214  frameInfo.xCoord(:,1) = frameInfo.xcom;
215  frameInfo.yCoord(:,1) = frameInfo.ycom;
216
217  frameInfo.path = [];
```

```
218  frameInfo.maskPath = [];
219
220
221
222
223  %=====================
224  % Subfunctions
225  %=====================
226  function result = significantCoefficientDenoising(img, S)
227  mask = zeros(size(img));
228  result = zeros(size(img));
229  W = awt(img, S);
230  for s = 1:S
231      tmp = W(:,:,s);
232      mask(abs(tmp) >= 3*std(tmp(:))) = 1;
233      result = result + tmp.*mask;
234  end
```

Bibliography

[1] Gregory Z Tau and Bradley S Peterson. Normal development of brain circuits. *Neuropsychopharmacology*, 35(1):147, 2010.

[2] Dale Purves, GJ Augustine, D Fitzpatrick, LC Katz, AS LaMantia, JO McNamara, and SM Williams. *Neuroscience 2nd Edition. Sunderland (MA) Sinauer Associates.* Inc, 2001.

[3] Maria J Pinto and Ramiro D Almeida. Puzzling out presynaptic differentiation. *Journal of neurochemistry*, 139(6):921–942, 2016.

[4] Martin M Riccomagno and Alex L Kolodkin. Sculpting neural circuits by axon and dendrite pruning. *Annual review of cell and developmental biology*, 31:779–805, 2015.

[5] Susanne Schoch and Eckart D Gundelfinger. Molecular organization of the presynaptic active zone. *Cell and tissue research*, 326(2):379–391, 2006.

[6] Thomas C Südhof. The presynaptic active zone. *Neuron*, 75(1):11–25, 2012.

[7] Thomas C Südhof. The synaptic vesicle cycle. *Annual review of neuroscience*, 27:509, 2004.

[8] Thomas C Südhof. The synaptic vesicle cycle: a cascade of protein–protein interactions. *Nature*, 375(6533):645, 1995.

[9] R Couteaux and M Pécot-Dechavassine. L'ouverture des vesicules synaptiques au niveau des "zones actives". *Septieme Congres International de Microscopie Electronique (Grenoble, France)*, 3:709–710, 1970.

[10] Morgan Sheng and Eunjoon Kim. The postsynaptic organization of synapses. *Cold Spring Harbor perspectives in biology*, 3(12):a005678, 2011.

[11] EG Gray. Electron microscopy of presynaptic organelles of the spinal cord. *Journal of Anatomy*, 97(Pt 1):101, 1963.

[12] Frauke Ackermann, Clarissa L Waites, and Craig C Garner. Presynaptic active zones in invertebrates and vertebrates. *EMBO reports*, 16(8):923–938, 2015.

[13] P García-Junco-Clemente, P Linares-Clemente, and R Fernandez-Chacon. Active zones for presynaptic plasticity in the brain. *Molecular psychiatry*, 10(2):185, 2005.

[14] Eckart D Gundelfinger, Carsten Reissner, and Craig C Garner. Role of Bassoon and Piccolo in assembly and molecular organization of the active zone. *Frontiers in synaptic neuroscience*, 7:19, 2016.

[15] Yun Wang, Masaya Okamoto, Frank Schmitz, Kay Hofmann, and Thomas C Südhof. RIM is a putative Rab3 effector in regulating synaptic-vesicle fusion. *Nature*, 388(6642):593, 1997.

[16] Yun Wang and Thomas C Südhof. Genomic definition of RIM proteins: evolutionary amplification of a family of synaptic regulatory proteins. *Genomics*, 81(2):126–137, 2003.

[17] Sandhya P Koushika, Janet E Richmond, Gayla Hadwiger, Robby M Weimer, Erik M Jorgensen, and Michael L Nonet. A post-docking role for active zone protein RIM. *Nature neuroscience*, 4(10):997, 2001.

[18] Susanne Schoch, Pablo E Castillo, Tobias Jo, Konark Mukherjee, Martin Geppert, Yun Wang, Frank Schmitz, Robert C Malenka, and Thomas C Südhof. RIM1α forms a protein scaffold for regulating neurotransmitter release at the active zone. *Nature*, 415(6869):321, 2002.

[19] Elena O Gracheva, Gayla Hadwiger, Michael L Nonet, and Janet E Richmond. Direct interactions between *C.elegans* Rab-3 and RIM provide a mechanism to target vesicles to the presynaptic density. *Neuroscience letters*, 444(2):137–142, 2008.

[20] Pascal S Kaeser, Lunbin Deng, Yun Wang, Irina Dulubova, Xinran Liu, Josep Rizo, and Thomas C Südhof. RIM proteins tether Ca^{2+} channels to presynaptic active zones via a direct PDZ-domain interaction. *Cell*, 144(2):282–295, 2011.

[21] Lunbin Deng, Pascal S Kaeser, Wei Xu, and Thomas C Südhof. RIM proteins activate vesicle priming by reversing autoinhibitory homodimerization of Munc13. *Neuron*, 69(2):317–331, 2011.

[22] Yunyun Han, Pascal S Kaeser, Thomas C Südhof, and Ralf Schneggenburger. RIM determines Ca^{2+} channel density and vesicle docking at the presynaptic active zone. *Neuron*, 69(2):304–316, 2011.

[23] Pablo E Castillo, Susanne Schoch, Frank Schmitz, Thomas C Südhof, and Robert C Malenka. Rim1α is required for presynaptic long-term potentiation. *Nature*, 415(6869):327, 2002.

[24] Toshihisa Ohtsuka, Etsuko Takao-Rikitsu, Eiji Inoue, Marie Inoue, Masakazu Takeuchi, Kaho Matsubara, Maki Deguchi-Tawarada, Keiko Satoh, Koji Morimoto, Hiroyuki Nakanishi, and Yoshimi Takai. CAST: a novel protein of the cytomatrix at the active zone of synapses that forms a ternary complex with RIM1 and Munc13-1. *J Cell Biol*, 158(3):577–590, 2002.

[25] Yun Wang, Xinran Liu, Thomas Biederer, and Thomas C Südhof. A family of RIM-binding proteins regulated by alternative splicing: Implications for the genesis of synaptic active zones. *Proceedings of the National Academy of Sciences*, 99(22):14464–14469, 2002.

[26] Yun Wang, Shuzo Sugita, and Thomas C Südhof. The RIM/NIM family of neuronal C2 domain proteins interactions with Rab3 and a new class of Src homology 3 domain protein. *Journal of Biological Chemistry*, 275(26):20033–20044, 2000.

[27] Tobias Mittelstaedt and Susanne Schoch. Structure and evolution of RIM-BP genes: identification of a novel family member. *Gene*, 403(1):70–79, 2007.

[28] Karen SY Liu, Matthias Siebert, Sara Mertel, Elena Knoche, Stephanie Wegener, Carolin Wichmann, Tanja Matkovic, Karzan Muhammad, Harald Depner, Christoph Mettke, Johanna Bückers, Stefan W Hell, Martin Müller, Graeme W Davis, Dietmar Schmitz, and Stephan J Sigrist. RIM-binding protein, a central part of the active zone, is essential for neurotransmitter release. *Science*, 334(6062):1565–1569, 2011.

[29] H Hibino, R Pironkova, O Onwumere, M Vologodskaia, AJ Hudspeth, and F Lesage. RIM binding proteins (RBPs) couple Rab3-interacting molecules (RIMs) to voltage-gated Ca^{2+} channels. *Neuron*, 34(3):411–423, 2002.

[30] Iris Augustin, Christian Rosenmund, Thomas C Südhof, and Nils Brose. Munc13-1 is essential for fusion competence of glutamatergic synaptic vesicles. *Nature*, 400(6743):457, 1999.

[31] Nils Brose, Kay Hofmann, Yutaka Hata, and Thomas C Südhof. Mammalian homologues of *Caenorhabditis elegans unc*-13 gene define novel family of C2-domain proteins. *Journal of Biological Chemistry*, 270(42):25273–25280, 1995.

[32] Jaewon Ko, Moonseok Na, Seho Kim, Jae-Ran Lee, and Eunjoon Kim. Interaction of the ERC family of RIM-binding proteins with the liprin-α family of multidomain proteins. *Journal of Biological Chemistry*, 278(43):42377–42385, 2003.

[33] Ya Dai, Hidenori Taru, Scott L Deken, Brock Grill, Brian Ackley, Michael L

Nonet, and Yishi Jin. Syd-2 liprin-α organizes presynaptic active zone formation through elks. *Nature neuroscience*, 9(12):1479, 2006.

[34] Olav Olsen, Kimberly A Moore, Masaki Fukata, Toshinari Kazuta, Jonathan C Trinidad, Fred W Kauer, Michel Streuli, Hidemi Misawa, Alma L Burlingame, Roger A Nicoll, and David S Bredt. Neurotransmitter release regulated by a MALS–liprin-α presynaptic complex. *J Cell Biol*, 170(7):1127–1134, 2005.

[35] C Serra-Pages, NL Kedersha, L Fazikas, Q Medley, A Debant, and M Streuli. The LAR transmembrane protein tyrosine phosphatase and a coiled-coil LAR-interacting protein co-localize at focal adhesions. *The EMBO Journal*, 14(12):2827–2838, 1995.

[36] Brian D Ackley, Robert J Harrington, Martin L Hudson, Lisa Williams, Cynthia J Kenyon, Andrew D Chisholm, and Yishi Jin. The two isoforms of the *Caenorhabditis elegans* leukocyte-common antigen related receptor tyrosine phosphatase PTP-3 function independently in axon guidance and synapse formation. *Journal of Neuroscience*, 25(33):7517–7528, 2005.

[37] Hidenori Taru and Yishi Jin. The liprin homology domain is essential for the homomeric interaction of syd-2/liprin-α protein in presynaptic assembly. *Journal of Neuroscience*, 31(45):16261–16268, 2011.

[38] Solange Monier, Florence Jollivet, Isabelle Janoueix-Lerosey, Ludger Johannes, and Bruno Goud. Characterization of novel Rab6-interacting proteins involved in endosome-to-TGN transport. *Traffic*, 3(4):289–297, 2002.

[39] Dhananjay A Wagh, Tobias M Rasse, Esther Asan, Alois Hofbauer, Isabell Schwenkert, Heike Dürrbeck, Sigrid Buchner, Marie-Christine Dabauvalle, Manuela Schmidt, Gang Qin, Carolin Wichmann, Robert Kittel, Stephan J Sigrist, and Erich Buchner. Bruchpilot, a protein with homology to ELKS/-CAST, is required for structural integrity and function of synaptic active zones in $Drosophila. Neuron, 49(6) : 833 − −844, 2006.$

[40] Claudia Cases-Langhoff, Britta Voss, Abigail M Garner, Ute Appeltauer, Koji Takei, Stefan Kindler, Rüdiger W Veh, P Camilli De, Eckart D Gundelfinger, and Craig C Garner. Piccolo, a novel 420 kDa protein associated with the presynaptic cytomatrix. *European journal of cell biology*, 69(3):214–223, 1996.

[41] Kristina Langnaese, Constanze Seidenbecher, Heike Wex, Bert Seidel, Kathrin Hartung, Ute Appeltauer, Abigail Garner, Britta Voss, Bettina Mueller, Craig C Garner, and Eckart D Gundelfinger. Protein components of a rat brain synaptic junctional protein preparation. *Molecular brain research*, 42(1):118–122, 1996.

[42] Susanne tom Dieck, Lydia Sanmartí-Vila, Kristina Langnaese, Karin Richter, Stefan Kindler, Antje Soyke, Heike Wex, Karl-Heinz Smalla, Udo Kämpf, Jürgen-Theodor Fränzer, Markus Stumm, Craig C Garner, and Eckart D Gundelfinger. Bassoon, a novel zinc-finger CAG/glutamine-repeat protein selectively localized at the active zone of presynaptic nerve terminals. *The Journal of cell biology*, 142(2):499–509, 1998.

[43] Xiaolu Wang, Mark Kibschull, Michael M Laue, Beate Lichte, Elisabeth Petrasch-Parwez, and Manfred W Kilimann. Aczonin, a 550-kD putative scaffolding protein of presynaptic active zones, shares homology regions with RIM and Bassoon and binds profilin. *The Journal of cell biology*, 147(1):151–162, 1999.

[44] Steven D Fenster, Wook Joon Chung, Rong Zhai, Claudia Cases-Langhoff, Britta Voss, Abigail M Garner, Udo Kaempf, Stefan Kindler, Eckart D Gundelfinger, and Craig C Garner. Piccolo, a presynaptic zinc finger protein structurally related to Bassoon. *Neuron*, 25(1):203–214, 2000.

[45] Stephan J Sigrist and Dietmar Schmitz. Structural and functional plasticity of the cytoplasmic active zone. *Current opinion in neurobiology*, 21(1):144–150, 2011.

[46] Joseph J Bruckner, Scott J Gratz, Jessica K Slind, Richard R Geske, Alexander M Cummings, Samantha E Galindo, Laura K Donohue, and Kate M O'Connor-Giles. Fife, a *Drosophila* Piccolo-RIM homolog, promotes active zone organization and neurotransmitter release. *Journal of Neuroscience*, 32(48):17048–17058, 2012.

[47] Wilko D Altrock, Susanne tom Dieck, Maxim Sokolov, Alexander C Meyer, Albrecht Sigler, Cord Brakebusch, Reinhard Fässler, Karin Richter, Tobias M Boeckers, Heidrun Potschka, Claudia Brandt, Wolfgang Löscher, Dörte Grimberg, Thomas Dresbach, Anne Hempelmann, Hadir Hassan, Detlef Balschun, Julietta U Frey, Johann H Brandstätter, Craig C Garner, Christian Rosenmund, and Eckart D Gundelfinger. Functional inactivation of a fraction of excitatory synapses in mice deficient for the active zone protein bassoon. *Neuron*, 37(5):787–800, 2003.

[48] Thomas Frank, Mark A Rutherford, Nicola Strenzke, Andreas Neef, Tina Pangršič, Darina Khimich, Anna Fejtova, Eckart D Gundelfinger, M Charles Liberman, Benjamin Harke, et al. Bassoon and the synaptic ribbon organize Ca^{2+} channels and vesicles to add release sites and promote refilling. *Neuron*, 68(4):724–738, 2010.

[49] Stefan Hallermann, Anna Fejtova, Hartmut Schmidt, Annika Weyhersmüller, R Angus Silver, Eckart D Gundelfinger, and Jens Eilers. Bassoon speeds vesicle reloading at a central excitatory synapse. *Neuron*, 68(4):710–723, 2010.

[50] Zhizi Jing, Mark A Rutherford, Hideki Takago, Thomas Frank, Anna Fejtova, Darina Khimich, Tobias Moser, and Nicola Strenzke. Disruption of the presynaptic cytoma-

trix protein Bassoon degrades ribbon anchorage, multiquantal release, and sound encoding at the hair cell afferent synapse. *Journal of Neuroscience*, 33(10):4456–4467, 2013.

[51] Alejandro Mendoza Schulz, Zhizi Jing, Juan María Sánchez Caro, Friederike Wetzel, Thomas Dresbach, Nicola Strenzke, Carolin Wichmann, and Tobias Moser. Bassoon-disruption slows vesicle replenishment and induces homeostatic plasticity at a CNS synapse. *The EMBO journal*, 33(5):512–527, 2014.

[52] Daria Davydova, Claudia Marini, Claire King, Julia Klueva, Ferdinand Bischof, Stefano Romorini, Carolina Montenegro-Venegas, Martin Heine, Romy Schneider, Markus S Schröder, et al. Bassoon specifically controls presynaptic P/Q-type Ca^{2+} channels via RIM-binding protein. *Neuron*, 82(1):181–194, 2014.

[53] Sergio Leal-Ortiz, Clarissa L Waites, Ryan Terry-Lorenzo, Pedro Zamorano, Eckart D Gundelfinger, and Craig C Garner. Piccolo modulation of Synapsin 1a dynamics regulates synaptic vesicle exocytosis. *The Journal of cell biology*, 181(5):831–846, 2008.

[54] Konark Mukherjee, Xiaofei Yang, Stefan H Gerber, Hyung-Bae Kwon, Angela Ho, Pablo E Castillo, Xinran Liu, and Thomas C Südhof. Piccolo and bassoon maintain synaptic vesicle clustering without directly participating in vesicle exocytosis. *Proceedings of the National Academy of Sciences*, 107(14):6504–6509, 2010.

[55] Thomas C Südhof. Neurotransmitter release: the last millisecond in the life of a synaptic vesicle. *Neuron*, 80(3):675–690, 2013.

[56] Agnes Nagy, RR Baker, SJ Morris, and VP Whittaker. The preparation and characterization of synaptic vesicles of high purity. *Brain research*, 109(2):285–309, 1976.

[57] WB Huttner, W Schiebler, P Greengard, and P De Camilli. Synapsin I (protein I), a nerve terminal-specific phosphoprotein. III. Its association with synaptic vesicles studied in a highly purified synaptic vesicle preparation. *The Journal of cell biology*, 96(5):1374–1388, 1983.

[58] Shigeo Takamori, Matthew Holt, Katinka Stenius, Edward A Lemke, Mads Grønborg, Dietmar Riedel, Henning Urlaub, Stephan Schenck, Britta Brügger, Philippe Ringler, Shirley A Müller, Burkhard Rammner, Frauke Gräter, Jochen S Hub, Bert L De Groot, Gottfried Mieskes, Yoshinori Moriyama, Jürgen Klingauf, Helmut Grubmüller, John Heuser, Felix Wieland, and Reinhard Jahn. Molecular anatomy of a trafficking organelle. *Cell*, 127(4):831–846, 2006.

[59] Silvio O Rizzoli. Synaptic vesicle recycling: steps and principles. *The EMBO journal*, 33(8):788–822, 2014.

[60] Qun-Fang Wan, Zhen-Yu Zhou, Pratima Thakur, Alejandro Vila, David M Sherry, Roger Janz, and Ruth Heidelberger. SV2 acts via presynaptic calcium to regulate neurotransmitter release. *Neuron*, 66(6):884–895, 2010.

[61] Silvio O Rizzoli and William J Betz. Synaptic vesicle pools. *Nature Reviews Neuroscience*, 6(1):57, 2005.

[62] D Elmqvist and DS Feldman. Calcium dependence of spontaneous acetylcholine release at mammalian motor nerve terminals. *The Journal of physiology*, 181(3):487–497, 1965.

[63] Steven Mennerick and Gary Matthews. Ultrafast exocytosis elicited by calcium current in synaptic terminals of retinal bipolar neurons. *Neuron*, 17(6):1241–1249, 1996.

[64] Guilherme Neves and Leon Lagnado. The kinetics of exocytosis and endocytosis in the synaptic terminal of goldfish retinal bipolar cells. *The Journal of physiology*, 515(1):181–202, 1999.

[65] Ralf Schneggenburger, Alexander C Meyer, and Erwin Neher. Released fraction and total size of a pool of immediately available transmitter quanta at a calyx synapse. *Neuron*, 23(2):399–409, 1999.

[66] Ricardo Delgado, Carlos Maureira, Carolina Oliva, Yoshiaki Kidokoro, and Pedro Labarca. Size of vesicle pools, rates of mobilization, and recycling at neuromuscular synapses of a *Drosophila* mutant, *shibire*. *Neuron*, 28(3):941–953, 2000.

[67] David A Richards, Cristina Guatimosim, Silvio O Rizzoli, and William J Betz. Synaptic vesicle pools at the frog neuromuscular junction. *Neuron*, 39(3):529–541, 2003.

[68] Hiroshi Kuromi and Yoshi Kidokoro. Two synaptic vesicle pools, vesicle recruitment and replenishment of pools at the *Drosophila* neuromuscular junction. *Journal of neurocytology*, 32(5-8):551–565, 2003.

[69] Nobutoshi Harata, Timothy A Ryan, Stephen J Smith, JoAnn Buchanan, and Richard W Tsien. Visualizing recycling synaptic vesicles in hippocampal neurons by FM 1-43 photoconversion. *Proceedings of the National Academy of Sciences*, 98(22):12748–12753, 2001.

[70] RPJ De Lange, ADG De Roos, and JGG Borst. Two modes of vesicle recycling in the rat calyx of held. *Journal of Neuroscience*, 23(31):10164–10173, 2003.

[71] JE Heuser and TS Reese. Evidence for recycling of synaptic vesicle membrane during transmitter release at the frog neuromuscular junction. *The Journal of cell biology*, 57(2):315–344, 1973.

[72] Kohji Takei, Olaf Mundigl, Laurie Daniell, and Pietro De Camilli. The synaptic vesicle cycle: a single vesicle budding step involving clathrin and dynamin. *The Journal of cell biology*, 133(6):1237–1250, 1996.

[73] Matthew B Dalva, Andrew C McClelland, and Matthew S Kayser. Cell adhesion molecules: signalling functions at the synapse. *Nature Reviews Neuroscience*, 8(3):206, 2007.

[74] Takeshi Yagi and Masatoshi Takeichi. Cadherin superfamily genes: functions, genomic organization, and neurologic diversity. *Genes & development*, 14(10):1169–1180, 2000.

[75] Alice M Elste and Deanna L Benson. Structural basis for developmentally regulated changes in cadherin function at synapses. *Journal of Comparative Neurology*, 495(3):324–335, 2006.

[76] Mika Shapira, R Grace Zhai, Thomas Dresbach, Tal Bresler, Viviana I Torres, Eckart D Gundelfinger, Noam E Ziv, and Craig C Garner. Unitary assembly of presynaptic active zones from Piccolo-Bassoon transport vesicles. *Neuron*, 38(2):237–252, 2003.

[77] James D Jontes, Michelle R Emond, and Stephen J Smith. *In vivo* trafficking and targeting of N-cadherin to nascent presynaptic terminals. *Journal of Neuroscience*, 24(41):9027–9034, 2004.

[78] A Stan, KN Pielarski, T Brigadski, N Wittenmayer, O Fedorchenko, A Gohla, V Lessmann, T Dresbach, and K Gottmann. Essential cooperation of N-cadherin and neuroligin-1 in the transsynaptic control of vesicle accumulation. *Proceedings of the National Academy of Sciences*, 107(24):11116–11121, 2010.

[79] Thai Nguyen and Thomas C Südhof. Binding properties of neuroligin 1 and neurexin 1β reveal function as heterophilic cell adhesion molecules. *Journal of Biological Chemistry*, 272(41):26032–26039, 1997.

[80] Ji-Ying Song, Konstantin Ichtchenko, Thomas C Südhof, and Nils Brose. Neuroligin 1 is a postsynaptic cell-adhesion molecule of excitatory synapses. *Proceedings of the National Academy of Sciences*, 96(3):1100–1105, 1999.

[81] Ethan R Graf, XueZhao Zhang, Shan-Xue Jin, Michael W Linhoff, and Ann Marie Craig. Neurexins induce differentiation of GABA and glutamate postsynaptic specializations via neuroligins. *Cell*, 119(7):1013–1026, 2004.

[82] Frédérique Varoqueaux, Stéphane Jamain, and Nils Brose. Neuroligin 2 is exclusively localized to inhibitory synapses. *European journal of cell biology*, 83(9):449–456, 2004.

[83] Elaine C Budreck and Peter Scheiffele. Neuroligin-3 is a neuronal adhesion protein at GABAergic and glutamatergic synapses. *European Journal of Neuroscience*, 26(7):1738–1748, 2007.

[84] Ml Irie, Y Hata, M Takeuchi, K Ichtchenko, A Toyoda, K Hirao, Y Takai, TW Rosahl, and TC Südhof. Binding of neuroligins to PSD-95. *Science*, 277(5331):1511–1515, 1997.

[85] Konstantin Ichtchenko, Yutaka Hata, Thai Nguyen, Beate Ullrich, Markus Missler, Carolyn Moomaw, and Thomas C Südhof. Neuroligin 1: a splice site-specific ligand for β-neurexins. *Cell*, 81(3):435–443, 1995.

[86] Peter Scheiffele, Jinhong Fan, Jenny Choih, Richard Fetter, and Tito Serafini. Neuroligin expressed in nonneuronal cells triggers presynaptic development in contacting axons. *Cell*, 101(6):657–669, 2000.

[87] Camin Dean, Francisco G Scholl, Jenny Choih, Shannon DeMaria, James Berger, Ehud Isacoff, and Peter Scheiffele. Neurexin mediates the assembly of presynaptic terminals. *Nature neuroscience*, 6(7):708, 2003.

[88] Joshua N Levinson and Alaa El-Husseini. Building excitatory and inhibitory synapses: balancing neuroligin partnerships. *Neuron*, 48(2):171–174, 2005.

[89] Rong Grace Zhai, Hagit Vardinon-Friedman, Claudia Cases-Langhoff, Birgit Becker, Eckart D Gundelfinger, Noam E Ziv, and Craig C Garner. Assembling the presynaptic active zone: a characterization of an active zone precursor vesicle. *Neuron*, 29(1):131–143, 2001.

[90] J-H Tao-Cheng. Ultrastructural localization of active zone and synaptic vesicle proteins in a preassembled multi-vesicle transport aggregate. *Neuroscience*, 150(3):575–584, 2007.

[91] Richard Fairless, Henriette Masius, Astrid Rohlmann, Katharina Heupel, Mohiuddin Ahmad, Carsten Reissner, Thomas Dresbach, and Markus Missler. Polarized targeting of neurexins to synapses is regulated by their C-terminal sequences. *Journal of Neuroscience*, 28(48):12969–12981, 2008.

[92] Christoph Maas, Viviana I Torres, Wilko D Altrock, Sergio Leal-Ortiz, Dhananjay Wagh, Ryan T Terry-Lorenzo, Anna Fejtova, Eckart D Gundelfinger, Noam E Ziv, and Craig C Garner. Formation of Golgi-derived active zone precursor vesicles. *Journal of Neuroscience*, 32(32):11095–11108, 2012.

[93] Thomas Dresbach, Viviana Torres, Nina Wittenmayer, Wilko D Altrock, Pedro Zamorano, Werner Zuschratter, Ralph Nawrotzki, Noam E Ziv, Craig C Garner,

and Eckart D Gundelfinger. Assembly of active zone precursor vesicles OBLIG-ATORY TRAFFICKING OF PRESYNAPTIC CYTOMATRIX PROTEINS BAS-SOON AND PICCOLO VIA A TRANS-GOLGI COMPARTMENT. *Journal of Biological Chemistry*, 281(9):6038–6047, 2006.

[94] Noam E Ziv and Craig C Garner. Cellular and molecular mechanisms of presynaptic assembly. *Nature Reviews Neuroscience*, 5(5):385, 2004.

[95] Shasta L Sabo, Raquel A Gomes, and A Kimberley McAllister. Formation of presynaptic terminals at predefined sites along axons. *Journal of Neuroscience*, 26(42):10813–10825, 2006.

[96] Susanne E Ahmari, JoAnn Buchanan, and Stephen J Smith. Assembly of presynaptic active zones from cytoplasmic transport packets. *Nature neuroscience*, 3(5):445, 2000.

[97] Michela Matteoli, Kohji Takei, Mark S Perin, Thomas C Südhof, and Pietro De Camilli. Exo-endocytotic recycling of synaptic vesicles in developing processes of cultured hippocampal neurons. *The Journal of cell biology*, 117(4):849–861, 1992.

[98] Kajetan Kraszewski, Olaf Mundigl, Laurie Daniell, Claudia Verderio, Michela Matteoli, and Pietro De Camilli. Synaptic vesicle dynamics in living cultured hippocampal neurons visualized with CY3-conjugated antibodies directed against the lumenal domain of synaptotagmin. *Journal of Neuroscience*, 15(6):4328–4342, 1995.

[99] Shasta L Sabo and A Kimberley McAllister. Mobility and cycling of synaptic protein–containing vesicles in axonal growth cone filopodia. *Nature neuroscience*, 6(12):1264, 2003.

[100] Noam E Ziv and Stephen J Smith. Evidence for a role of dendritic filopodia in synaptogenesis and spine formation. *Neuron*, 17(1):91–102, 1996.

[101] Philip Washbourne, Jennie E Bennett, and A Kimberley McAllister. Rapid recruitment of NMDA receptor transport packets to nascent synapses. *Nature neuroscience*, 5(8):751, 2002.

[102] Hagit Vardinon Friedman, Tal Bresler, Craig C Garner, and Noam E Ziv. Assembly of new individual excitatory synapses: time course and temporal order of synaptic molecule recruitment. *Neuron*, 27(1):57–69, 2000.

[103] Luke AD Bury and Shasta L Sabo. Coordinated trafficking of synaptic vesicle and active zone proteins prior to synapse formation. *Neural development*, 6(1):24, 2011.

[104] Ye E Wu, Lin Huo, Celine I Maeder, Wei Feng, and Kang Shen. The balance between capture and dissociation of presynaptic proteins controls the spatial distribution of synapses. *Neuron*, 78(6):994–1011, 2013.

[105] Stefan R Krueger, Annette Kolar, and Reiko Maki Fitzsimonds. The presynaptic release apparatus is functional in the absence of dendritic contact and highly mobile within isolated axons. *Neuron*, 40(5):945–957, 2003.

[106] Arjuna Ratnayaka, Vincenzo Marra, Tiago Branco, and Kevin Staras. Extrasynaptic vesicle recycling in mature hippocampal neurons. *Nature communications*, 2:531, 2011.

[107] Christopher D Hazuka, Davide L Foletti, Shu-Chan Hsu, Yun Kee, F Woodward Hopf, and Richard H Scheller. The sec6/8 complex is located at neurite outgrowth and axonal synapse-assembly domains. *Journal of Neuroscience*, 19(4):1324–1334, 1999.

[108] Linda J Pike. Rafts defined: a report on the keystone symposium on lipid rafts and cell function. *Journal of lipid research*, 47(7):1597–1598, 2006.

[109] Shingo Suzuki, Kazuyuki Kiyosue, Shunsuke Hazama, Akihiko Ogura, Megumi Kashihara, Tomoko Hara, Hisatsugu Koshimizu, and Masami Kojima. Brain-derived neurotrophic factor regulates cholesterol metabolism for synapse development. *Journal of Neuroscience*, 27(24):6417–6427, 2007.

[110] Oswald Steward and Paula M Falk. Protein-synthetic machinery at postsynaptic sites during synaptogenesis: a quantitative study of the association between polyribosomes and developing synapses. *Journal of Neuroscience*, 6(2):412–423, 1986.

[111] Xiao-Bo Liu, Alberto Muñoz, and Edward G Jones. Changes in subcellular localization of metabotropic glutamate receptor subtypes during postnatal development of mouse thalamus. *Journal of Comparative Neurology*, 395(4):450–465, 1998.

[112] Nathalie Sans, Kate Prybylowski, Ronald S Petralia, Kai Chang, Ya-Xian Wang, Claudia Racca, Stefano Vicini, and Robert J Wenthold. NMDA receptor trafficking through an interaction between PDZ proteins and the exocyst complex. *Nature cell biology*, 5(6):520, 2003.

[113] Philip Washbourne, Xiao-Bo Liu, Edward G Jones, and A Kimberley McAllister. Cycling of NMDA receptors during trafficking in neurons before synapse formation. *Journal of Neuroscience*, 24(38):8253–8264, 2004.

[114] Clarissa L Waites, Ann Marie Craig, and Craig C Garner. Mechanisms of vertebrate synaptogenesis. *Annu. Rev. Neurosci.*, 28:251–274, 2005.

[115] Kimberly Gerrow, Stefano Romorini, Shahin M Nabi, Michael A Colicos, Carlo Sala, and Alaa El-Husseini. A preformed complex of postsynaptic proteins is involved in excitatory synapse development. *Neuron*, 49(4):547–562, 2006.

[116] James W Hinds and Patricia L Hinds. Synapse formation in the mouse olfactory bulb quantitative studies. *Journal of Comparative Neurology*, 169(1):15–40, 1976.

[117] Mary E Blue and John G Parnavelas. The formation and maturation of synapses in the visual cortex of the rat. II. Quantitative analysis. *Journal of neurocytology*, 12(4):697–712, 1983.

[118] John C Fiala, Marcia Feinberg, Viktor Popov, and Kristen M Harris. Synaptogenesis via dendritic filopodia in developing hippocampal area CA1. *Journal of Neuroscience*, 18(21):8900–8911, 1998.

[119] Liqun Luo. Actin cytoskeleton regulation in neuronal morphogenesis and structural plasticity. *Annual review of cell and developmental biology*, 18(1):601–635, 2002.

[120] Lukas C Kapitein and Casper C Hoogenraad. Which way to go? cytoskeletal organization and polarized transport in neurons. *Molecular and Cellular Neuroscience*, 46(1):9–20, 2011.

[121] Reinhard L Friede and T Samorajski. Axon caliber related to neurofilaments and microtubules in sciatic nerve fibers of rats and mice. *The Anatomical Record*, 167(4):379–387, 1970.

[122] Osamu Ohara, Yoshinari Gahara, Toshihiko Miyake, Hiroshi Teraoka, and Tadahisa Kitamura. Neurofilament deficiency in quail caused by nonsense mutation in neurofilament-l gene. *The Journal of Cell Biology*, 121(2):387–395, 1993.

[123] Qinzhang Zhu, Sébastien Couillard-Després, and Jean-Pierre Julien. Delayed maturation of regenerating myelinated axons in mice lacking neurofilaments. *Experimental neurology*, 148(1):299–316, 1997.

[124] Phillip R Gordon-Weeks and Alyson E Fournier. Neuronal cytoskeleton in synaptic plasticity and regeneration. *Journal of neurochemistry*, 129(2):206–212, 2014.

[125] Richard Eva and James Fawcett. Integrin signalling and traffic during axon growth and regeneration. *Current opinion in neurobiology*, 27:179–185, 2014.

[126] Wim Robberecht and Thomas Philips. The changing scene of amyotrophic lateral sclerosis. *Nature Reviews Neuroscience*, 14(4):248, 2013.

[127] Hans Zempel, Julia Luedtke, Yatender Kumar, Jacek Biernat, Hana Dawson, Eckhard Mandelkow, and Eva-Maria Mandelkow. Amyloid-β oligomers induce synaptic damage via Tau-dependent microtubule severing by TTLL6 and spastin. *The EMBO journal*, 32(22):2920–2937, 2013.

[128] Anna Akhmanova and Michel O Steinmetz. Tracking the ends: a dynamic protein network controls the fate of microtubule tips. *Nature reviews Molecular cell biology*, 9(4):309, 2008.

[129] Tim Mitchison and Marc Kirschner. Dynamic instability of microtubule growth. *nature*, 312(5991):237, 1984.

[130] Marc Kirschner and Tim Mitchison. Beyond self-assembly: from microtubules to morphogenesis. *Cell*, 45(3):329–342, 1986.

[131] Srinivas Honnappa, Susana Montenegro Gouveia, Anke Weisbrich, Fred F Damberger, Neel S Bhavesh, Hatim Jawhari, Ilya Grigoriev, Frederik JA van Rijssel, Ruben M Buey, Aleksandra Lawera, Ilian Jelesarov, Fritz K Winkler, Kurt Wüthrich, Anna Akhmanova, and Michel O Steinmetz. An EB1-binding motif acts as a microtubule tip localization signal. *Cell*, 138(2):366–376, 2009.

[132] Kai Jiang, Shasha Hua, Renu Mohan, Ilya Grigoriev, Kah Wai Yau, Qingyang Liu, Eugene A Katrukha, AF Maarten Altelaar, Albert JR Heck, Casper C Hoogenraad, and Anna Akhmanova. Microtubule minus-end stabilization by polymerization-driven CAMSAP deposition. *Developmental cell*, 28(3):295–309, 2014.

[133] Paul R Burton and Jeffrey L Paige. Polarity of axoplasmic microtubules in the olfactory nerve of the frog. *Proceedings of the National Academy of Sciences*, 78(5):3269–3273, 1981.

[134] Peter W Baas, Jeffrey S Deitch, Mark M Black, and Gary A Banker. Polarity orientation of microtubules in hippocampal neurons: uniformity in the axon and nonuniformity in the dendrite. *Proceedings of the National Academy of Sciences*, 85(21):8335–8339, 1988.

[135] Tatiana Stepanova, Jenny Slemmer, Casper C Hoogenraad, Gideon Lansbergen, Bjorn Dortland, Chris I De Zeeuw, Frank Grosveld, Gert van Cappellen, Anna Akhmanova, and Niels Galjart. Visualization of microtubule growth in cultured neurons via the use of EB3-GFP (end-binding protein 3-green fluorescent protein). *Journal of Neuroscience*, 23(7):2655–2664, 2003.

[136] Alex C Kwan, Daniel A Dombeck, and Watt W Webb. Polarized microtubule arrays in apical dendrites and axons. *Proceedings of the National Academy of Sciences*, 105(32):11370–11375, 2008.

[137] Tatjana Kleele, Petar Marinković, Philip R Williams, Sina Stern, Emily E Weigand, Peter Engerer, Ronald Naumann, Jana Hartmann, Rosa M Karl, Frank Bradke, Derron Bishop, Jochen Herms, Arthur Konnerth, Martin Kerschensteiner, Leanne Godinho, and Thomas Misgeld. An assay to image neuronal microtubule dynamics in mice. *Nature communications*, 5:4827, 2014.

[138] Rodolfo J Rivas and Mary E Hatten. Motility and cytoskeletal organization of migrating cerebellar granule neurons. *Journal of Neuroscience*, 15(2):981–989, 1995.

[139] Oscar Marín, Manuel Valiente, Xuecai Ge, and Li-Huei Tsai. Guiding neuronal cell migrations. *Cold Spring Harbor perspectives in biology*, 2(2):a001834, 2010.

[140] Jonathan A Cooper. Mechanisms of cell migration in the nervous system. *J Cell Biol*, 202(5):725–734, 2013.

[141] Alfredo Cáceres, Bing Ye, and Carlos G Dotti. Neuronal polarity: demarcation, growth and commitment. *Current opinion in cell biology*, 24(4):547–553, 2012.

[142] Erik W Dent, Stephanie L Gupton, and Frank B Gertler. The growth cone cytoskeleton in axon outgrowth and guidance. *Cold Spring Harbor perspectives in biology*, 3(3):a001800, 2011.

[143] Kevin C Flynn, Farida Hellal, Dorothee Neukirchen, Sonja Jacob, Sabina Tahirovic, Sebastian Dupraz, Sina Stern, Boyan K Garvalov, Christine Gurniak, Alisa E Shaw, Liane Meyn, Roland Wedlich-Söldner, James R Bamburg, J Victor Small, Walter Witke, and Frank Bradke. ADF/cofilin-mediated actin retrograde flow directs neurite formation in the developing brain. *Neuron*, 76(6):1091–1107, 2012.

[144] Carlos G Dotti, Christopher A Sullivan, and Gary A Banker. The establishment of polarity by hippocampal neurons in culture. *Journal of Neuroscience*, 8(4):1454–1468, 1988.

[145] Harald Witte, Dorothee Neukirchen, and Frank Bradke. Microtubule stabilization specifies initial neuronal polarization. *J Cell Biol*, 180(3):619–632, 2008.

[146] Takao Nakata and Nobutaka Hirokawa. Microtubules provide directional cues for polarized axonal transport through interaction with kinesin motor head. *The Journal of cell biology*, 162(6):1045–1055, 2003.

[147] Takao Nakata, Shinsuke Niwa, Yasushi Okada, Franck Perez, and Nobutaka Hirokawa. Preferential binding of a kinesin-1 motor to GTP-tubulin–rich microtubules underlies polarized vesicle transport. *The Journal of cell biology*, 194(2):245–255, 2011.

[148] Daniel M Suter and Kyle E Miller. The emerging role of forces in axonal elongation. *Progress in neurobiology*, 94(2):91–101, 2011.

[149] Wen Lu, Pangkong Fox, Margot Lakonishok, Michael W Davidson, and Vladimir I Gelfand. Initial neurite outgrowth in *Drosophila* neurons is driven by kinesin-powered microtubule sliding. *Current biology*, 23(11):1018–1023, 2013.

[150] Douglas H Roossien, Phillip Lamoureux, and Kyle E Miller. Cytoplasmic dynein pushes the cytoskeletal meshwork forward during axonal elongation. *J Cell Sci*, 127(16):3593–3602, 2014.

[151] Nobutaka Hirokawa, Shinsuke Niwa, and Yosuke Tanaka. Molecular motors in neurons: transport mechanisms and roles in brain function, development, and disease. *Neuron*, 68(4):610–638, 2010.

[152] Sandra Maday, Alison E Twelvetrees, Armen J Moughamian, and Erika LF Holzbaur. Axonal transport: cargo-specific mechanisms of motility and regulation. *Neuron*, 84(2):292–309, 2014.

[153] EG Gray. Presynaptic microtubules and their association with synaptic vesicles. *Proc. R. Soc. Lond. B*, 190(1100):369–372, 1975.

[154] Margaret M Bird. Microtubule-synaptic vesicle associations in cultured rat spinal cord neurons. *Cell and tissue research*, 168(1):101–115, 1976.

[155] Greg R Phillips, Jeffrey K Huang, Yun Wang, Hidekazu Tanaka, Lawrence Shapiro, Wandong Zhang, Wei-Song Shan, Kirsten Arndt, Marcus Frank, Ronald E Gordon, Mary Ann Gawinowicz, Yingming Zhao, and David R Colman. The presynaptic particle web: ultrastructure, composition, dissolution, and reconstitution. *Neuron*, 32(1):63–77, 2001.

[156] R Grace Zhai and Hugo J Bellen. The architecture of the active zone in the presynaptic nerve terminal. *Physiology*, 19(5):262–270, 2004.

[157] Marco Morciano, Tobias Beckhaus, Michael Karas, Herbert Zimmermann, and Walter Volknandt. The proteome of the presynaptic active zone: from docked synaptic vesicles to adhesion molecules and maxi-channels. *Journal of neurochemistry*, 108(3):662–675, 2009.

[158] Melanie Laßek, Jens Weingarten, and Walter Volknandt. The proteome of the murine presynaptic active zone. *Proteomes*, 2(2):243–257, 2014.

[159] William P Bartlett and Gary A Banker. An electron microscopic study of the development of axons and dendrites by hippocampal neurons in culture. I. Cells which develop without intercellular contacts. *Journal of Neuroscience*, 4(8):1944–1953, 1984.

[160] Yanping Yan and Kendal Broadie. *In vivo* assay of presynaptic microtubule cytoskeleton dynamics in *Drosophila*. *Journal of neuroscience methods*, 162(1-2):198–205, 2007.

[161] Catherine Pawson, Benjamin A Eaton, and Graeme W Davis. Formin-dependent synaptic growth: evidence that Dlar signals via Diaphanous to modulate synaptic actin and dynamic pioneer microtubules. *Journal of Neuroscience*, 28(44):11111–11123, 2008.

[162] Thomas Hummel, Karin Krukkert, Jack Roos, Graeme Davis, and Christian Klämbt. *Drosophila* Futsch/22C10 is a MAP1B-like protein required for dendritic and axonal development. *Neuron*, 26(2):357–370, 2000.

[163] Simon Lepicard, Bénédicte Franco, Frédéric de Bock, and Marie-Laure Parmentier. A presynaptic role of microtubule-associated protein 1/Futsch in *Drosophila*: regulation of active zone number and neurotransmitter release. *Journal of Neuroscience*, 34(20):6759–6771, 2014.

[164] Jack Roos, Thomas Hummel, Norman Ng, Christian Klämbt, and Graeme W Davis. *Drosophila* Futsch regulates synaptic microtubule organization and is necessary for synaptic growth. *Neuron*, 26(2):371–382, 2000.

[165] Vinay K Godena, Giulia Romano, Maurizio Romano, Chiara Appocher, Raffaella Klima, Emanuele Buratti, Francisco E Baralle, and Fabian Feiguin. TDP-43 regulates *Drosophila* neuromuscular junctions growth by modulating Futsch/MAP1B levels and synaptic microtubules organization. *PloS one*, 6(3):e17808, 2011.

[166] Bl J Schnapp and TS Reese. Cytoplasmic structure in rapid-frozen axons. *The Journal of Cell Biology*, 94(3):667–669, 1982.

[167] Nobutaka Hirokawa, Kenji Sobue, Keiko Kanda, Akihiro Harada, and Hiroshi Yorifuji. The cytoskeletal architecture of the presynaptic terminal and molecular structure of synapsin 1. *The Journal of cell biology*, 108(1):111–126, 1989.

[168] T Gotow, K Miyaguchi, and PH Hashimoto. Cytoplasmic architecture of the axon terminal: filamentous strands specifically associated with synaptic vesicles. *Neuroscience*, 40(2):587–598, 1991.

[169] Atsuko Honda, Mitsunori Yamada, Hideo Saisu, Hitoshi Takahashi, Kazuhiro J Mori, and Teruo Abe. Direct, Ca^{2+}-dependent interaction between Tubulin and Synaptotagmin I, A POSSIBLE MECHANISM FOR ATTACHING SYNAPTIC VESICLES TO MICROTUBULES. *Journal of Biological Chemistry*, 277(23):20234–20242, 2002.

[170] Xindao Hu, Chris Viesselmann, Sookin Nam, Elliott Merriam, and Erik W Dent. Activity-dependent dynamic microtubule invasion of dendritic spines. *Journal of Neuroscience*, 28(49):13094–13105, 2008.

[171] Jacek Jaworski, Lukas C Kapitein, Susana Montenegro Gouveia, Bjorn R Dortland, Phebe S Wulf, Ilya Grigoriev, Paola Camera, Samantha A Spangler, Paola Di Stefano, Jeroen Demmers, Harm Krugers, Paola Defilipi, Anna Akhmanova, and Casper C Hoogenraad. Dynamic microtubules regulate dendritic spine morphology and synaptic plasticity. *Neuron*, 61(1):85–100, 2009.

[172] Elliott B Merriam, Matthew Millette, Derek C Lumbard, Witchuda Saengsawang, Thomas Fothergill, Xindao Hu, Lotfi Ferhat, and Erik W Dent. Synaptic regulation of microtubule dynamics in dendritic spines by calcium, F-actin, and drebrin. *Journal of Neuroscience*, 33(42):16471–16482, 2013.

[173] Kwan Y Chan and Ann H Bunt. An association between mitochondria and microtubules in synaptosomes and axon terminals of cerebral cortex. *Journal of neurocytology*, 7(2):137–143, 1978.

[174] F Hajos, A Csillag, and M Kalman. The morphology of microtubules in incubated synaptosomes. Effect of low temperature and vinblastine. *Experimental brain research*, 35(2):387–393, 1979.

[175] Guy A Perkins, Jonathan Tjong, Joshua M Brown, Patrick H Poquiz, Raymond T Scott, Douglas R Kolson, Mark H Ellisman, and George A Spirou. The microarchitecture of mitochondria at active zones: electron tomography reveals novel anchoring scaffolds and cristae structured for high-rate metabolism. *Journal of Neuroscience*, 30(3):1015–1026, 2010.

[176] Malkolm Graffe, David Zenisek, and Justin W Taraska. A marginal band of microtubules transports and organizes mitochondria in retinal bipolar synaptic terminals. *The Journal of general physiology*, 146(1):109–117, 2015.

[177] Laurent Blanchoin, Rajaa Boujemaa-Paterski, Cécile Sykes, and Julie Plastino. Actin dynamics, architecture, and mechanics in cell motility. *Physiological reviews*, 94(1):235–263, 2014.

[178] Ke Xu, Guisheng Zhong, and Xiaowei Zhuang. Actin, spectrin, and associated proteins form a periodic cytoskeletal structure in axons. *Science*, 339(6118):452–456, 2013.

[179] Elisa D'Este, Dirk Kamin, Fabian Göttfert, Ahmed El-Hady, and Stefan W Hell. STED nanoscopy reveals the ubiquity of subcortical cytoskeleton periodicity in living neurons. *Cell reports*, 10(8):1246–1251, 2015.

[180] Archan Ganguly, Yong Tang, Lina Wang, Kelsey Ladt, Jonathan Loi, Bénédicte Dargent, Christophe Leterrier, and Subhojit Roy. A dynamic formin-dependent deep F-actin network in axons. *Journal of Cell Biology*, pages jcb–201506110, 2015.

[181] Marco B Rust and Tanja Maritzen. Relevance of presynaptic actin dynamics for synapse function and mouse behavior. *Experimental cell research*, 335(2):165–171, 2015.

[182] Poh Hui Chia, Maulik R Patel, and Kang Shen. NAB-1 instructs synapse assembly by

linking adhesion molecules and F-actin to active zone proteins. *Nature neuroscience*, 15(2):234, 2012.

[183] Poh Hui Chia, Baoyu Chen, Pengpeng Li, Michael K Rosen, and Kang Shen. Local F-actin network links synapse formation and axon branching. *Cell*, 156(1):208–220, 2014.

[184] Wandong Zhang and Deanna L Benson. Stages of synapse development defined by dependence on f-actin. *Journal of Neuroscience*, 21(14):5169–5181, 2001.

[185] Shernaz X Bamji, Kazuhiro Shimazu, Nikole Kimes, Joerg Huelsken, Walter Birchmeier, Bai Lu, and Louis F Reichardt. Role of β-catenin in synaptic vesicle localization and presynaptic assembly. *Neuron*, 40(4):719–731, 2003.

[186] Martin Bähler, Fabio Benfenati, Flavia Valtorta, Andrew J Czernik, and Paul Greengard. Characterization of synapsin I fragments produced by cysteine-specific cleavage: a study of their interactions with F-actin. *The Journal of cell biology*, 108(5):1841–1849, 1989.

[187] F Cesca, P Baldelli, F Valtorta, and F Benfenati. The synapsins: key actors of synapse function and plasticity. *Progress in neurobiology*, 91(4):313–348, 2010.

[188] Clarissa L Waites, Sergio A Leal-Ortiz, Till FM Andlauer, Stefan J Sigrist, and Craig C Garner. Piccolo regulates the dynamic assembly of presynaptic F-actin. *Journal of Neuroscience*, 31(40):14250–14263, 2011.

[189] Harukata Miki, Mitsutoshi Setou, Kiyofumi Kaneshiro, and Nobutaka Hirokawa. All kinesin superfamily protein, kif, genes in mouse and human. *Proceedings of the National Academy of Sciences*, 98(13):7004–7011, 2001.

[190] Hiroyuki Aizawa, Yoko Sekine, Reiko Takemura, Zhizeng Zhang, Masaomi Nangaku, and Nobutaka Hirokawa. Kinesin family in murine central nervous system. *The Journal of cell biology*, 119(5):1287–1296, 1992.

[191] Nobutaka Hirokawa and Yasuko Noda. Intracellular transport and kinesin superfamily proteins, KIFs: structure, function, and dynamics. *Physiological reviews*, 88(3):1089–1118, 2008.

[192] Carolyn J Lawrence, R Kelly Dawe, Karen R Christie, Don W Cleveland, Scott C Dawson, Sharyn A Endow, Lawrence SB Goldstein, Holly V Goodson, Nobutaka Hirokawa, Jonathon Howard, et al. A standardized kinesin nomenclature. *The Journal of cell biology*, 167(1):19–22, 2004.

[193] Faneng Sun, Chuanmei Zhu, Ram Dixit, and Valeria Cavalli. Sunday Driver/JIP3 binds kinesin heavy chain directly and enhances its motility. *The EMBO Journal*, 30(16):3416–3429, 2011.

[194] Yoshimitsu Kanai, Yasushi Okada, Yosuke Tanaka, Akihiro Harada, Sumio Terada, and Nobutaka Hirokawa. KIF5C, a novel neuronal kinesin enriched in motor neurons. *Journal of Neuroscience*, 20(17):6374–6384, 2000.

[195] Dara S Friedman and Ronald D Vale. Single-molecule analysis of kinesin motility reveals regulation by the cargo-binding tail domain. *Nature cell biology*, 1(5):293, 1999.

[196] David D Hackney and Maryanne F Stock. Kinesin's iak tail domain inhibits initial microtubule-stimulated ADP release. *Nature Cell Biology*, 2(5):257, 2000.

[197] Kristen A Dietrich, Charles V Sindelar, Paul D Brewer, Kenneth H Downing, Christine R Cremo, and Sarah E Rice. The kinesin-1 motor protein is regulated by a direct interaction of its head and tail. *Proceedings of the National Academy of Sciences*, 105(26):8938–8943, 2008.

[198] David D Hackney, Nahyeon Baek, and Avin C Snyder. Half-site inhibition of dimeric kinesin head domains by monomeric tail domains. *Biochemistry*, 48(15):3448–3456, 2009.

[199] Yao Liang Wong, Kristen A Dietrich, Nariman Naber, Roger Cooke, and Sarah E Rice. The kinesin-1 tail conformationally restricts the nucleotide pocket. *Biophysical Journal*, 96(7):2799–2807, 2009.

[200] Hung Yi Kristal Kaan, David D Hackney, and Frank Kozielski. The structure of the kinesin-1 motor-tail complex reveals the mechanism of autoinhibition. *Science*, 333(6044):883–885, 2011.

[201] Qian Cai, Ping-Yue Pan, and Zu-Hang Sheng. Syntabulin–kinesin-1 family member 5B-mediated axonal transport contributes to activity-dependent presynaptic assembly. *Journal of Neuroscience*, 27(27):7284–7296, 2007.

[202] T Lynne Blasius, Dawen Cai, Gloria T Jih, Christopher P Toret, and Kristen J Verhey. Two binding partners cooperate to activate the molecular motor kinesin-1. *The Journal of cell biology*, 176(1):11–17, 2007.

[203] Takanori Kawano, Masahiko Araseki, Yoichi Araki, Masataka Kinjo, Tohru Yamamoto, and Toshiharu Suzuki. A small peptide sequence is sufficient for initiating kinesin-1 activation through part of TPR region of KLC1. *Traffic*, 13(6):834–848, 2012.

[204] Kristen J Verhey and Jennetta W Hammond. Traffic control: regulation of kinesin motors. *Nature reviews Molecular cell biology*, 10(11):765, 2009.

[205] Meng-meng Fu and Erika LF Holzbaur. Integrated regulation of motor-driven or-

ganelle transport by scaffolding proteins. *Trends in cell biology*, 24(10):564–574, 2014.

[206] Qingning Su, Qian Cai, Claudia Gerwin, Carolyn L Smith, and Zu-Hang Sheng. Syntabulin is a microtubule-associated protein implicated in syntaxin transport in neurons. *Nature cell biology*, 6(10):941, 2004.

[207] John Jia En Chua, Eugenia Butkevich, Josephine M Worseck, Maike Kittelmann, Mads Grønborg, Elmar Behrmann, Ulrich Stelzl, Nathan J Pavlos, Maciej M Lalowski, Stefan Eimer, Erich E Wanker, Dieter Robert Klopfenstein, and Reinhard Jahn. Phosphorylation-regulated axonal dependent transport of syntaxin 1 is mediated by a kinesin-1 adapter. *Proceedings of the National Academy of Sciences*, 109(15):5862–5867, 2012.

[208] Russell J Diefenbach, Eve Diefenbach, Mark W Douglas, and Anthony L Cunningham. The heavy chain of conventional kinesin interacts with the SNARE proteins SNAP25 and SNAP23. *Biochemistry*, 41(50):14906–14915, 2002.

[209] April M Morton, Anthony L Cunningham, and Russell J Diefenbach. Kinesin-1 plays a role in transport of SNAP-25 to the plasma membrane. *Biochemical and biophysical research communications*, 391(1):388–393, 2010.

[210] Frédéric J Hoerndli, Dane A Maxfield, Penelope J Brockie, Jerry E Mellem, Erica Jensen, Rui Wang, David M Madsen, and Andres V Maricq. Kinesin-1 regulates synaptic strength by mediating the delivery, removal, and redistribution of AMPA receptors. *Neuron*, 80(6):1421–1437, 2013.

[211] R Sato-Yoshitake, H Yorifuji, M Inagaki, and N Hirokawa. The phosphorylation of kinesin regulates its binding to synaptic vesicles. *Journal of Biological Chemistry*, 267(33):23930–23936, 1992.

[212] Dana Thyra Byrd, Masato Kawasaki, Mercy Walcoff, Naoki Hisamoto, Kunihiro Matsumoto, and Yishi Jin. UNC-16, a JNK-signaling scaffold protein, regulates vesicle transport in *C.elegans*. *Neuron*, 32(5):787–800, 2001.

[213] Hirofumi Toda, Hiroaki Mochizuki, Rafael Flores, Rebecca Josowitz, Tatiana B Krasieva, Vickie J LaMorte, Emiko Suzuki, Joseph G Gindhart, Katsuo Furukubo-Tokunaga, and Toshifumi Tomoda. UNC-51/ATG1 kinase regulates axonal transport by mediating motor–cargo assembly. *Genes & development*, 22(23):3292–3307, 2008.

[214] Dennis J Selkoe. Amyloid β-protein and the genetics of Alzheimer's disease. *Journal of Biological Chemistry*, 271(31):18295–18298, 1996.

[215] Adeela Kamal, Gorazd B Stokin, Zhaohaui Yang, Chun-Hong Xia, and Lawrence SB

Goldstein. Axonal transport of amyloid precursor protein is mediated by direct binding to the kinesin light chain subunit of kinesin-I. *Neuron*, 28(2):449–459, 2000.

[216] Shermali Gunawardena and Lawrence SB Goldstein. Disruption of axonal transport and neuronal viability by amyloid precursor protein mutations in *Drosophila*. *Neuron*, 32(3):389–401, 2001.

[217] Gorazd B Stokin, Concepción Lillo, Tomás L Falzone, Richard G Brusch, Edward Rockenstein, Stephanie L Mount, Rema Raman, Peter Davies, Eliezer Masliah, David S Williams, and Lawrence SB Goldstein. Axonopathy and transport deficits early in the pathogenesis of Alzheimer's disease. *Science*, 307(5713):1282–1288, 2005.

[218] Zoia Muresan and Virgil Muresan. Coordinated transport of phosphorylated amyloid-β precursor protein and c-Jun NH2-terminal kinase–interacting protein-1. *The Journal of cell biology*, 171(4):615–625, 2005.

[219] Nobutaka Hirokawa, Reiko Sato-Yoshitake, Toshimichi Yoshida, and Takao Kawashima. Brain dynein (MAP1C) localizes on both anterogradely and retrogradely transported membranous organelles *in vivo*. *The Journal of cell biology*, 111(3):1027–1037, 1990.

[220] Alison E Twelvetrees, Stefano Pernigo, Anneri Sanger, Pedro Guedes-Dias, Giampietro Schiavo, Roberto A Steiner, Mark P Dodding, and Erika LF Holzbaur. The dynamic localization of cytoplasmic dynein in neurons is driven by kinesin-1. *Neuron*, 90(5):1000–1015, 2016.

[221] James F Dillman, Lewis P Dabney, and K Kevin Pfister. Cytoplasmic dynein is associated with slow axonal transport. *Proceedings of the National Academy of Sciences*, 93(1):141–144, 1996.

[222] Dieter R Klopfenstein and Ronald D Vale. The lipid binding pleckstrin homology domain in UNC-104 kinesin is necessary for synaptic vesicle transport in *caenorhabditis elegans*. *Molecular biology of the cell*, 15(8):3729–3739, 2004.

[223] Dieter R Klopfenstein, Michio Tomishige, Nico Stuurman, and Ronald D Vale. Role of phosphatidylinositol (4, 5) bisphosphate organization in membrane transport by the Unc104 kinesin motor. *Cell*, 109(3):347–358, 2002.

[224] David H Hall and Edward M Hedgecock. Kinesin-related gene *unc-104* is required for axonal transport of synaptic vesicles in *C.elegans*. *Cell*, 65(5):837–847, 1991.

[225] Michio Tomishige, Dieter R Klopfenstein, and Ronald D Vale. Conversion of Unc104/KIF1A kinesin into a processive motor after dimerization. *Science*, 297(5590):2263–2267, 2002.

[226] Yasushi Okada, Hiroto Yamazaki, Yoko Sekine-Aizawa, and Nobutaka Hirokawa. The neuron-specific kinesin superfamily protein KIF1A is a unique monomeric motor for anterograde axonal transport of synaptic vesicle precursors. *Cell*, 81(5):769–780, 1995.

[227] Norihiro Nakamura, Yoshihide Miyake, Masafumi Matsushita, Shingo Tanaka, Hiroki Inoue, and Hiroshi Kanazawa. KIF1Bβ2, capable of interacting with CHP, is localized to synaptic vesicles. *The Journal of Biochemistry*, 132(3):483–491, 2002.

[228] Eunju Pack-Chung, Peri T Kurshan, Dion K Dickman, and Thomas L Schwarz. A *Drosophila* kinesin required for synaptic bouton formation and synaptic vesicle transport. *Nature neuroscience*, 10(8):980, 2007.

[229] KY Lo, A Kuzmin, SM Unger, JD Petersen, and MA Silverman. KIF1A is the primary anterograde motor protein required for the axonal transport of dense-core vesicles in cultured hippocampal neurons. *Neuroscience letters*, 491(3):168–173, 2011.

[230] Makoto Kondo, Yosuke Takei, and Nobutaka Hirokawa. Motor protein kif1a is essential for hippocampal synaptogenesis and learning enhancement in an enriched environment. *Neuron*, 73(4):743–757, 2012.

[231] Masaomi Nangaku, Reiko Sato-Yoshitake, Yasushi Okada, Yasuko Noda, Reiko Takemura, Hiroto Yamazaki, and Nobutaka Hirokawa. KIF1B, a novel microtubule plus end-directed monomeric motor protein for transport of mitochondria. *Cell*, 79(7):1209–1220, 1994.

[232] Marcin J Wozniak, Martina Melzer, Cornelia Dorner, Hans-Ulrich Haring, and Reiner Lammers. The novel protein KBP regulates mitochondria localization by interaction with a kinesin-like protein. *BMC cell biology*, 6(1):35, 2005.

[233] Anthony J Otsuka, Ayyamperumal Jeyaprakash, Jaime García-Añoveros, Lan Zhao Tang, Gregory Fisk, Toinette Hartshorne, Rodrigo Franco, and Teresa Bornt. The *C.elegans unc-104* gene encodes a putative kinesin heavy chain-like protein. *Neuron*, 6(1):113–122, 1991.

[234] Yoshiaki Yonekawa, Akihiro Harada, Yasushi Okada, Takeshi Funakoshi, Yoshimitsu Kanai, Yosuke Takei, Sumio Terada, Tetsuo Noda, and Nobutaka Hirokawa. Defect in synaptic vesicle precursor transport and neuronal cell death in KIF1A motor protein–deficient mice. *The Journal of cell biology*, 141(2):431–441, 1998.

[235] Shinsuke Niwa, Yosuke Tanaka, and Nobutaka Hirokawa. KIF1Bβ- and KIF1A-mediated axonal transport of presynaptic regulator Rab3 occurs in a GTP-dependent manner through DENN/MADD. *Nature Cell Biology*, 10(11):1269, 2008.

[236] Miki Tanaka, Jun Miyoshi, Hiroyoshi Ishizaki, Atsushi Togawa, Katsunori Ohnishi, Katsuaki Endo, Kaho Matsubara, Akira Mizoguchi, Takashi Nagano, Makoto Sato, Takuya Sasaki, and Yoshimi Takai. Role of Rab3 GDP/GTP exchange protein in synaptic vesicle trafficking at the mouse neuromuscular junction. *Molecular biology of the cell*, 12(5):1421–1430, 2001.

[237] Timothy R Mahoney, Qiang Liu, Takashi Itoh, Shuo Luo, Gayla Hadwiger, Rose Vincent, Zhao-Wen Wang, Mitsunori Fukuda, and Michael L Nonet. Regulation of synaptic transmission by RAB-3 and RAB-27 in *Caenorhabditis elegans*. *Molecular biology of the cell*, 17(6):2617–2625, 2006.

[238] Hyewon Shin, Michael Wyszynski, Kyung-Hye Huh, Juli G Valtschanoff, Jae-Ran Lee, Jaewon Ko, Michel Streuli, Richard J Weinberg, Morgan Sheng, and Eunjoon Kim. Association of the kinesin motor KIF1A with the multimodular protein liprin-α. *Journal of Biological Chemistry*, 278(13):11393–11401, 2003.

[239] Mei Zhen and Yishi Jin. The liprin protein SYD-2 regulates the differentiation of presynaptic termini in *C.elegans*. *Nature*, 401(6751):371, 1999.

[240] Oliver I Wagner, Alessandro Esposito, Barbara Köhler, Chih-Wei Chen, Che-Piao Shen, Gong-Her Wu, Eugenia Butkevich, Sailaja Mandalapu, Dirk Wenzel, Fred S Wouters, and Dieter R Klopfenstein. Synaptic scaffolding protein SYD-2 clusters and activates kinesin-3 UNC-104 in *C.elegans*. *Proceedings of the National Academy of Sciences*, 106(46) : 19605 − −19610, 2009.

[241] Yasushi Okada, Hideo Higuchi, and Nobutaka Hirokawa. Processivity of the single-headed kinesin KIF1A through biased binding to tubulin. *Nature*, 424(6948):574, 2003.

[242] Luke AD Bury and Shasta L Sabo. Building a terminal: mechanisms of presynaptic development in the CNS. *The Neuroscientist*, 22(4):372–391, 2016.

[243] Ritsu Kamiya. Functional diversity of axonemal dyneins as studied in Chlamydomonas mutants. 219:115–155, 2002.

[244] Yosuke Tanaka, Zhizeng Zhang, and Nobutaka Hirokawa. Identification and molecular evolution of new dynein-like protein sequences in rat brain. *Journal of Cell Science*, 108(5):1883–1893, 1995.

[245] Joel L Rosenbaum and George B Witman. Intraflagellar transport. *Nature reviews Molecular cell biology*, 3(11):813, 2002.

[246] Sher Karki and Erika LF Holzbaur. Cytoplasmic dynein and dynactin in cell division and intracellular transport. *Current opinion in cell biology*, 11(1):45–53, 1999.

[247] K Kevin Pfister, Paresh R Shah, Holger Hummerich, Andreas Russ, James Cotton, Azlina Ahmad Annuar, Stephen M King, and Elizabeth MC Fisher. Genetic analysis of the cytoplasmic dynein subunit families. *PLoS genetics*, 2(1):e1, 2006.

[248] Trina A Schroer. Dynactin. *Annu. Rev. Cell Dev. Biol.*, 20:759–779, 2004.

[249] Daisuke Satoh, Daichi Sato, Taiichi Tsuyama, Motoki Saito, Hiroyuki Ohkura, Melissa M Rolls, Fuyuki Ishikawa, and Tadashi Uemura. Spatial control of branching within dendritic arbors by dynein-dependent transport of Rab5-endosomes. *Nature cell biology*, 10(10):1164, 2008.

[250] Yi Zheng, Jill Wildonger, Bing Ye, Ye Zhang, Angela Kita, Susan H Younger, Sabina Zimmerman, Lily Yeh Jan, and Yuh Nung Jan. Dynein is required for polarized dendritic transport and uniform microtubule orientation in axons. *Nature cell biology*, 10(10):1172, 2008.

[251] Anna Fejtova, Daria Davydova, Ferdinand Bischof, Vesna Lazarevic, Wilko D Altrock, Stefano Romorini, Cornelia Schöne, Werner Zuschratter, Michael R Kreutz, Craig C Garner, Noam E Ziv, and Eckart D Gundelfinger. Dynein light chain regulates axonal trafficking and synaptic levels of Bassoon. *The Journal of cell biology*, 185(2):341–355, 2009.

[252] Christoph Maas, Nadia Tagnaouti, Sven Loebrich, Bardo Behrend, Corinna Lappe-Siefke, and Matthias Kneussel. Neuronal cotransport of glycine receptor and the scaffold protein gephyrin. *The Journal of cell biology*, 172(3):441–451, 2006.

[253] Jens C Fuhrmann, Stefan Kins, Philippe Rostaing, Oussama El Far, Joachim Kirsch, Morgan Sheng, Antoine Triller, Heinrich Betz, and Matthias Kneussel. Gephyrin interacts with dynein light chains 1 and 2, components of motor protein complexes. *Journal of Neuroscience*, 22(13):5393–5402, 2002.

[254] Mariangela Lo Giudice, Marcella Neri, Michele Falco, Maurizio Sturnio, Elisa Calzolari, Daniela Di Benedetto, and Marco Fichera. A missense mutation in the coiled-coil domain of the KIF5A gene and late-onset hereditary spastic paraplegia. *Archives of neurology*, 63(2):284–287, 2006.

[255] Marcia A Blair, Shaochun Ma, and Peter Hedera. Mutation in KIF5A can also cause adult-onset hereditary spastic paraplegia. *Neurogenetics*, 7(1):47–50, 2006.

[256] M Fichera, M Lo Giudice, M Falco, M Sturnio, S Amata, O Calabrese, S Bigoni, E Calzolari, and M Neri. Evidence of kinesin heavy chain (KIF5A) involvement in pure hereditary spastic paraplegia. *Neurology*, 63(6):1108–1110, 2004.

[257] Evan Reid, Mark Kloos, Allison Ashley-Koch, Lori Hughes, Simon Bevan, Ingrid K Svenson, Felicia Lennon Graham, Perry C Gaskell, Andrew Dearlove, Margaret A

Pericak-Vance, David C Rubinsztein, and Douglas A Marchuk. A kinesin heavy chain (KIF5A) mutation in hereditary spastic paraplegia (SPG10). *The American Journal of Human Genetics*, 71(5):1189–1194, 2002.

[258] Bettina Ebbing, Klaudiusz Mann, Agata Starosta, Johann Jaud, Ludger Schöls, Rebecca Schüle, and Günther Woehlke. Effect of spastic paraplegia mutations in KIF5A kinesin on transport activity. *Human molecular genetics*, 17(9):1245–1252, 2008.

[259] Karine Poirier, Nicolas Lebrun, Loic Broix, Guoling Tian, Yoann Saillour, Cécile Boscheron, Elena Parrini, Stephanie Valence, Benjamin Saint Pierre, Madison Oger, Didier Lacombe, David Geneviève, Elena Fontana, Franscesca Darra, Claude Cances, Magalie Barth, Dominique Bonneau, Bernardo Dalla Bernadina, Sylvie N'Guyen, Cyril Gitiaux, Philippe Parent, Vincent des Portes, Jean Michel Pedespan, Victoire Legrez, Laetitia Castelnau-Ptakine, Patrick Nitschke, Thierry Hieu, Cecile Masson, Diana Zelenika, Annie Andrieux, Fiona Francis, Renzo Guerrini, Nicholas J Cowan, Nadia Bahi-Buisson, and Jamel Chelly. Mutations in TUBG1, DYNC1H1, KIF5C and KIF2A cause malformations of cortical development and microcephaly. *Nature genetics*, 45(6):639, 2013.

[260] Yosuke Tanaka, Yoshimitsu Kanai, Yasushi Okada, Shigenori Nonaka, Sen Takeda, Akihiro Harada, and Nobutaka Hirokawa. Targeted disruption of mouse conventional kinesin heavy chain kif5B, results in abnormal perinuclear clustering of mitochondria. *Cell*, 93(7):1147–1158, 1998.

[261] Chunjie Zhao, Junko Takita, Yosuke Tanaka, Mitsutoshi Setou, Terunaga Nakagawa, Sen Takeda, Hong Wei Yang, Sumio Terada, Takao Nakata, Yosuke Takei, Masaaki Saito, Shoji Tsuji, Yasuhide Hayashi, and Nobutaka Hirokawa. Charcot-marie-tooth disease type 2A caused by mutation in a microtubule motor KIF1Bβ. *Cell*, 105(5):587–597, 2001.

[262] David A Lyons, Stephen G Naylor, Anja Scholze, and William S Talbot. Kif1b is essential for mRNA localization in oligodendrocytes and development of myelinated axons. *Nature genetics*, 41(7):854, 2009.

[263] Michael E Shy, John Kamholz, and Robert E Lovelace. Introduction to the third international symposium on charcot-marie-tooth disorders. *Annals of the New York Academy of Sciences*, 883(1), 1999.

[264] A Harada, Y Takei, Y Kanai, Y Tanaka, S Nonaka, and N Hirokawa. Golgi vesiculation and lysosome dispersion in cells lacking cytoplasmic dynein. *The Journal of cell biology*, 141(1):51–59, 1998.

[265] Eran Perlson, Shlomit Hanz, Keren Ben-Yaakov, Yael Segal-Ruder, Rony Seger, and Mike Fainzilber. Vimentin-dependent spatial translocation of an activated MAP kinase in injured nerve. *Neuron*, 45(5):715–726, 2005.

[266] Valeria Cavalli, Pekka Kujala, Judith Klumperman, and Lawrence SB Goldstein. Sunday driver links axonal transport to damage signaling. *The Journal of cell biology*, 168(5):775–787, 2005.

[267] Brinda Ravikumar, Abraham Acevedo-Arozena, Sara Imarisio, Zdenek Berger, Coralie Vacher, Cahir J O'Kane, Steve DM Brown, and David C Rubinsztein. Dynein mutations impair autophagic clearance of aggregate-prone proteins. *Nature genetics*, 37(7):771, 2005.

[268] Shinji Sasaki, Daisuke Mori, Kazuhito Toyo-Oka, Amy Chen, Lisa Garrett-Beal, Masami Muramatsu, Shuji Miyagawa, Noriko Hiraiwa, Atsushi Yoshiki, Anthony Wynshaw-Boris, and Shinji Hirotsune. Complete loss of *Ndel*1 results in neuronal migration defects and early embryonic lethality. *Molecular and cellular biology*, 25(17):7812–7827, 2005.

[269] Sandra E Encalada, Lukasz Szpankowski, Chun-hong Xia, and Lawrence SB Goldstein. Stable kinesin and dynein assemblies drive the axonal transport of mammalian prion protein vesicles. *Cell*, 144(4):551–565, 2011.

[270] Adam G Hendricks, Eran Perlson, Jennifer L Ross, Harry W Schroeder III, Mariko Tokito, and Erika LF Holzbaur. Motor coordination via a tug-of-war mechanism drives bidirectional vesicle transport. *Current Biology*, 20(8):697–702, 2010.

[271] Sandra Maday, Karen E Wallace, and Erika LF Holzbaur. Autophagosomes initiate distally and mature during transport toward the cell soma in primary neurons. *J Cell Biol*, 196(4):407–417, 2012.

[272] Virupakshi Soppina, Stephen R Norris, Aslan S Dizaji, Matt Kortus, Sarah Veatch, Michelle Peckham, and Kristen J Verhey. Dimerization of mammalian kinesin-3 motors results in superprocessive motion. *Proceedings of the National Academy of Sciences*, 111(15):5562–5567, 2014.

[273] Adam G Hendricks, Erika LF Holzbaur, and Yale E Goldman. Force measurements on cargoes in living cells reveal collective dynamics of microtubule motors. *Proceedings of the National Academy of Sciences*, 109(45):18447–18452, 2012.

[274] Lukasz Szpankowski, Sandra E Encalada, and Lawrence SB Goldstein. Subpixel colocalization reveals amyloid precursor protein-dependent kinesin-1 and dynein association with axonal vesicles. *Proceedings of the National Academy of Sciences*, 109(22):8582–8587, 2012.

[275] Melanie JI Müller, Stefan Klumpp, and Reinhard Lipowsky. Tug-of-war as a cooperative mechanism for bidirectional cargo transport by molecular motors. *Proceedings of the National Academy of Sciences*, 105(12):4609–4614, 2008.

[276] Ram Dixit, Jennifer L Ross, Yale E Goldman, and Erika LF Holzbaur. Differential regulation of dynein and kinesin motor proteins by tau. *Science*, 319(5866):1086–1089, 2008.

[277] Benjamin H Blehm, Trina A Schroer, Kathleen M Trybus, Yann R Chemla, and Paul R Selvin. *In vivo* optical trapping indicates kinesin's stall force is reduced by dynein during intracellular transport. *Proceedings of the National Academy of Sciences*, 110(9):3381–3386, 2013.

[278] Elizabeth E Glater, Laura J Megeath, R Steven Stowers, and Thomas L Schwarz. Axonal transport of mitochondria requires milton to recruit kinesin heavy chain and is light chain independent. *The Journal of cell biology*, 173(4):545–557, 2006.

[279] Xinnan Wang and Thomas L Schwarz. The mechanism of Ca^{2+}-dependent regulation of kinesin-mediated mitochondrial motility. *Cell*, 136(1):163–174, 2009.

[280] Andrew F MacAskill, Johanne E Rinholm, Alison E Twelvetrees, I Lorena Arancibia-Carcamo, James Muir, Asa Fransson, Pontus Aspenstrom, David Attwell, and Josef T Kittler. Miro1 is a calcium sensor for glutamate receptor-dependent localization of mitochondria at synapses. *Neuron*, 61(4):541–555, 2009.

[281] Emilie Colin, Diana Zala, Geraldine Liot, Helene Rangone, Maria Borrell-Pagès, Xiao-Jiang Li, Frédéric Saudou, and Sandrine Humbert. Huntingtin phosphorylation acts as a molecular switch for anterograde/retrograde transport in neurons. *The EMBO journal*, 27(15):2124–2134, 2008.

[282] Kristen J Verhey, Debra Meyer, Reneé Deehan, John Blenis, Bruce J Schnapp, Tom A Rapoport, and Ben Margolis. Cargo of kinesin identified as JIP scaffolding proteins and associated signaling molecules. *The Journal of cell biology*, 152(5):959–970, 2001.

[283] Meng-meng Fu and Erika LF Holzbaur. JIP1 regulates the directionality of APP axonal transport by coordinating kinesin and dynein motors. *J Cell Biol*, 202(3):495–508, 2013.

[284] Laird Bloom and H Robert Horvitz. The *Caenorhabditis elegans* gene *unc-76* and its human homologs define a new gene family involved in axonal outgrowth and fasciculation. *Proceedings of the National Academy of Sciences*, 94(7):3414–3419, 1997.

[285] Toshitsugu Fujita, Junko Ikuta, Juri Hamada, Toshihide Okajima, Kenji Tatematsu, Katsuyuki Tanizawa, and Shun'ichi Kuroda. Identification of a tissue-non-specific

homologue of axonal fasciculation and elongation protein zeta-1. *Biochemical and biophysical research communications*, 313(3):738–744, 2004.

[286] Edward M Hedgecock, Joseph G Culotti, J Nichol Thomson, and Lizabeth A Perkins. Axonal guidance mutants of *Caenorhabditis elegans* identified by filling sensory neurons with fluorescein dyes. *Developmental biology*, 111(1):158–170, 1985.

[287] Chand Desai, Gian Garriga, Steven L Mclntire, and H Robert Horvitz. A genetic pathway for the development of the *Caenorhabditis elegans* HSN motor neurons. *Nature*, 336(6200):638, 1988.

[288] Steven L McIntire, Gian Garriga, John White, Dean Jacobson, and H Robert Horvitz. Genes necessary for directed axonal elongation or fasciculation in *C.elegans*. *Neuron*, 8(2):307–322, 1992.

[289] Joseph G Gindhart, Jinyun Chen, Melissa Faulkner, Rita Gandhi, Karl Doerner, Tiffany Wisniewski, and Aline Nandlestadt. The kinesin-associated protein UNC-76 is required for axonal transport in the *Drosophila* nervous system. *Molecular biology of the cell*, 14(8):3356–3365, 2003.

[290] Eugenia Butkevich, Wolfgang Härtig, Miroslav Nikolov, Christian Erck, Jens Grosche, Henning Urlaub, Christoph F Schmidt, Dieter R Klopfenstein, and John Jia En Chua. Phosphorylation of FEZ1 by microtubule affinity regulating kinases regulates its function in presynaptic protein trafficking. *Scientific reports*, 6:26965, 2016.

[291] Neville E Sanjana, Ophir Shalem, and Feng Zhang. Improved vectors and genome-wide libraries for CRISPR screening. *Nature methods*, 11(8):783, 2014.

[292] David M Walter, Olivia S Venancio, Elizabeth L Buza, John W Tobias, Charuhas Deshpande, A Andrea Gudiel, Caroline Kim-Kiselak, Michelle Cicchini, Travis J Yates, and David M Feldser. Systematic *in vivo* inactivation of chromatin-regulating enzymes identifies Setd2 as a potent tumor suppressor in lung adenocarcinoma. *Cancer research*, 77(7):1719–1729, 2017.

[293] Thomas Dresbach, Anne Hempelmann, Christina Spilker, Susanne tom Dieck, Wilko D Altrock, Werner Zuschratter, Craig C Garner, and Eckart D Gundelfinger. Functional regions of the presynaptic cytomatrix protein bassoon: significance for synaptic targeting and cytomatrix anchoring. *Molecular and Cellular Neuroscience*, 23(2):279–291, 2003.

[294] Camin Dean, Huisheng Liu, Thorsten Staudt, Markus A Stahlberg, Siv Vingill, Johanna Bückers, Dirk Kamin, Johann Engelhardt, Meyer B Jackson, Stefan W Hell, et al. Distinct subsets of Syt-IV/BDNF vesicles are sorted to axons versus dendrites

and recruited to synapses by activity. *Journal of Neuroscience*, 32(16):5398–5413, 2012.

[295] Sheila A Stewart, Derek M Dykxhoorn, Deborah Palliser, Hana Mizuno, Evan Y Yu, Dong Sung An, David M Sabatini, Irvin SY Chen, William C Hahn, Phillip A Sharp, Robert A Weinberg, and Carl D Novina. Lentivirus-delivered stable gene silencing by RNAi in primary cells. *Rna*, 9(4):493–501, 2003.

[296] Johannes Schindelin, Ignacio Arganda-Carreras, Erwin Frise, Verena Kaynig, Mark Longair, Tobias Pietzsch, Stephan Preibisch, Curtis Rueden, Stephan Saalfeld, Benjamin Schmid, Jean-Yves Tinevaz, Daniel James White, Volker Hartenstein, Kevin Eliceiri, Pavel Tomancak, and Albert Cardona. Fiji: an open-source platform for biological-image analysis. *Nature methods*, 9(7):676, 2012.

[297] Jean-Christophe Olivo-Marin. Extraction of spots in biological images using multiscale products. *Pattern recognition*, 35(9):1989–1996, 2002.

[298] Dariusz Orlowski and Carsten R Bjarkam. A simple reproducible and time saving method of semi-automatic dendrite spine density estimation compared to manual spine counting. *Journal of neuroscience methods*, 208(2):128–133, 2012.

[299] Jean-Yves Tinevez, Nick Perry, Johannes Schindelin, Genevieve M Hoopes, Gregory D Reynolds, Emmanuel Laplantine, Sebastian Y Bednarek, Spencer L Shorte, and Kevin W Eliceiri. TrackMate: An open and extensible platform for single-particle tracking. *Methods*, 115:80–90, 2017.

[300] Tiago A Ferreira, Arne V Blackman, Julia Oyrer, Sriram Jayabal, Andrew J Chung, Alanna J Watt, P Jesper Sjöström, and Donald J Van Meyel. Neuronal morphometry directly from bitmap images. *Nature methods*, 11(10):982, 2014.

[301] Viacheslav Malikov, Eveline Santos Da Silva, Vladimir Jovasevic, Geoffrey Bennett, Daniel A de Souza Aranha Vieira, Bianca Schulte, Felipe Diaz-Griffero, Derek Walsh, and Mojgan H Naghavi. HIV-1 capsids bind and exploit the kinesin-1 adaptor FEZ1 for inward movement to the nucleus. *Nature communications*, 6:6660, 2015.

[302] Viacheslav Malikov and Mojgan H Naghavi. Localized phosphorylation of a kinesin-1 adaptor by a capsid-associated kinase regulates HIV-1 motility and uncoating. *Cell reports*, 20(12):2792–2799, 2017.

[303] Nectarios Klonis, Melanie Rug, Ian Harper, Mark Wickham, Alan Cowman, and Leann Tilley. Fluorescence photobleaching analysis for the study of cellular dynamics. *European Biophysics Journal*, 31(1):36–51, 2002.

[304] Cécile Leduc, Kathrin Padberg-Gehle, Vladimir Varga, Dirk Helbing, Stefan Diez, and Jonathon Howard. Molecular crowding creates traffic jams of kinesin motors on

microtubules. *Proceedings of the National Academy of Sciences*, 109(16):6100–6105, 2012.

[305] Jitendra Kumar, Bikash C Choudhary, Raghu Metpally, Qun Zheng, Michael L Nonet, Sowdhamini Ramanathan, Dieter R Klopfenstein, and Sandhya P Koushika. The *Caenorhabditis elegans* Kinesin-3 motor UNC-104/KIF1A is degraded upon loss of specific binding to cargo. *PLoS genetics*, 6(11):e1001200, 2010.

[306] Celine I Maeder, Adriana San-Miguel, Emily Ye Wu, Hang Lu, and Kang Shen. *In vivo* neuron-wide analysis of synaptic vesicle precursor trafficking. *Traffic*, 15(3):273–291, 2014.

[307] Arpan K Rai, Ashim Rai, Avin J Ramaiya, Rupam Jha, and Roop Mallik. Molecular adaptations allow dynein to generate large collective forces inside cells. *Cell*, 152(1-2):172–182, 2013.

[308] Paul Greengard, Flavia Valtorta, Andrew J Czernik, and Fabio Benfenati. Synaptic vesicle phosphoproteins and regulation of synaptic function. *Science*, 259(5096):780–785, 1993.

[309] Sabine Hilfiker, Vincent A Pieribone, Andrew J Czernik, Hung-Teh Kao, George J Augustine, and Paul Greengard. Synapsins as regulators of neurotransmitter release. *Philosophical Transactions of the Royal Society B: Biological Sciences*, 354(1381):269–279, 1999.

[310] Pietro Baldelli, Anna Fassio, Flavia Valtorta, and Fabio Benfenati. Lack of synapsin I reduces the readily releasable pool of synaptic vesicles at central inhibitory synapses. *Journal of Neuroscience*, 27(49):13520–13531, 2007.

[311] Anders Kielland, Alev Erisir, S Ivar Walaas, and Paul Heggelund. Synapsin utilization differs among functional classes of synapses on thalamocortical cells. *Journal of Neuroscience*, 26(21):5786–5793, 2006.

[312] David A Scott, Utpal Das, Yong Tang, and Subhojit Roy. Mechanistic logic underlying the axonal transport of cytosolic proteins. *Neuron*, 70(3):441–454, 2011.

[313] A Ferreira and M Rapoport. The synapsins: beyond the regulation of neurotransmitter release. *Cellular and Molecular Life Sciences CMLS*, 59(4):589–595, 2002.

[314] E Evergren, F Benfenati, and O Shupliakov. The synapsin cycle: a view from the synaptic endocytic zone. *Journal of neuroscience research*, 85(12):2648–2656, 2007.

[315] Christoph Kaether, Paul Skehel, and Carlos G Dotti. Axonal membrane proteins are transported in distinct carriers: a two-color video microscopy study in cultured hippocampal neurons. *Molecular biology of the cell*, 11(4):1213–1224, 2000.

[316] Takao Nakata, Sumio Terada, and Nobutaka Hirokawa. Visualization of the dynamics of synaptic vesicle and plasma membrane proteins in living axons. *The Journal of cell biology*, 140(3):659–674, 1998.

[317] Cheng-Wen Su, Suzanne Tharin, Yishi Jin, Bruce Wightman, Mona Spector, David Meili, Nancy Tsung, Christa Rhiner, Dimitris Bourikas, Esther Stoeckli, et al. The short coiled-coil domain-containing protein UNC-69 cooperates with UNC-76 to regulate axonal outgrowth and normal presynaptic organization in *Caenorhabditis elegans*. *Journal of biology*, 5(4):9, 2006.

[318] Kristen M Harris and John K Stevens. Dendritic spines of CA1 pyramidal cells in the rat hippocampus: serial electron microscopy with reference to their biophysical characteristics. *Journal of Neuroscience*, 9(8):2982–2997, 1989.

[319] Thomas Schikorski and Charles F Stevens. Quantitative ultrastructural analysis of hippocampal excitatory synapses. *Journal of Neuroscience*, 17(15):5858–5867, 1997.

[320] Louise Kay, Lawrence Humphreys, Britta J Eickholt, and Juan Burrone. Neuronal activity drives matching of pre-and postsynaptic function during synapse maturation. *Nature neuroscience*, 14(6):688, 2011.

[321] Arava Fisher-Lavie and Noam E Ziv. Matching dynamics of presynaptic and postsynaptic scaffolds. *Journal of Neuroscience*, 33(32):13094–13100, 2013.

[322] Shigeo Okabe, Akiko Miwa, and Haruo Okado. Spine formation and correlated assembly of presynaptic and postsynaptic molecules. *Journal of Neuroscience*, 21(16):6105–6114, 2001.

[323] Florian Engert and Tobias Bonhoeffer. Dendritic spine changes associated with hippocampal long-term synaptic plasticity. *Nature*, 399(6731):66, 1999.

[324] Heike Hering and Morgan Sheng. Dentritic spines: structure, dynamics and regulation. *Nature Reviews Neuroscience*, 2(12):880, 2001.

[325] Tobias Bonhoeffer and Rafael Yuste. Spine motility: phenomenology, mechanisms, and function. *Neuron*, 35(6):1019–1027, 2002.

[326] Rafael Yuste and Tobias Bonhoeffer. Genesis of dendritic spines: insights from ultrastructural and imaging studies. *Nature Reviews Neuroscience*, 5(1):24, 2004.

[327] Yi Zuo, Guang Yang, Elaine Kwon, and Wen-Biao Gan. Long-term sensory deprivation prevents dendritic spine loss in primary somatosensory cortex. *Nature*, 436(7048):261, 2005.

[328] Min Fu and Yi Zuo. Experience-dependent structural plasticity in the cortex. *Trends in neurosciences*, 34(4):177–187, 2011.

[329] Anthony J Koleske. Molecular mechanisms of dendrite stability. *Nature Reviews Neuroscience*, 14(8):536, 2013.

[330] Carlo Sala and Menahem Segal. Dendritic spines: the locus of structural and functional plasticity. *Physiological reviews*, 94(1):141–188, 2014.

[331] Mara Dierssen and Ger JA Ramakers. Dendritic pathology in mental retardation: from molecular genetics to neurobiology. *Genes, Brain and Behavior*, 5(s2):48–60, 2006.

[332] Leisa A Glantz and David A Lewis. Decreased dendritic spine density on prefrontal cortical pyramidal neurons in schizophrenia. *Archives of general psychiatry*, 57(1):65–73, 2000.

[333] Robert A Sweet, Ruth A Henteleff, Wei Zhang, Allan R Sampson, and David A Lewis. Reduced dendritic spine density in auditory cortex of subjects with schizophrenia. *Neuropsychopharmacology*, 34(2):374, 2009.

[334] Jeffrey J Hutsler and Hong Zhang. Increased dendritic spine densities on cortical projection neurons in autism spectrum disorders. *Brain research*, 1309:83–94, 2010.

[335] Dominick P Purpura. Dendritic spine "dysgenesis" and mental retardation. *Science*, 186(4169):1126–1128, 1974.

[336] Scott A Irwin, Biraju Patel, Madhuri Idupulapati, Jennifer B Harris, Ralph A Crisostomo, Brian P Larsen, Frank Kooy, Patrick J Willems, Patrick Cras, Piotr B Kozlowski, Rodney A Swain, Ivan Jeanne Weiler, and William T Greenough. Abnormal dendritic spine characteristics in the temporal and visual cortices of patients with fragile-X syndrome: a quantitative examination. *American Journal of Medical Genetics Part A*, 98(2):161–167, 2001.

[337] Miguel Marin-Padilla. Pyramidal cell abnormalities in the motor cortex of a child with down's syndrome. A Golgi study. *Journal of Comparative Neurology*, 167(1):63–81, 1976.

[338] Sachio Takashima, Laurence E Becker, Dawna L Armstrong, and Fuwah Chan. Abnormal neuronal development in the visual cortex of the human fetus and infant with Down's syndrome. A quantitative and qualitative Golgi study. *Brain research*, 225(1):1–21, 1981.

[339] I Ferrer and F Gullotta. Down's dyndrome and Alzheimer's disease: dendritic spine counts in the hippocampus. *Acta neuropathologica*, 79(6):680–685, 1990.

[340] Sachio Takashima, K Iida, T Mito, and M Arima. Dendritic and histochemical development and ageing in patients with Down's syndrome. *Journal of Intellectual Disability Research*, 38(3):265–273, 1994.

[341] Eunchai Kang, Katherine E Burdick, Ju Young Kim, Xin Duan, Junjie U Guo, Kurt A Sailor, Dhong-Eun Jung, Sundar Ganesan, Sungkyung Choi, Dennis Pradhan, et al. Interaction between FEZ1 and DISC1 in regulation of neuronal development and risk for schizophrenia. *Neuron*, 72(4):559–571, 2011.

[342] Yasuhito Watanabe, Konstantin Khodosevich, and Hannah Monyer. Dendrite development regulated by the schizophrenia-associated gene FEZ1 involves the ubiquitin proteasome system. *Cell reports*, 7(2):552–564, 2014.

[343] K Miyoshi, A Honda, K Baba, M Taniguchi, K Oono, T Fujita, S Kuroda, T Katayama, and M Tohyama. Disrupted-in-schizophrenia 1, a candidate gene for schizophrenia, participates in neurite outgrowth. *Molecular psychiatry*, 8(7):685, 2003.

[344] Dd A Sholl. Dendritic organization in the neurons of the visual and motor cortices of the cat. *Journal of anatomy*, 87(Pt 4):387, 1953.

[345] Yunfeng Hua, Raunak Sinha, Cora S Thiel, Roman Schmidt, Jana Hüve, Henrik Martens, Stefan W Hell, Alexander Egner, and Jurgen Klingauf. A readily retrievable pool of synaptic vesicles. *Nature neuroscience*, 14(7):833, 2011.

[346] Daryl D Hurd and William M Saxton. Kinesin mutations cause motor neuron disease phenotypes by disrupting fast axonal transport in *Drosophila*. *Genetics*, 144(3):1075–1085, 1996.

[347] Hideru Togashi, Kentaro Abe, Akira Mizoguchi, Kanna Takaoka, Osamu Chisaka, and Masatoshi Takeichi. Cadherin regulates dendritic spine morphogenesis. *Neuron*, 35(1):77–89, 2002.

[348] Ozlem Bozdagi, Martin Valcin, Kira Poskanzer, Hidekazu Tanaka, and Deanna L Benson. Temporally distinct demands for classic cadherins in synapse formation and maturation. *Molecular and Cellular Neuroscience*, 27(4):509–521, 2004.

[349] Anthony Holtmaat and Karel Svoboda. Experience-dependent structural synaptic plasticity in the mammalian brain. *Nature Reviews Neuroscience*, 10(9):647, 2009.

[350] Haruo Kasai, Masahiro Fukuda, Satoshi Watanabe, Akiko Hayashi-Takagi, and Jun Noguchi. Structural dynamics of dendritic spines in memory and cognition. *Trends in neurosciences*, 33(3):121–129, 2010.

[351] Miguel Marin-Padilla. Structural abnormalities of the cerebral cortex in human chromosomal aberrations: a Golgi study. *Brain research*, 44(2):625–629, 1972.

[352] Miguel Marin-Padilla. Structural organization of the cerebral cortex (motor area) in human chromosomal aberrations. A Golgi study. I. D_1 (13–15) trisomy, patau syndrome. *Brain Research*, 66(3):375–391, 1974.

[353] P Von Bossanyi and M Becher. Quantitative Untersuchungen an Dendritenspines von Lamina V-Pyramidenneuronen des Frontalhirns nach frühkindlicher Hirnschädigung. *Journal für Hirnforschung*, 31(2):181–192, 1990.

[354] Octavio Garcia, Maria Torres, Pablo Helguera, Pinar Coskun, and Jorge Busciglio. A role for thrombospondin-1 deficits in astrocyte-mediated spine and synaptic pathology in Down's syndrome. *PloS one*, 5(12):e14200, 2010.

[355] John A Hammer III and James R Sellers. Walking to work: roles for class V myosins as cargo transporters. *Nature Reviews Molecular Cell Biology*, 13(1):13, 2012.

[356] Susana S Correia, Silvia Bassani, Tyler C Brown, Marie-France Lisé, Donald S Backos, Alaa El-Husseini, Maria Passafaro, and José A Esteban. Motor protein–dependent transport of AMPA receptors into spines during long-term potentiation. *Nature neuroscience*, 11(4):457, 2008.

[357] Zhiping Wang, Jeffrey G Edwards, Nathan Riley, D William Provance Jr, Ryan Karcher, Xiang-dong Li, Ian G Davison, Mitsuo Ikebe, John A Mercer, Julie A Kauer, and Michael D Ehlers. Myosin Vb mobilizes recycling endosomes and AMPA receptors for postsynaptic plasticity. *Cell*, 135(3):535–548, 2008.

[358] Wolfgang Wagner, Stephan D Brenowitz, and John A Hammer III. Myosin-Va transports the endoplasmic reticulum into the dendritic spines of Purkinje neurons. *Nature cell biology*, 13(1):40, 2011.

[359] Jiaping Gu, Bonnie L Firestein, and James Q Zheng. Microtubules in dendritic spine development. *Journal of Neuroscience*, 28(46):12120–12124, 2008.

[360] Xindao Hu, Lauren Ballo, Lauren Pietila, Chris Viesselmann, Jason Ballweg, Derek Lumbard, Matt Stevenson, Elliott Merriam, and Erik W Dent. BDNF-induced increase of PSD-95 in dendritic spines requires dynamic microtubule invasions. *Journal of Neuroscience*, 31(43):15597–15603, 2011.

[361] Derrick P McVicker, Adam M Awe, Karl E Richters, Rebecca L Wilson, Diana A Cowdrey, Xindao Hu, Edwin R Chapman, and Erik W Dent. Transport of a kinesin-cargo pair along microtubules into dendritic spines undergoing synaptic plasticity. *Nature communications*, 7:12741, 2016.

[362] Xintong Dong, Kang Shen, and Hannes E Bülow. Intrinsic and extrinsic mechanisms of dendritic morphogenesis. *Annual review of physiology*, 77:271–300, 2015.

[363] Fernanda Ledda and Gustavo Paratcha. Mechanisms regulating dendritic arbor patterning. *Cellular and Molecular Life Sciences*, 74(24):4511–4537, 2017.

[364] L Becker, T Mito, S Takashima, and K Onodera. Growth and development of the

brain in Down syndrome. *Progress in clinical and biological research*, 373:133–152, 1991.

[365] Sachio Takashima, Atsushi Ieshima, Haruomi Nakamura, and Laurence E Becker. Dendrites, dementia and the Down syndrome. *Brain and Development*, 11(2):131–133, 1989.

[366] E Schulz and B Scholz. Neurohistological findings in the parietal cortex of children with chromosome aberrations. *Journal fur Hirnforschung*, 33(1):37–62, 1992.

[367] M Prinz, B Prinz, and E Schulz. The growth of non-pyramidal neurons in the primary motor cortex of man: a Golgi study. *Histology and histopathology*, 12(4):895–900, 1997.

[368] Minhan Ka, Divyan A Chopra, Shashank M Dravid, and Woo-Yang Kim. Essential roles for ARID1B in dendritic arborization and spine morphology of developing pyramidal neurons. *Journal of Neuroscience*, 36(9):2723–2742, 2016.

[369] Thomas Schikorski and Charles F Stevens. Morphological correlates of functionally defined synaptic vesicle populations. *Nature neuroscience*, 4(4):391, 2001.

[370] Shigeki Watanabe, Benjamin R Rost, Marcial Camacho-Pérez, M Wayne Davis, Berit Söhl-Kielczynski, Christian Rosenmund, and Erik M Jorgensen. Ultrafast endocytosis at mouse hippocampal synapses. *Nature*, 504(7479):242, 2013.

[371] William J Tyler and Lucas D Pozzo-Miller. BDNF enhances quantal neurotransmitter release and increases the number of docked vesicles at the active zones of hippocampal excitatory synapses. *Journal of Neuroscience*, 21(12):4249–4258, 2001.

[372] Akiko Honda, Ko Miyoshi, Kousuke Baba, Manabu Taniguchi, Yoshihisa Koyama, Shun'ichi Kuroda, Taiichi Katayama, and Masaya Tohyama. Expression of fasciculation and elongation protein zeta-1 (FEZ1) in the developing rat brain. *Molecular brain research*, 122(1):89–92, 2004.

Acknowledgments

I would like to thank my thesis advisor, Dr. John Chua, for his support and guidance throughout my project.

I would like to thank Prof. Dr. Reinhard Jahn, for generously hosting our group in the department of neurobiology and for his scientific and personal support.

I am grateful to the members of my thesis committee, Dr. Dieter Klopfenstein and Prof. Dr. Stefan Jakobs, for our discussions during the committee meetings.

I would like to express my appreciation to Prof. Dr. Silvio Rizzoli, for taking the time to help me plan, analyze and interpret the FRAP experiments. I also would like to thank Dr. Andrew Woehler for his invaluable help with the image analysis, which saved me a great deal of time and effort. Special thanks also go to Sven Trockenbrudt for his help with performing and analysis of the synaptic release assays. I also would like to thank Dr. Dietmar Riedel for the electron microcopy.

I highly appreciate the technical assistance provided by Brigitte Barg-Kues and Sigrid Schmidt. I also would like to particularly thank our excellent animal facility, especially Sascha Krause and Thomas Gundlach.

I am also grateful to my friends and colleagues in the department for the nice and calm atmosphere. My special thanks go to Oleksandr Yagensky for his positivity and scientific input during our group meetings. I would like to thank Dr. Mahdokht Kohansal for her encouragement and scientific feedbacks. I also would like to thank Dr. Zohreh Farsi, for the her help with microscopy, scientific discussions and moral support. I am also thankful to Dr. Agata Witkowska for her advice on microscopy and data analysis, and for being a kind and supportive office-mate during the writing days.

I am particularly thankful to the wonderful people in Göttingen, whose friendships made the good moments unforgettable and the low ones tolerable: Ehsan, Elham, Vedran, Farnaz, Goran, Gianmarco, Matteo, Mario, Ricardo and Raffaella. I would like to especially thank Claudia Schmidt, my friend and roommate, for proofreading my thesis, her unfailing positivity and for making our home a great place to live.

My gratitude also goes to my friends from home, especially Nikoo, Layla and Shiva for their love and support. Last but not least, I would like to thank my parents and sister for their boundless love and continual encouragement, and for teaching me patience, persistence and resilience by example.

Curriculum Vitae

Personal information

Name	**Tahere Kalantary Dehaghi**
Address	Department of Neurobiology Max Planck Institute for Biophysical Chemistry Am Faßberg 11 37077 Göttingen, Germany
Email	tkalant@mpibpc.mpg.de
Nationality	Iranian

Education

2014 - present — **PhD in Molecular Biology**

International Max Planck Research School for Molecular Biology (IMPRS), Göttingen, Germany
Dissertation: Intracellular trafficking of proteins to presynaptic sites
Laboratory of Prof. Reinhard Jahn
Advisor: Dr. John J.E. Chua

2012 - 2014 — **M.Sc.**

International Max Planck Research School for Molecular Biology (IMPRS), Göttingen, Germany
Thesis title: Functional consequences of Sip1 inactivation in oligodendrocyte lineage cell of the CNS
Laboratory of Prof. Klaus-Armin Nave
Advisor: Dr. Sandra Göbbels

2007 - 2012 — **B.Sc.**

University of Tehran, Tehran, Iran
Biotechnology (Direct PhD program)

Research Experience

2014 - present — **PhD candidate**

Max Planck Institute for Biophysical Chemistry, Göttingen, Germany
Lab of Prof. Reinhard Jahn under supervision of Dr. John Chua

2013 - 2014 — **Master student**

Max Planck Institute for Experimental Medicine, Göttingen, Germany

	Lab of Prof. Klaus-Armin Nave under supervision of Dr. Sandra Göbbels
May - Jul. 2013	**Rotation student**
	Max Planck Institute for Biophysical Chemistry, Göttingen, Germany
	Department of Mass Spectrometry, Prof. Henning Urlaub
	Establishing the 18O-labeling protocol for phosphoproteome analysis by mass spectrometry
Mar. - May 2013	**Rotation student**
	Max Planck Institute for Biophysical Chemistry, Göttingen, Germany
	Research Group Macromolecular Crystallography, Dr. Vladimir Pena
	Cloning and expression of SF3b multiprotein complex by using multibac expression system
Jan. - Mar. 2013	**Rotation student**
	Georg-August University Göttingen Department of Molecular Enzymology, Prof. Kai Tittmann
	Expression, purification and characterization of the E. coli PDH E3 component
Apr. 2012 - Jun. 2012	**Research Intern**
	Tarbiat Modares University, Prof. Khosro Khajeh
	Designing a construct expressing small RNA fragments controlling the expression of a reporter protein in a NAND logical gate-dependent manner
Jun. 2008 - Sep. 2008	**Research Intern**
	Pasteur Institute of Iran Biotechnology Research Center, Prof. Vahid Khalaj
	Summer Internship

Teaching Experience

2016 and 2017	Tutor for international Max Planck school Lecture series on various molecular biology topics

Conferences

2017	Gordon Conference for Excitatory Synapse and Brain Function (Poster Presentation)
2016	Organizer of the International PhD symposium "Horizons in Molecular Biology", Göttingen, Germany

	Responsible for correspondence with the conference participants, organising the poster sessions and conference advertisement
2015	Organizer of the 9th career fair of the International PhD symposium "Horizons in Molecular Biology", Göttingen, Germany

Honors and Awards

2014 - 2017	Max Planck Society PhD Stipend
2012 - 2013	Stipend of the excellence foundation for the promotion of the Max Planck Society
2007 - 2012	University of Tehran fellowship for exceptional talents
2007	Ministry of Education distinction for outstanding performance in the national university entrance exams in the (ranked 51st among 400,000 participants in the mathematics and physics sciences), Tehran, Iran
2007	Ministry of Education distinction for outstanding performance in the national university entrance exams in the (ranked 9th among 400,000 participants in English literature), Tehran, Iran

Publications

Oleksandr Yagensky*, **Kalantary Dehaghi*, Tahere**, and John Jia En Chua. The roles of microtubule-based transport at presynaptic nerve terminals. *Frontiers in synaptic neuroscience*, 8:3, 2016.

*These authors have contributed equally to this work.

Languages

Mother tongue	**Persian**
Other languages	English (Fluent)
	German (Advanced)
	Arabic (Intermediate)

	References
1	**Prof. Reinhard Jahn**
	Department of Neurobiology, Max Planck institute for biophysical chemistry, Am Faßberg 11, 37077 Göttingen, Germany
E-mail:	rjahn@mpibpc.mpg.de
Phone:	+49 551 201 1635
2	**Dr. John Chua**
	Center for Life Sciences, National University of Singapore, 28 Medical Drive, 04-05 117456, Singapore
E-mail:	john.chua@mpibpc.mpg.de
	phsjcje@nus.edu.sg
Phone:	+65 66015178
3	**Prof. Klaus-Armin Nave**
	Department of Neurogenetics, Max Planck institute for experimental medicine, Hermann-Rein-Straße 3, 37075 Göttingen, Germany
E-mail:	nave@em.mpg.de
Phone:	+49 551 3899 757